NASA TECHNICAL MEMORANDUM

NASA TM X-71991

COPY NO.

NASA TM X-71991

# COMPARISON OF INTERFERENCE-FREE NUMERICAL RESULTS WITH SAMPLE EXPERIMENTAL DATA FOR THE AEDC WALL-INTERFERENCE MODEL AT TRANSONIC AND SUBSONIC FLOW CONDITIONS

By Perry A. Newman and Dennis O. Allison

July 1974

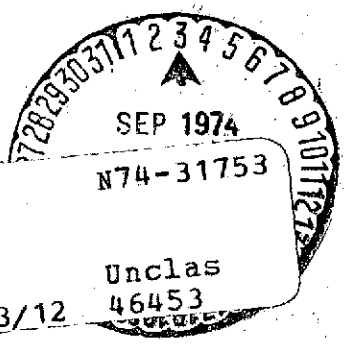






NATIONAL AERONAUTICS AND SPACE ADMINISTRATION

LANGLEY RESEARCH CENTER, HAMPTON, VIRGINIA 23665

| 1. Report No. | 2. Government Accession No. | 3. Recipient's Catalog No. |
|---|---|---|
| NASA TM X-71991 | | |

| 4. Title and Subtitle | 5. Report Date |
|---|---|
| Comparison of Interference-Free Numerical Results With Sample Experimental Data for the AEDC Wall-Interference Model at Transonic and Subsonic Flow Conditions. | July 1974 |
| | 6. Performing Organization Code |
| 7. Author(s) | 8. Performing Organization Report No. |
| Perry A. Newman and Dennis O. Allison | |
| 9. Performing Organization Name and Address | 10. Work Unit No. |
| NASA-Langley Research Center<br>Hampton, Virginia 23665 | 501-06-01-02 |
| | 11. Contract or Grant No. |
| 12. Sponsoring Agency Name and Address | 13. Type of Report and Period Covered |
| National Aeronautics and Space Administration<br>Washington, D.C. 20546 | NASA Technical Memorandum |
| | 14. Sponsoring Agency Code |

15. Supplementary Notes

Special technical information release, not planned for formal NASA publication.

16. Abstract

Numerical results obtained from two computer programs recently developed with NASA support and now available for use by others are compared with some sample experimental data taken on a rectangular-wing configuration in the AEDC 16-Foot Transonic Tunnel at transonic and subsonic flow conditions. This data was used in an AEDC investigation as reference data to deduce the tunnel-wall interference effects for corresponding data taken in a smaller tunnel. The comparisons were originally intended to see how well a current state-of-the-art transonic flow calculation for a simple 3-D wing agreed with data which was felt by experimentalists to be relatively interference-free. As a result of the discrepancies between the experimental data and computational results at the quoted angle of attack, it was then deduced from an approximate stress analysis that the sting had deflected appreciably. Thus, the comparisons themselves are not so meaningful, since the calculations must be repeated at the proper angle of attack. Of more importance, however, is a demonstration of the utility of currently available computational tools in the analysis and correlation of transonic experimental data.

| 17. Key Words (Suggested by Author(s)) (STAR category underlined) | 18. Distribution Statement |
|---|---|
| Aerodynamics<br>Transonic Flow<br>Compressible Flow<br>Wings | Unclassified-unlimited |

| 19. Security Classif. (of this report) | 20. Security Classif. (of this page) | 21. No. of Pages | 22. Price* |
|---|---|---|---|
| Unclassified | Unclassified | 92 | $4.00 |

*Available from { The National Technical Information Service, Springfield, Virginia 22151
STIF/NASA Scientific and Technical Information Facility, P.O. Box 33, College Park, MD 20740

# COMPARISON OF INTERFERENCE-FREE NUMERICAL RESULTS WITH SAMPLE EXPERIMENTAL DATA FOR THE AEDC WALL-INTERFERENCE MODEL AT TRANSONIC AND SUBSONIC FLOW CONDITIONS

By Perry A. Newman and Dennis O. Allison
Langley Research Center

## SUMMARY

Numerical results obtained from two computer programs recently developed with NASA support and now available for use by others are compared with some sample experimental data taken on a rectangular-wing configuration in the AEDC 16-Foot Transonic Tunnel at transonic and subsonic flow conditions. This data was used in an AEDC investigation as reference data to deduce the tunnel-wall interference effects for corresponding data taken in a smaller tunnel. The comparisons were originally intended to see how well a current state-of-the-art transonic flow calculation for a simple 3-D wing agreed with data which was felt by experimentalists to be relatively interference-free. As a result of the discrepancies between the experimental data and computational results at the quoted angle of attack, it was deduced from an approximate stress analysis that the sting had deflected appreciably. Thus, the comparisons themselves are not so meaningful, since the calculations must be repeated at the proper angle of attack. Of more importance, however, is a demonstration of the utility of currently available computational tools in the analysis and correlation of transonic experimental data.

## INTRODUCTION

The possibility of calculating inviscid three-dimensional transonic flow about simple lifting wings by using large present-generation computers has been demonstrated (Refs. 1-7). However, very few comparisons have been made with experiments and those which have are of limited value. Older data, generally taken on semispan models, may have large inaccuracies due to tunnel-wall interference and recent data is generally for more complicated configurations than can presently be modeled in 3-D calculations. Such comparisons were made in references 3, 4, and 5 for a swept wing panel and a wing simulating the C-141 wing; discrepancies were observed and were attributed to viscous and wall-interference effects. A current review (Ref. 8) of the computation of steady 2-D and 3-D transonic flow based on relaxation methods indicates the present status and concludes that even though significant advances have been made in the last several years further improvements regarding shock jumps and viscous effects are clearly needed in order to adequately simulate transonic flow problems. Jameson's solutions (Refs. 6 and 7) for the

exact isentropic transonic flow about finite yawed wings incorporate a number of ideas which are now recognized as being important for a successful iterative calculation of transonic flow. A version of his program is operational and available (Ref. 9); it represents one of the most advanced state-of-the-art computational tools.

Recently Binion (Ref. 10) of AEDC (ARO, Inc.) completed a series of transonic experiments on a simple configuration which could be approximated by existing transonic 3-D wing programs. It was the AEDC Wall Interference Model, a full span rectangular-planform wing centrally mounted on a circular cross-section sting-body. The purpose of these experiments was to investigate the three-dimensional tunnel-wall interference in the AEDC 4-Foot Transonic Tunnel (4T) by comparison with data obtained from the AEDC 16-Foot Transonic Tunnel (16T) under identical flow conditions. A differential pressure measurement near the tip of the sting-body was used to ascertain that the flow conditions were the same. Thus pressure distributions obtained in the two tunnels could be compared directly rather than as a function of angle of attack.

Sample experimental data from the AEDC Tunnel 16T was made available in order that comparisons could be made with numerical results from Jameson's transonic-flow program for 3-D wings (Refs. 6,7,9). The first calculation for a lifting transonic flow indicated that the comparisons were not quantitatively as good as had been anticipated. Since the experimental sting-body could not be modeled in the nonlinear Jameson program, it was decided to make calculations for wings and wing-body configurations using the linear-theory subsonic-supersonic program recently developed by Woodward (Ref. 11). These latter calculations were made into the transonic range to show where the linear theory departs from the experimental results for the particular configuration.

The comparisons between the present calculated and experimental results show a systematic discrepancy with respect to the lift which is opposite to what would be expected due to viscous effects alone. As a result, an approximate stress analysis was made and it indicated an appreciable sting deflection. Several calculations were made to take this deflection into account and the comparisons with experiment are greatly improved.

## SOURCE OF RESULTS

### Experimental Data

A detailed description of the AEDC wall interference tests recently completed by Binion is contained in Reference 10. The sample experimental data used in the present comparisons was taken in the AEDC Tunnel 16T. This data was used as reference data to deduce the tunnel-wall interference corrections for corresponding data taken in the AEDC Tunnel 4T. Tunnel 16T is a closed-circuit continuous-flow variable-density wind tunnel capable of operating at Mach numbers from 0.2 to 1.6. The test section is 16 ft. square and 40 ft. long; its walls are perforated with 60° slanted holes at a fixed 6% porosity.

Figure 1 is an AEDC photograph of the experimental model mounted in tunnel 16T with the tail in the forward position. The experimental data quoted in the present report was taken on the wing with the tail mounted in the aft position, whereas that quoted for the tail was taken with the wing removed from the tunnel. The geometric configuration most closely approximating the experimental model (with tail mounted in the aft position) is shown in Figure 2. This plot was generated by the program of Reference 12 and is the geometry which was used for several wing-body-tail calculations in the linear-theory Woodward program (Ref. 11). Both the wing and tail have a rectangular planform with a NACA 63A006 airfoil section; the aspect ratio of the wing is 32/9 (~ 3.556) whereas that of the tail is 13/4.5 (~ 2.889).

In these experiments, the boundary layer was tripped at about 5% chord. An experimentally determined correction for flow angularity is the only correction which was made to the data. The sample AEDC experimental cases which are compared with numerical calculations in this report are identified in Table I. In each case, chordwise pressure data was taken on the upper and lower wing (tail) surfaces at the 50% semispan station and streamwise pressure data was taken on the upper and lower surface of the sting-body.

TABLE I

SAMPLE AEDC EXPERIMENTAL CASES TO BE COMPARED WITH NUMERICAL CALCULATIONS

| AEDC Identification | $M_\infty$ | $\alpha$ | Experimental Configuration |
|---|---|---|---|
| 116/4 | 0.599 | 0.06 | Wing* with tail* aft |
| 116/5 | 0.599 | 2.03** | " " " " |
| 113/3 | 0.699 | 0.02 | " " " " |
| 113/4 | 0.699 | 2.03** | " " " " |
| 112/4 | 0.802 | -0.01 | " " " " |
| 112/6 | 0.800 | 2.00** | " " " " |
| 136/6 | 0.900 | -0.03 | " " " " |
| 136/8 | 0.896 | 1.97** | " " " " |
| 175/4 | 0.599 | -0.02 | Tail* alone |
| 175/5 | 0.600 | 1.99** | " " |
| 174/5 | 0.700 | -0.03 | " " |
| 174/7 | 0.699 | 1.96** | " " |
| 171/4 | 0.800 | -0.06 | " " |
| 171/5 | 0.800 | 1.94** | " " |
| 167/6 | 0.898 | -0.09 | " " |
| 167/7 | 0.895 | 1.91** | " " |

*Both the wing and tail are full-span models and are mounted on sting-bodies as shown in Figure 1.

**Need to be corrected for sting deflection.

Again the reader is referred to Reference 10 for details concerning the experiment.

## Computational Programs

As already mentioned, two recently developed computer programs were used to generate the numerical results which are presented in the next section. A few brief comments on each program are given below; however, one must see the appropriate references for details concerning either program. Both were developed with NASA support and are available for use by others.

The Jameson Three-Dimensional Transonic Airfoil Analysis Program (Refs. 6,7,9) computes inviscid isentropic transonic flow over yawed or unyawed wings with straight leading and arbitrary trailing edges. The solution is based on the full nonlinear potential equation and the free-stream Mach number is restricted only by the isentropic assumption. Thus, computations can be made for low supersonic free-stream velocities even though no such examples are included here. Weak shock waves are automatically located wherever they occur in the flow. An analytical transformation of wing-section planes (i.e., normal to the leading edge) maps the region of physical space outside the airfoil to an upper half-plane as indicated in Figure A1 of the Appendix. This procedure allows for exact specification of both the surface boundary conditions and the far-field boundary data appropriate to supersonic free stream velocities. In supersonic flow regions the finite difference operator is locally rotated so as to properly account for the domain of dependence. The line relaxation algorithm has been stabilized using criteria from a time-like analogy.

The Woodward Unified Subsonic-Supersonic Aerodynamics Program (Ref. 11) computes the inviscid pressure distribution and aerodynamic characteristics for wing-body-tail configurations in subsonic and supersonic potential flow. The solution is based on a linear superposition of aerodynamic singularities (source and vortex) distributed on a large number of panels which approximate the geometrical configuration. For a lifting surface two options are available. In one, singularities are located on the mean plane of the surface and approximate planar boundary conditions are used to determine the singularity strengths. In the other, singularities are located on the upper and lower surfaces of the lifting element and exact boundary conditions are used. There are apparently still some bugs in the latter nonplanar option; therefore, all of the Woodward program results quoted here were generated using the planar option. For either option, the resulting system of equations which determines the singularity strengths is solved using an iterative procedure.

The numerical calculations were made at the nominal Mach numbers ($M_\infty$ = 0.6,0.7,0.8,0.9) and angles of attack ($\alpha = 0^o, 2^o$) of the sample experimental cases listed in Table I. Since various geometric configurations were used to approximate the experimental model, the particular cases which were calculated are given in the next section. The NACA 63A006 airfoil ordinates used in the calculations are listed in Table II. These were furnished by Ching Lo of AEDC (ARO, Inc.) and they are consistent with those given in Reference 13.

TABLE II

NACA 63A006 AIRFOIL ORDINATES USED IN CALCULATIONS
(BASED ON CHORD OF 100.)

| NACA 63A006 | |
|---|---|
| X(I) | Y(I) |
| 0. | 0. |
| .055555 | .16235 |
| .11111 | .22444 |
| .22222 | .32222 |
| .33333 | .401111 |
| .44444 | .46777 |
| .55555 | .52 |
| .83333 | .62277 |
| 1.11111 | .71111 |
| 1.66666 | .86478 |
| 2.2222 | .98961 |
| 2.7777 | 1.0978 |
| 3.3333 | 1.1962 |
| 3.8888 | 1.2877 |
| 4.4444 | 1.3696 |
| 5. | 1.447 |
| 7.5 | 1.7466 |
| 10. | 1.9889 |
| 15. | 2.3622 |
| 20. | 2.6311 |
| 25. | 2.82 |
| 30. | 2.9422 |
| 35. | 2.9955 |
| 40. | 2.9844 |
| 45. | 2.9144 |
| 50. | 2.7877 |
| 55. | 2.6133 |
| 60. | 2.3955 |
| 65. | 2.1433 |
| 70. | 1.8589 |
| 75. | 1.5555 |
| 80. | 1.2478 |
| 85. | .93889 |
| 90. | .63 |
| 95. | .32222 |
| 100. | .013 |

## COMPARISON OF RESULTS

### General

It should be pointed out here that the numerical calculations are for interference-free inviscid flow conditions. These calculations were made with programs which are now readily available for use by others. No attempt has been made to model the tunnel walls or to correlate the present experimental data by matching additional experimental parameters (such as the lift) or adjusting the flow conditions. These ideas, however, have been demonstrated to be fruitful in 2-D transonic-flow relaxation calculations (Refs. 14 and 15).

Numerical results were generated in one or both computer programs at several flow conditions for five geometric configurations which approximate the experimental model. Comparisons with experimental data have been grouped accordingly as rectangular wing, rectangular tail, wing with sting-body and tail with sting-body. In addition, four cases were run in the Woodward program for a wing-body-tail configuration as depicted in Figure 2. The computed pressure distributions on the wing and sting-body with the tail in the aft position were essentially the same as those obtained for the wing with sting-body without the tail. This indicates that the tail in the aft position had little effect on the wing data; thus, wing-body-tail configuration results are not presented here.

Since all of these comparisons show a systematic discrepancy in lift, opposite to that expected due to viscosity alone, approximate stress analyses of the model and sting were made to see if significant aeroelastic deformations were present. It was found that the sting deflections were appreciable; in the last section, results from several rectangular-wing calculations for the approximate corrected angle of attack are compared with experimental data.

### Rectangular Wing

The rectangular wing approximating the experimental model is depicted in Figure 3. Four cases were run in both programs in order to compare sample subsonic ($M_\infty = 0.6$) nonlifting ($\alpha = 0^o$) and lifting ($\alpha = 2^o$) flows and transonic ($M_\infty = 0.9$) nonlifting ($\alpha = 0^o$) and lifting ($\alpha = 2^o$) flows. The comparisons are presented in this order in Figures 5 to 18. For each case the first figure compares chordwise distributions of surface pressure coefficient at the 50 percent semispan location while the second figure shows the calculated results at the wing root. Section aerodynamic coefficients (computed from the Jameson program) are printed near the bottom of these figures. The sonic value of $C_p$ is indicated by a long tick mark on the ordinate. The third figure shows total aerodynamic coefficients and the Mach number (times 100) distribution in the root-section plane of the computational grid as obtained from the Jameson program. One can refer to the Appendix to see how information on this chart can be transferred to the root-section plane of physical space. For lifting cases, a fourth figure shows the spanwise distribution of section lift coefficient as calculated from both programs.

It can be seen from Figures 5 and 8 that for the sample subsonic cases at $M_\infty = 0.6$ the experimental and theoretical (both linear and nonlinear) pressure results compare favorably. Figure 11 shows the spanwise distribution of computed section lift coefficients; the nonlinear Jameson program values are observed to be about 6 percent higher than those from the linear theory Woodward program. One can see how such a difference in section lift shows up in the pressure plot at the 50 percent semispan station by referring to Figure 8 and suspect that the experimental section lift coefficient is larger than the Jameson value by at least the same amount, and probably even more.

Comparisons of pressure results for the sample transonic ($M_\infty = 0.9$) nonlifting ($\alpha = 0^o$) and lifting ($\alpha = 2^o$) flows are shown in Figures 12 and 15 respectively. The nonlinear-theory Jameson results and experimental data qualitatively agree; however, shock locations and section lifts do not compare well. In both cases the experimental shock wave is downstream of the Jameson inviscid theoretical location for a wing alone in free air. Referring to Figure 15 one can see that the lower surface pressure distributions (Jameson and experiment) tend to agree, but the upper surface pressures do not. In fact the $\Delta C_p$, and thus the section lift, appears to be much larger in the experiment. The discrepancy in both shock location and section lift is in the opposite direction from what viscous effects alone would produce. This is discussed further in the last section. Note again that the nonlinear-theory Jameson program is for a wing alone. The sting-body has not been accounted for and its effect at transonic speeds may be important at angles of attack. The supersonic bubbles both above and below the wing are clearly visible in Figures 14 and 17, the Mach charts at the root-section plane of the computational space.

It is certainly obvious that at $M_\infty = 0.9$ the wing pressure results from the linear-theory Woodward program do not exhibit the correct qualitative behavior. The chordwise distribution of lifting pressure ($\Delta C_p$) is not right and thus the section moments will be wrong even though the section lift values, as shown on Figure 18, are not nearly so much in error.

## Rectangular Tail

Figure 4 shows the rectangular-tail configuration to the same scale as that used in Figure 3 for the wing. The results in this section are presented on the same type figures as described in the last section. The comparisons and results are shown on Figures 19 to 32; they exhibit the same trends as the wing results just discussed. The agreement with experiment is somewhat better though. One can note, by comparing the pressure plots for the transonic cases, that the shock location changes with the aspect ratio.

## Wing with Sting-Body

Experimental data was taken on the upper and lower surfaces of the sting-body and in several cases the flow on the body did not become supersonic. These cases have been computed in the linear-theory Woodward program to see if there was any indication that the sting-body was affecting transonic lifting flows to the extent indicated by the wing and tail alone comparisons just described.

Figure 33 depicts the wing with sting-body configuration which was used in the Woodward program. Computations were made for this configuration at Mach numbers of 0.6, 0.7, 0.8, and 0.9 and angles of attack of $0^{o}$ and $2^{o}$. For each case the first figure compares the chordwise distribution of wing pressures at the 50 percent semispan station while the second figure compares the axial distribution of pressures on the upper and lower surfaces of the sting-body, starting from the tip. For the lifting cases, a plot of the spanwise distribution of section lift coefficients computed by the Woodward program is also given. The comparisons for this configuration are given on Figures 34 to 53.

At Mach numbers of 0.6 and 0.7 as well as the zero incidence case at 0.8 the experimental data and linear-theory Woodward results compare well. It can be seen in Figure 46 though that at $2^{o}$ incidence and $M_{\infty} = 0.8$ there is a shock wave on the wing which of course is not predicted by the linear-theory Woodward program. Figure 47 shows that the flow on the sting-body is still subsonic but that the linear-theory $C_p$ distribution does not agree too well with experiment over the first 1/3 of the wing chord. At $M_{\infty} = 0.9$ the linear-theory pressure results are not even qualitatively right over the wing.

Inclusion of the sting-body had very little effect on the linear-theory pressure distribution at the 50 percent semispan location on the wing. There was no indication from these linear-theory results that the discrepancies in the transonic lifting flows was due to the sting-body. Some preliminary non-linear (transonic) calculations (Ref. 16) for this wing mounted on a circular-cylindrical body did not seem to indicate the effect either. However, this latter calculation did not allow for a change in the cross-sectional area to match that of the experimental sting-body.

## Tail With Sting-Body

Figure 54 shows the tail with sting-body to the same scale as that in Figure 3 for the wing. The results in this section are presented on the same type figures as discussed in the last section. The tail with sting-body comparisons are shown on Figures 55 to 74. The trends and agreement with experiment are similar to those for the wing with sting-body configuration.

### Rectangular Wing at Corrected Angle of Attack

As already pointed out the previous comparisons show a systematic discrepancy in section lift between the calculations and experiment at the 50% semispan station. The difference is opposite to that expected due to viscous effects alone since the inviscid calculations, which impose the Kutta condition at the trailing edge of the wing, should overpredict the lift. This is not the case, however, as can be seen from Figure 15. For that case, one would say that the experimental lift was about half again as much as that obtained from the Jameson program at $\alpha = 2^{o}$. In fact, it can be seen from Figure 75 that when the calculation is made at $\alpha = 3^{o}$, the resulting agreement with the experimental data is indeed very good. The detailed pressure distributions on both the upper and lower wing surface including the shock wave locations on both agree well except near the trailing edge where viscous effects are present.

An approximate aeroelastic analysis of the model indicated that the torsional deflections of the wing itself (assumed to be a homogeneous solid) were very small and could not be responsible for the large differences. An approximate analysis of the sting (obtained from an AEDC stress analysis program) indicated that it deflected appreciably. For the $M_{\infty} = 0.9$, $\alpha = 2^{o}$ wing case (136/8 of Table I) $\Delta\alpha$ due to sting deflection obtained from the approximate stress analysis was $0.81^{o}$ whereas that for the $M_{\infty} = 0.6$, $\alpha = 2^{o}$ wing case (116/5 of Table I) was $0.37^{o}$. These two cases were computed in the Jameson program and the chordwise distribution of pressure coefficient at the 50% semispan station is shown in Figures 76 and 77 respectively. It can be seen that the agreement is much better than that shown in Figures 15 and 8.

It is apparent that the sting deflection must be taken into account before meaningful comparisons can be made. The sting can be statically loaded to determine fairly accurately just what the angular deflections were at the model position. The results shown in Figure 75 would lead us to believe that $\Delta\alpha$ is probably more like $1^{o}$ or larger rather than the approximate $0.81^{o}$. Inclusion of viscous effects would tend to require an even larger angle of attack in order to obtain the same lift.

## CONCLUDING REMARKS

Comparisons of interference-free theoretical results and some sample experimental data taken on the AEDC Wall Interference Model in tunnel 16T indicated how presently available computational programs can and should be used in the analysis and correlation of experimental transonic data. Meaningful comparisons can be made only after the actual angular corrections at the model position (due to sting deflection) have been experimentally measured for each case.

The present comparisons do show where and how linear-theory results (Woodward program) become inadequate in the transonic-flow region. However, it was concluded from the Woodward program that the presence of the body and tail was not the cause of the observed lift discrepancy between the Jameson wing-alone results and the experimental data. Note that the sting-body has

not been accounted for in a nonlinear calculation; its effect at transonic speeds may be important at angle of attack.

The numerical results given here are only a sample of what can be generated using presently available computer programs. Comparisons with much more of the experimental data can and should be made when the angle of attack is corrected, since both the Jameson and Woodward programs will treat supersonic free-stream velocities.

# APPENDIX

## TRANSFORMATION OF MACH CHART TO PHYSICAL SPACE

In the Jameson program, a parabolic transformation is used in planes normal to the leading edge of the wing. Figure A1 depicts how the airfoil contour in such planes appears in both physical and computational space while Figure A2 shows a portion of the wing-section plane computational grid plotted on physical space. This plot was obtained from a program supplied by J. D. Keller of NASA-Langley. The Mach number charts which Jameson's program produces as part of the printed output are for computational space, not physical space. Figure A3 is a sample root-section Mach chart with annotations on it which locate the wing and free stream. The solid line near the border of the Mach chart encloses that portion of computational grid which is plotted in Figure A2. One can transpose the Mach number (times 100) at each computational grid point of a Mach chart, such as Figure A3, to Figure A2 in order to see the Mach number distribution (or some other feature such as sonic line or shock wave) of the flow in the physical wing-section plane.

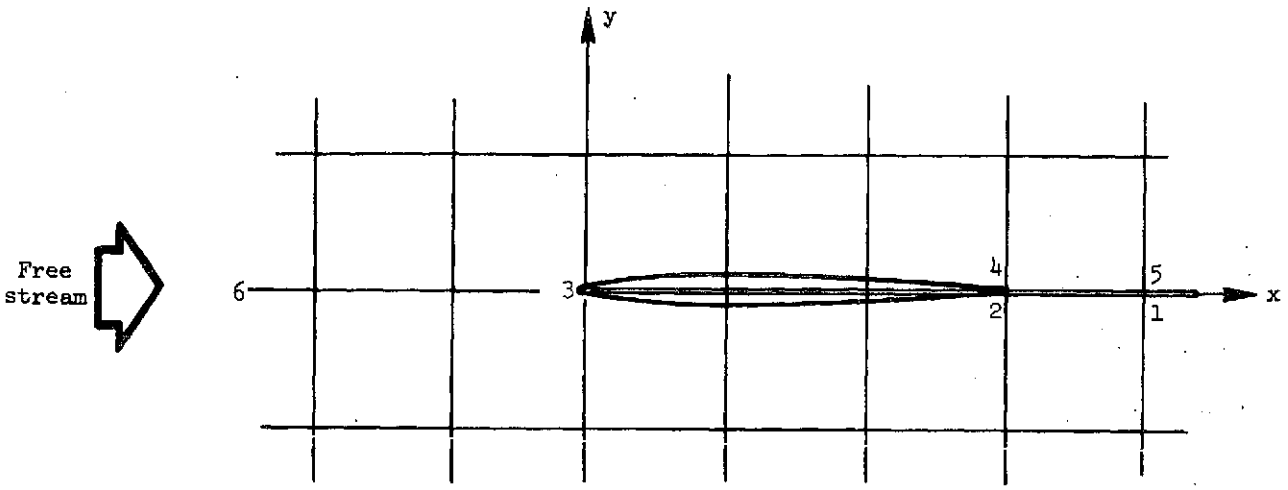


Physical space - Cartesian coordinates

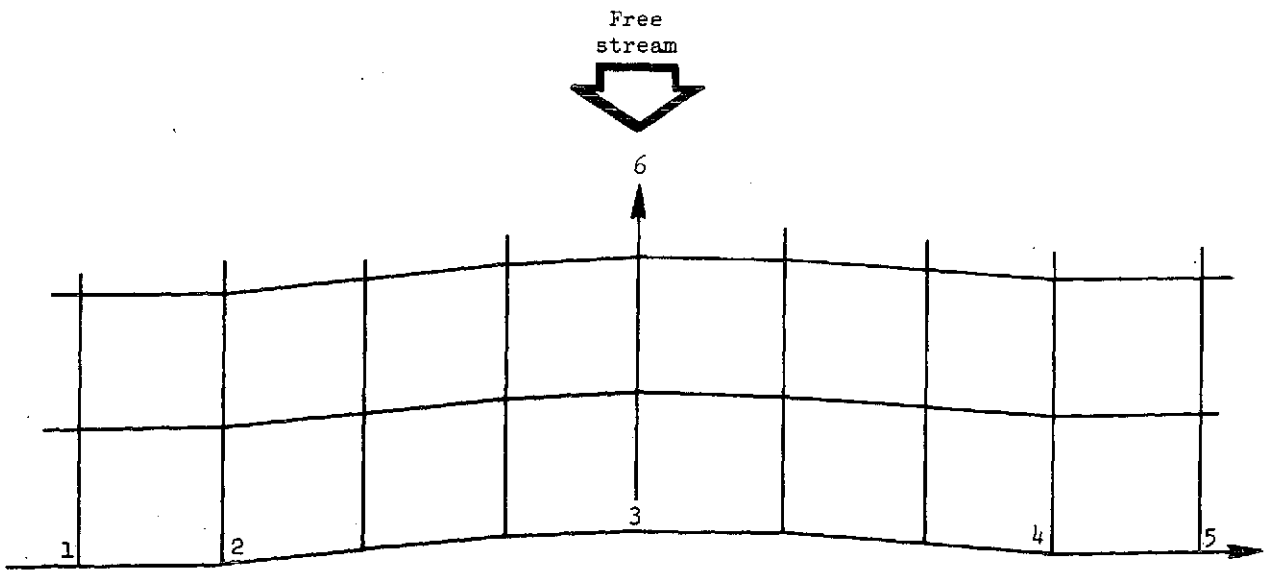


Computational space - sheared parabolic coordinates

Figure A1.- Physical and computational coordinate systems in wing section plane.

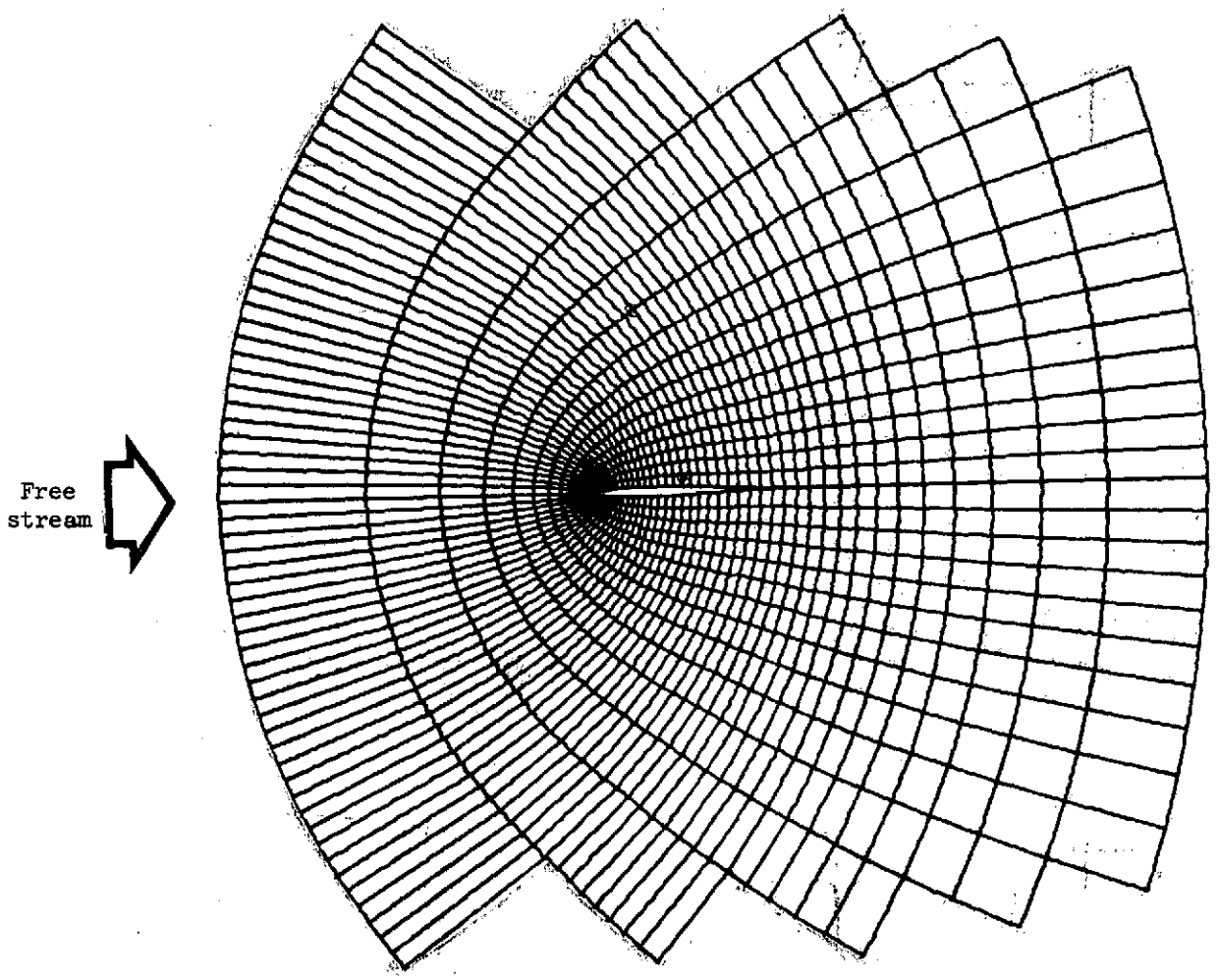


Figure A2.- Portion of wing section computational grid plotted in physical space.

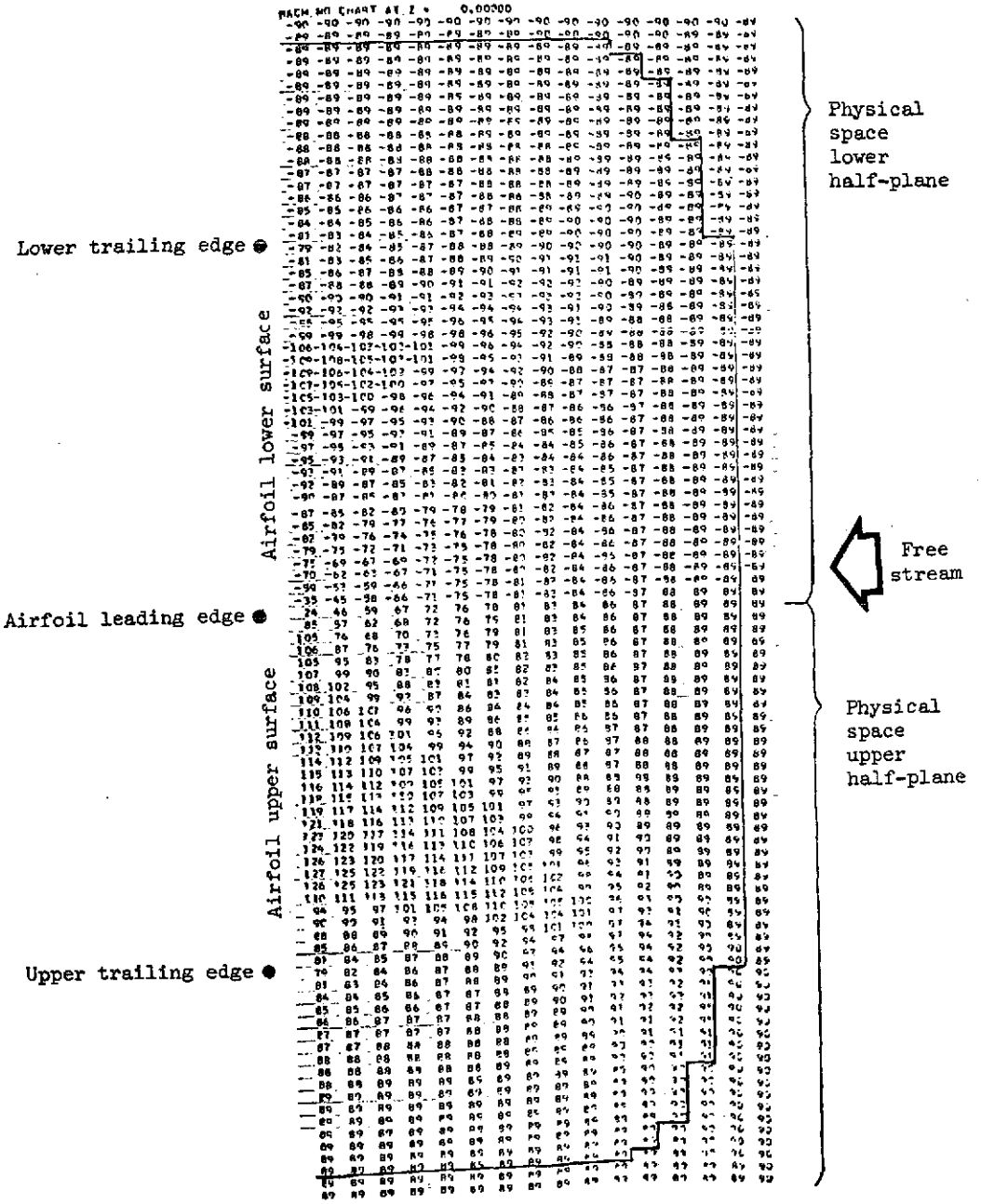


Figure A3.- Mach chart at root section of wing in computation plane.

## REFERENCES


1. Bailey, F.R.; and Steger, J.L.: Relaxation Techniques for Three-Dimensional Transonic Flow About Wings. AIAA J., vol. 11, no. 3, Mar. 1973, pp. 318-325.

2. Newman, P.A.; and Klunker, E.B.: Computation of Transonic Flow About Finite Lifting Wings. AIAA J., vol. 10, no. 7, July 1972, pp. 971-973.

3. Ballhaus, W.F.; and Bailey, F.R.: Numerical Calculation of Transonic Flow About Swept Wings. AIAA Paper No. 72-677, June 1972.

4. Bailey, F.R.; and Ballhaus, W.F.: Relaxation Methods for Transonic Flow About Wing-Cylinder Combinations and Lifting Swept Wings. Proceedings of the Third International Conference on Numerical Methods in Fluid Mechanics. Vol. 19 of Lecture Notes in Physics, Henri Cabannes and Roger Temain, eds., Springer-Verlag, 1973, pp. 2-9.

5. Lomax, H.; Bailey, F.R.; and Ballhaus, W.F.: On the Numerical Simulation of Three-Dimensional Transonic Flow With Application to the C-141 Wing. NASA TN D-6933, 1973.

6. Jameson, A.: Numerical Calculation of the Three-Dimensional Transonic Flow Over a Yawed Wing. Proceedings of the AIAA Computational Fluid Dynamics Conference. Palm Springs, California, July 19-20, 1973. pp. 18-26.

7. Jameson, A.: Three Dimensional Flows Around Airfoils With Shocks. Proceedings of the IFIP Symposium on Computing Methods in Applied Sciences and Engineering, December 17-21, 1973, Versailles, France. To be published by Springer-Verlag (available in Colloques IRIA Methodes Calqul Scientifique et Technique, 1973).

8. Bailey, F.R.: On the Computation of Two- and Three-Dimensional Steady Transonic Flows by Relaxation Methods. Presented in Von Karman Institute Lecture Series on Progress in Numerical Dynamics, 11-15 February 1974, Brussels, Belgium. To be published.

9. Newman, P.A.; and Davis, R.M.: Input Description for Jameson's Three-Dimensional Transonic Airfoil Anlaysis Program. NASA TM X-71919, 1974.

10. Binion, T.W., Jr.: An Investigation of Three-Dimensional Wall Interference in a Variable Porosity Transonic Wind Tunnel. To be published as an AEDC TR, 1974.

11. Woodward, F.A.: An Improved Method for the Aerodynamic Analysis of Wing-Body-Tail Configurations in Subsonic and Supersonic Flow. NASA CR-2228, 1973.

12. Craidon, C.B.: Description of a Digital Computer Program for Airplane Configuration Plots. NASA TM X-2074, 1970.

13. Loftin, L.K., Jr.: Theoretical and Experimental Data for a Number of NACA 6A-Series Airfoil Sections. NACA Rept. 903, 1948.

14. Murman, E.M.: Computation of Wall Effects in Ventilated Transonic Wind Tunnels. AIAA Paper No. 72-1007, Sept. 1972.

15. Melnik, R.E.; and Ives, D.C.: On Viscous and Wind-Tunnel Wall Effects in Transonic Flows Over Airfoils. AIAA Paper No. 73-660, July 1973.

16. Klunker, E.B.; and Newman, P.A.: Computation of Transonic Flow About Lifting Wing-Cylinder Combinations. J. Aircraft, vol. 11, no. 4, Apr. 1974, pp. 254-256.

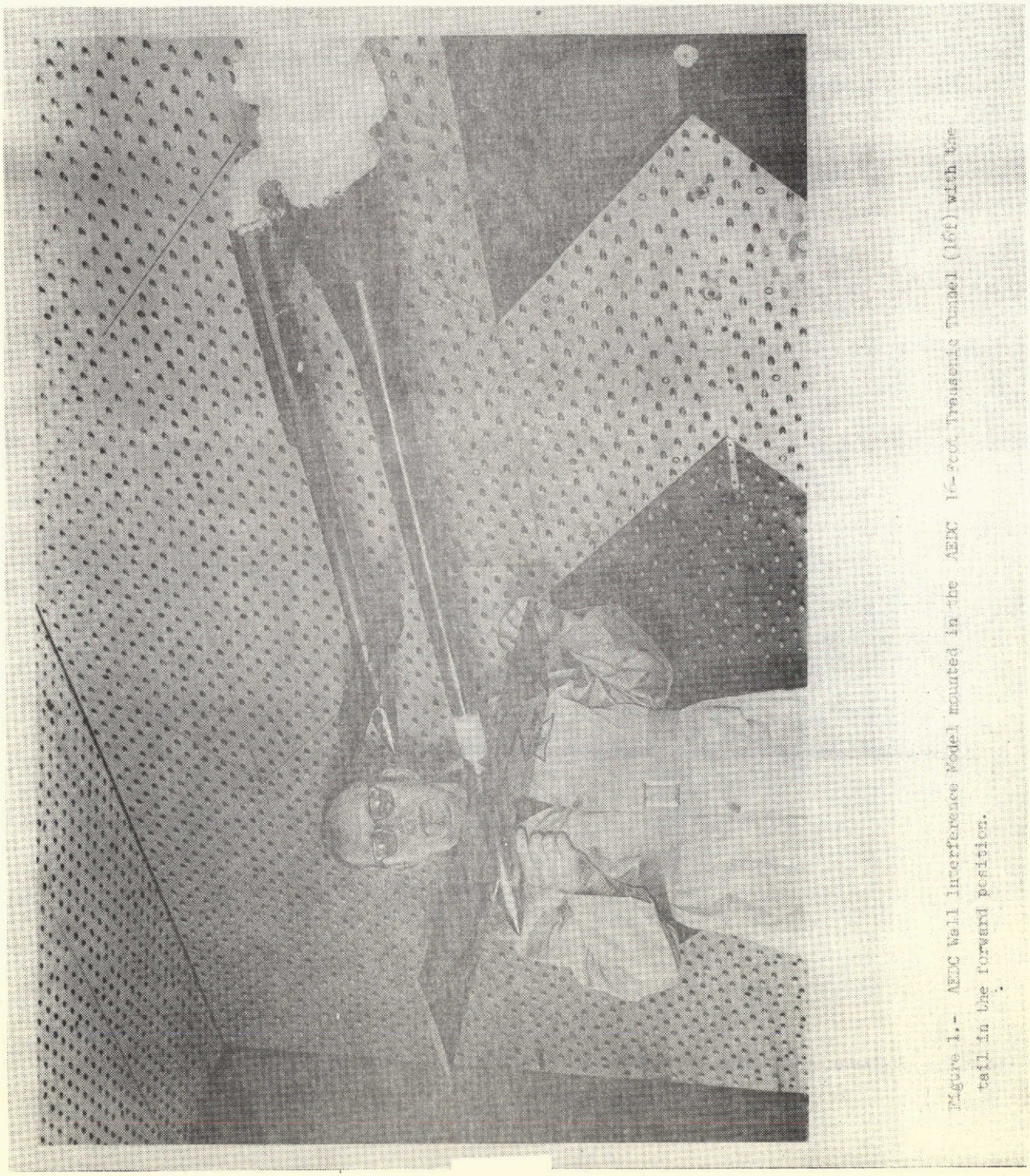

Figure 1.- AEDC Wall Interference Model mounted in the AEDC 16-Foot Transonic Tunnel (16T) with the tail in the forward position.

RECTANGULAR WING WITH EXPERIMENTAL STING-BODY AND
RECTANGULAR TAIL IN AFT POSITION

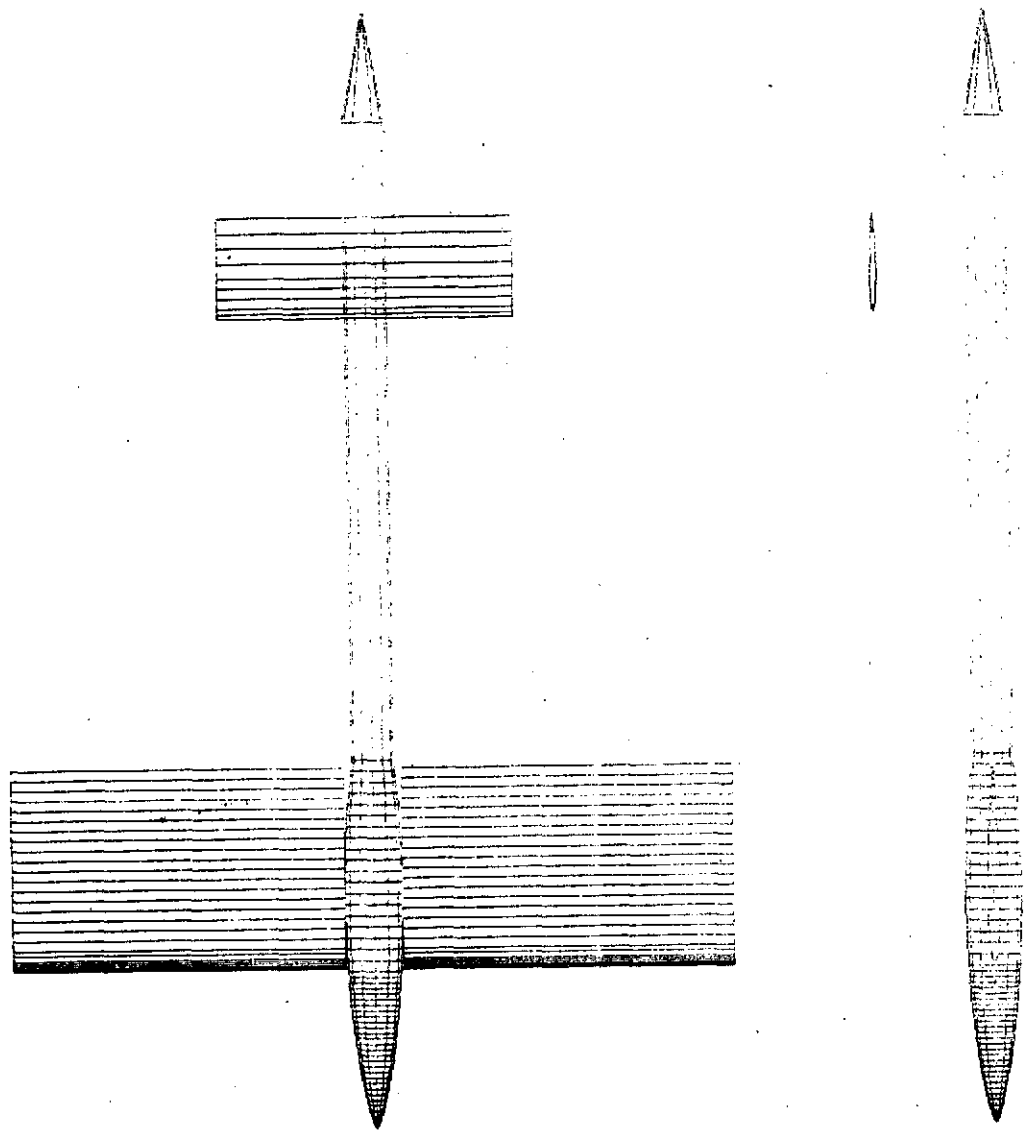

FIGURE 2.- RECTANGULAR WING PLUS EXPERIMENTAL STING-BODY AND TAIL CONFIGURATION USED IN CALCULATIONS.

RECTANGULAR WING NACA 63A006 SECTION AR = 32/9

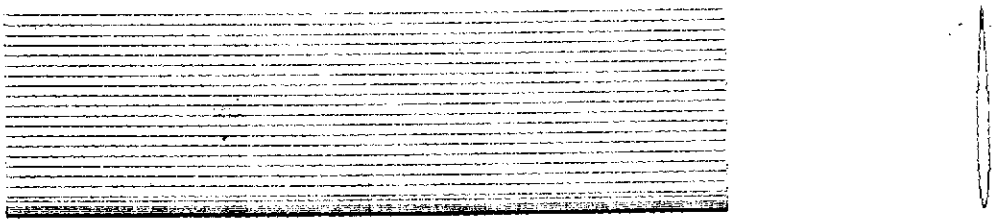

FIGURE 3.- RECTANGULAR WING CONFIGURATION USED IN CALCULATIONS.

RECTANGULAR TAIL NACA 63A006 SECTION AR = 13/4.5

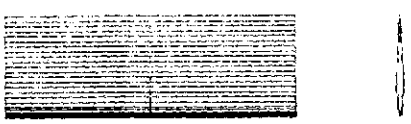

FIGURE 4.- RECTANGULAR TAIL CONFIGURATION USED IN CALCULATIONS.

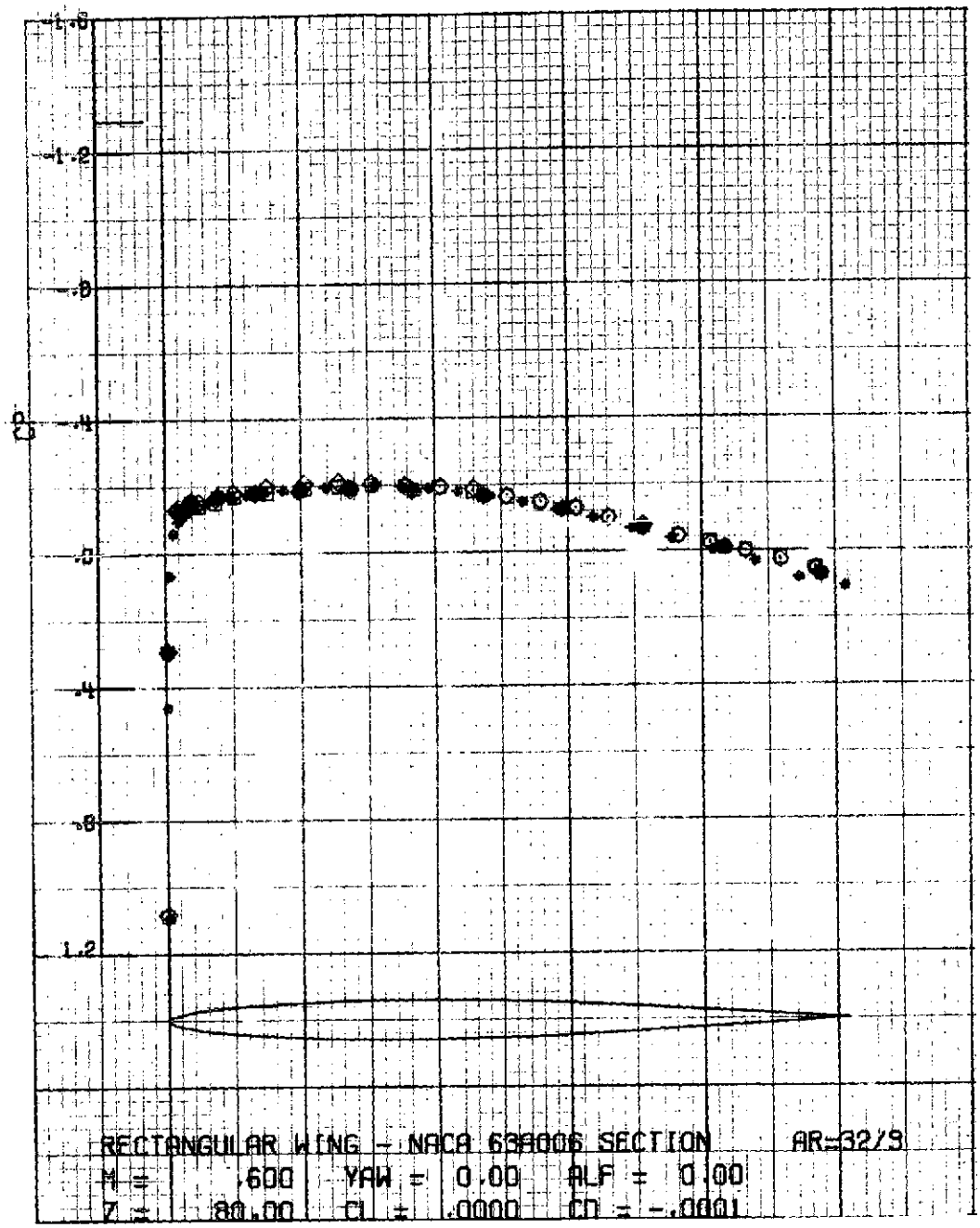


Figure 5.- Chordwise distribution of surface pressure coefficients at the 50 percent semispan location.

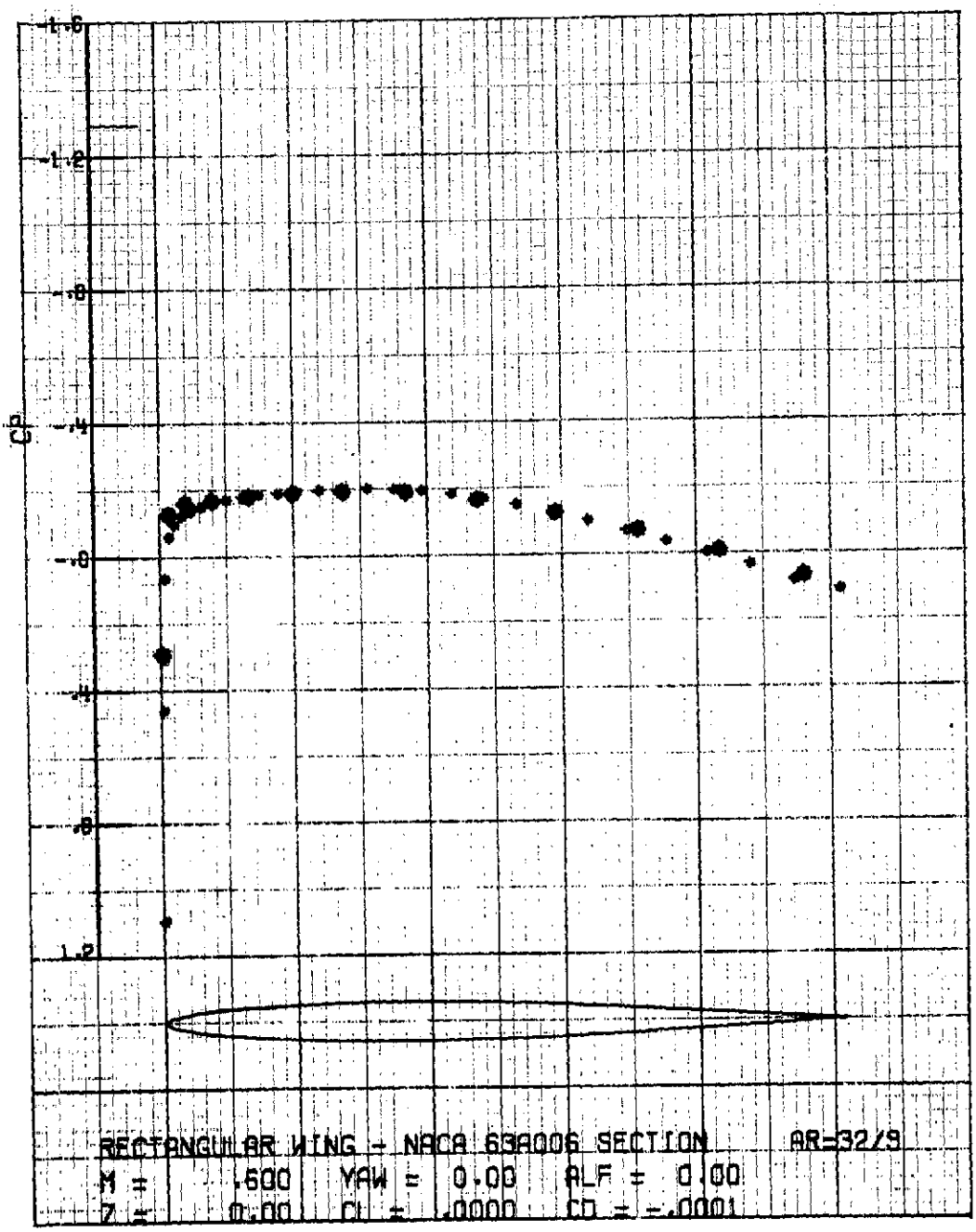


Figure 6.- Chordwise distribution of surface pressure coefficients at the root section.

RECTANGULAR WING - NACA 63A006 SECTION AR = 32/9

TOTAL WING COEFFICIENTS

| YAW | ANG OF ATTACK | MACH NO | CL | LD FORM | LM |
|---|---|---|---|---|---|
| 0.0000 | 0.0000 | .8000 | .0000 | -.0001 | .0000 |

| CD FRICTION | CD | L/D FORM | L/D |
|---|---|---|---|
| 0.0006 | -.0101 | -.0000 | -.0000 |

MACH NO CHART AT $\alpha$ = 0.00000

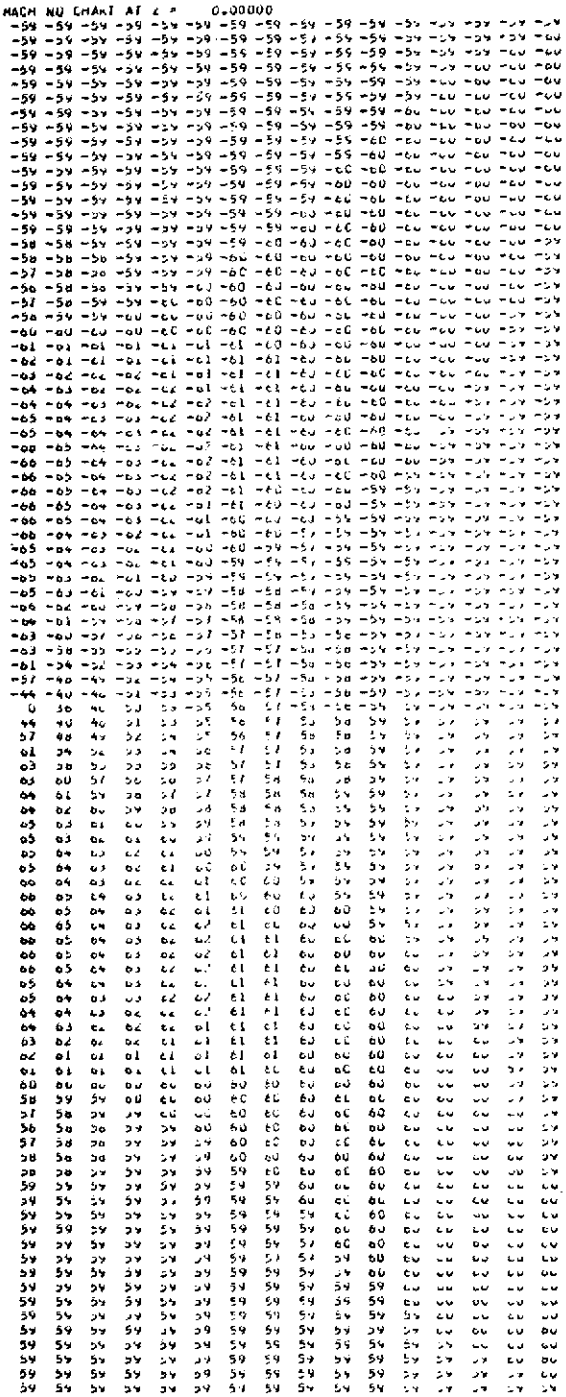

FIGURE 7.- TOTAL AERODYNAMIC COEFFICIENTS AND MACH CHART AT ROOT SECTION IN COMPUTATIONAL PLANE OF JAMESON PROGRAM (SEE APPENDIX FOR COMMENTS).

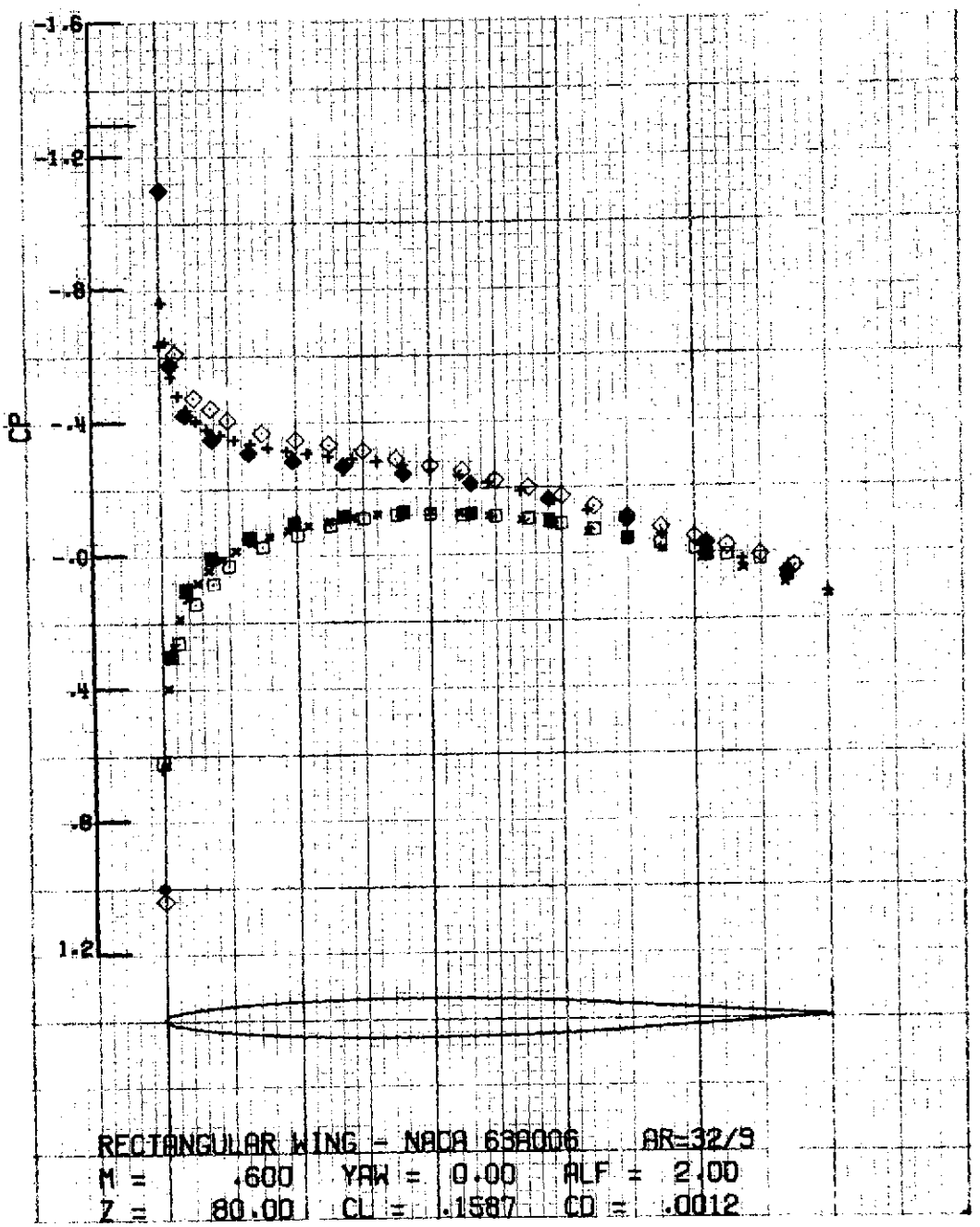


Figure 8.- Chordwise distribution of surface pressure coefficients at the 50 percent semispan location.

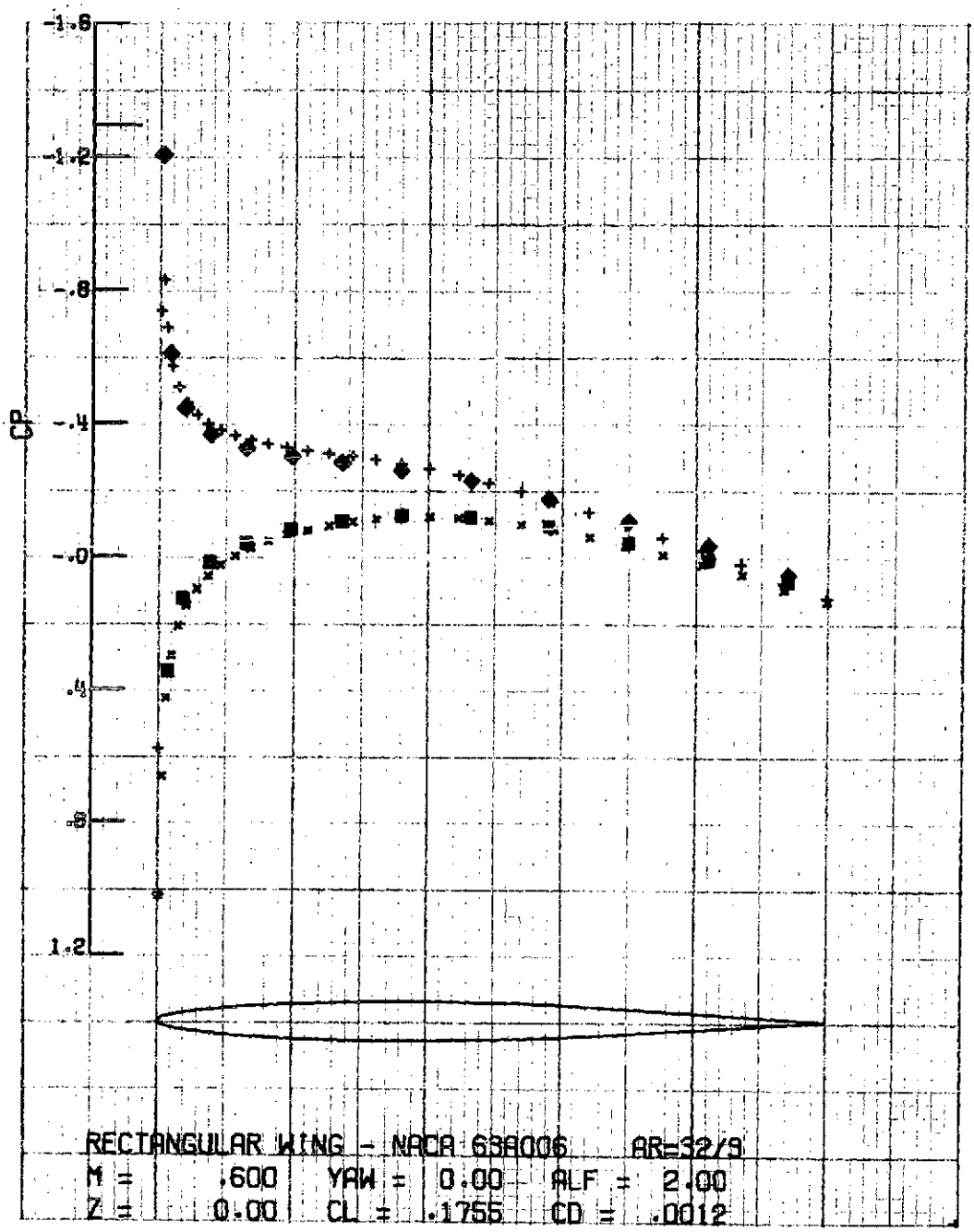


Figure 9.- Chordwise distribution of surface pressure coefficients at the root section.

RECTANGULAR WING - NACA 63A006 SECTION AR = 32/9

TOTAL WING COEFFICIENTS

| YAW | ANG OF ATTACK | MACH NO | CL | CD FORM | CM |
|---|---|---|---|---|---|
| 0.0000 | 2.0000 | .6000 | .1479 | .0012 | -.0344 |

| CD FRICTION | CD | L/D FORM | L/D |
|---|---|---|---|
| 0.0000 | .0012 | 124.1315 | 124.1315 |

MACH NO CHART AT Z = 0.00000

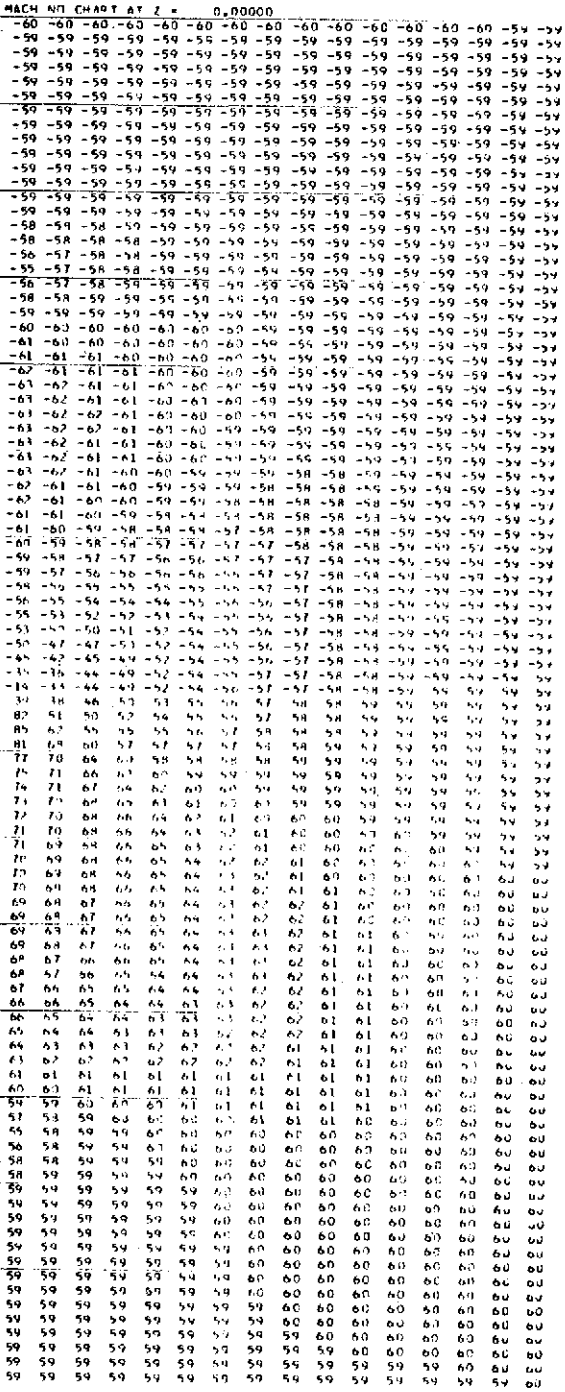

REPRODUCIBILITY OF THE ORIGINAL PAGE IS POOR

FIGURE 10.- TOTAL AERODYNAMIC COEFFICIENTS AND MACH CHART AT ROOT SECTION IN COMPUTATIONAL PLANE OF JAMESON PROGRAM (SEE APPENDIX FOR COMMENTS).

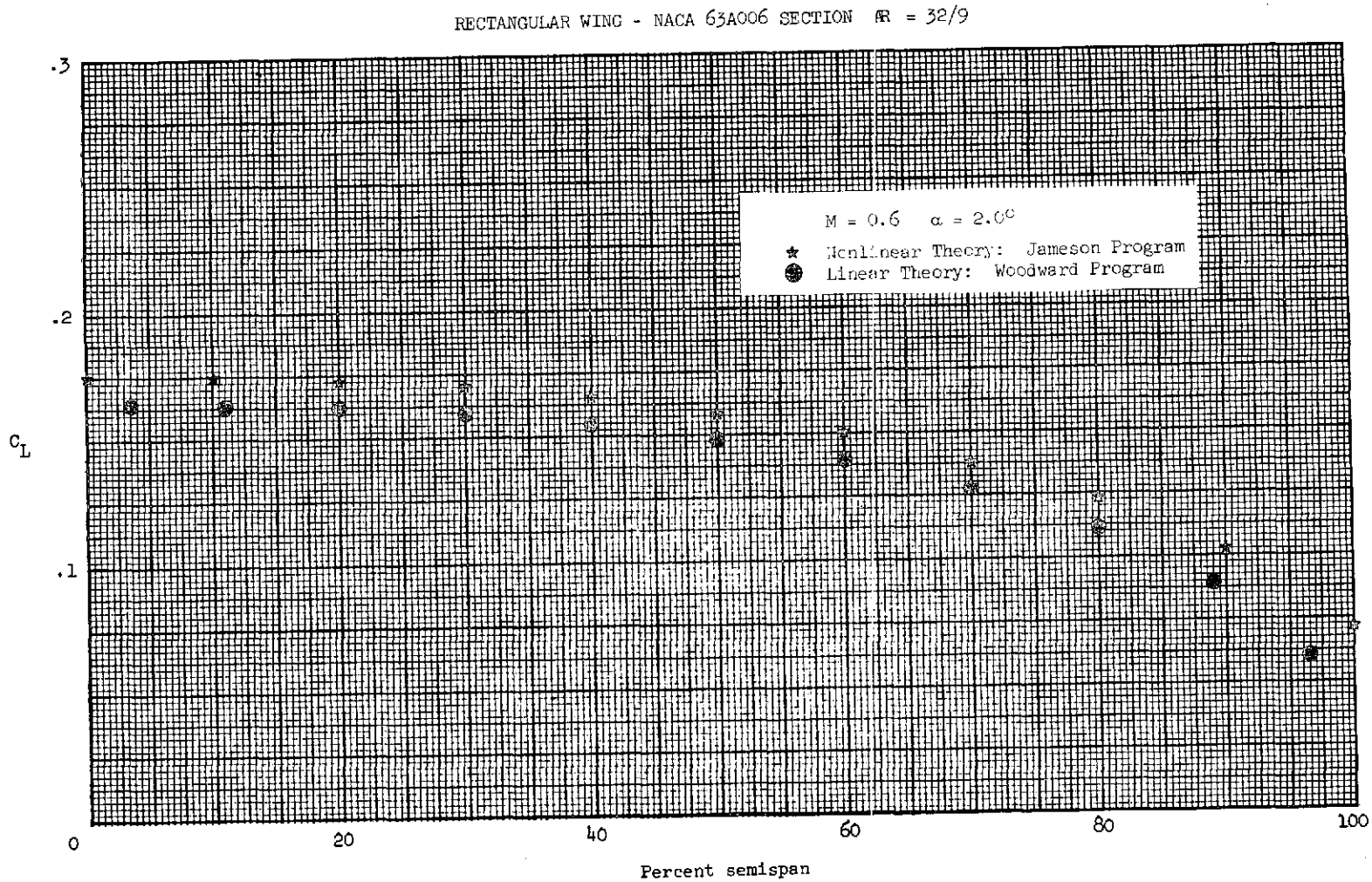


Figure 11.- Spanwise distribution of section lift coefficient.

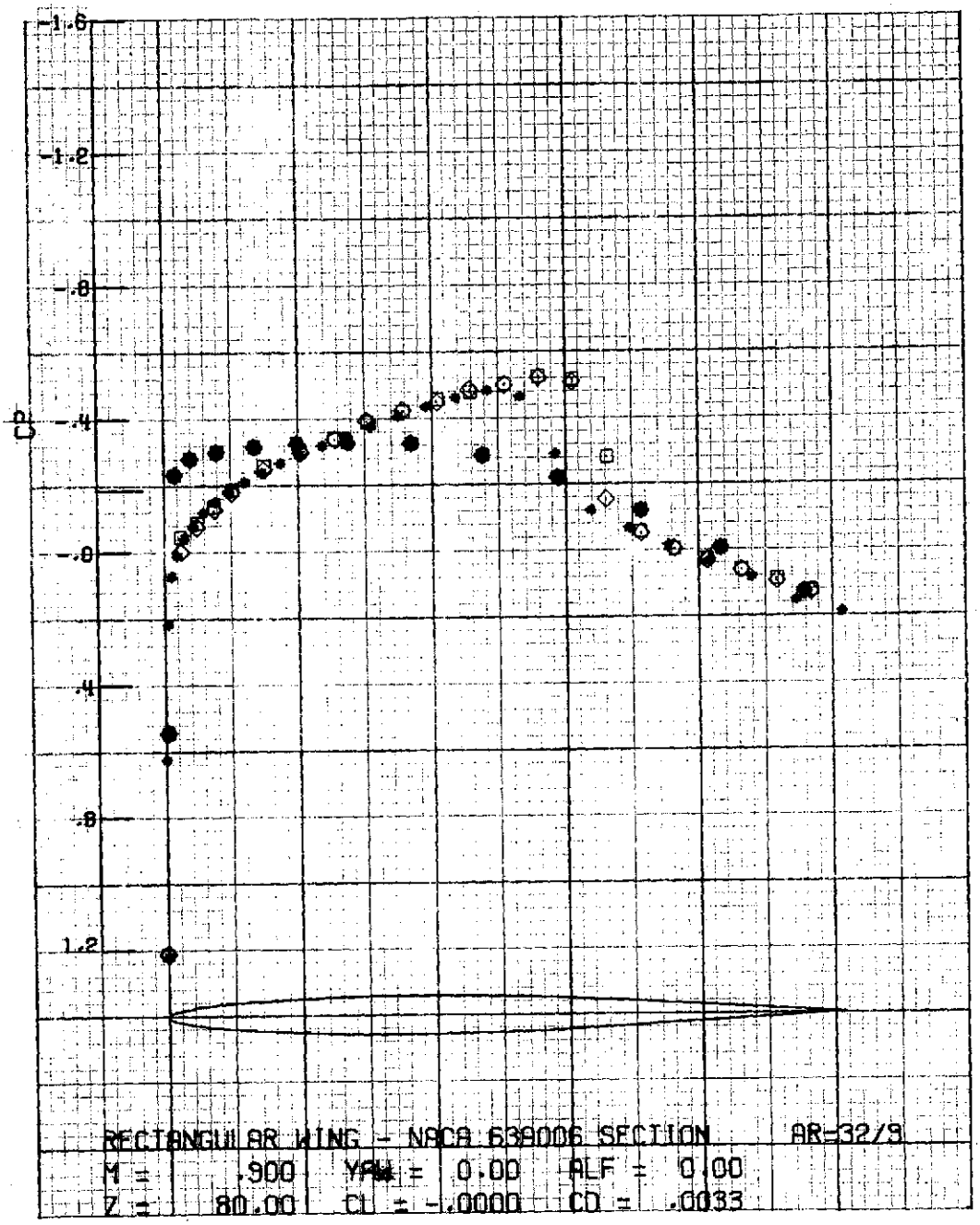


+ Upper surface
× Lower surface
} Nonlinear Theory: Jameson Program

◆ Upper surface
■ Lower surface
} Linear Theory: Woodward Program

◇ Upper surface
□ Lower surface
} Experiment: AEDC (136/6)
M = 0.900 $\alpha$ = -0.03°

Figure 12.- Chordwise distribution of surface pressure coefficients at the 50 percent semispan location.

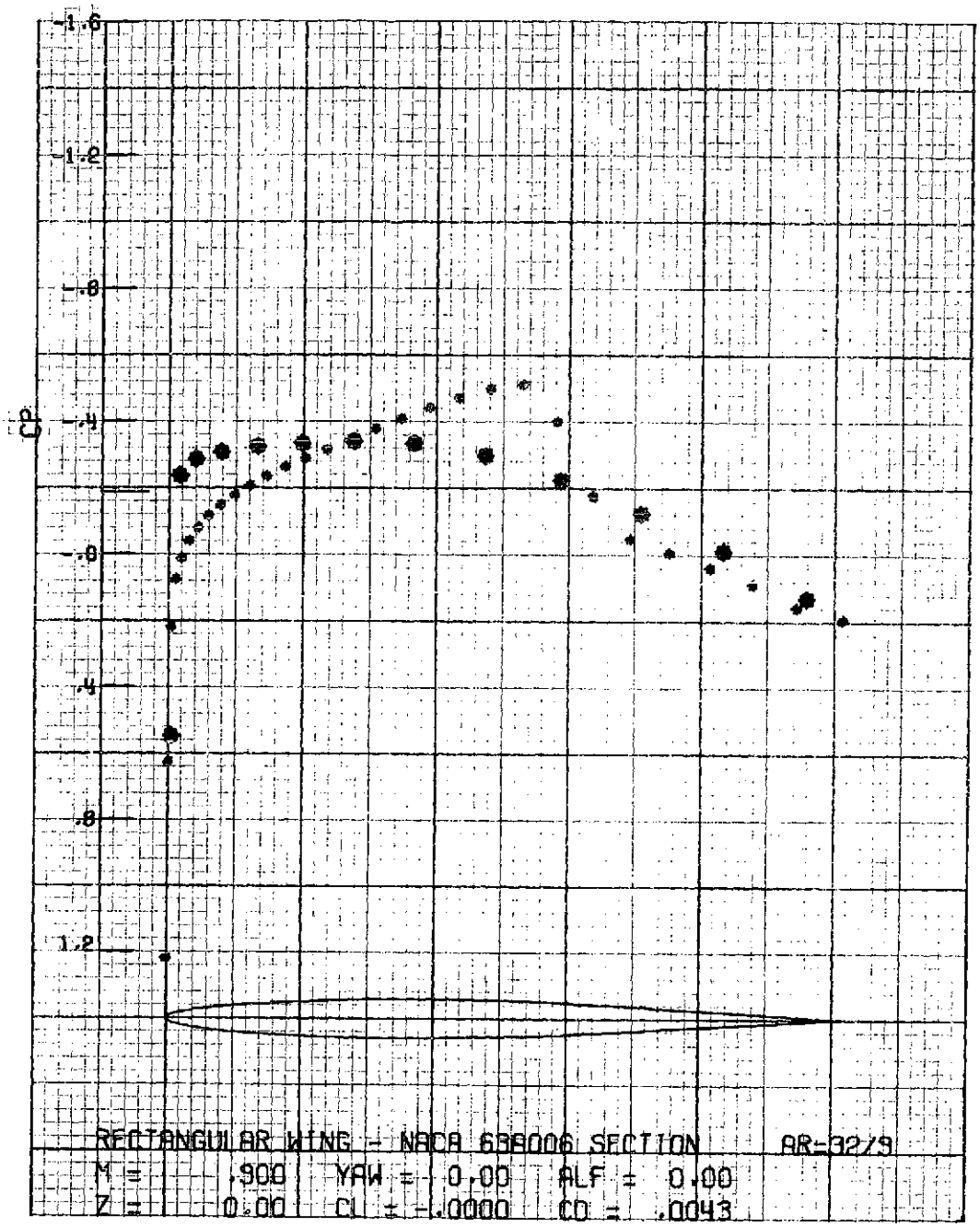


Figure 13.- Chordwise distribution of surface pressure coefficients at the root section.

RECTANGULAR WING - NACA 63A006 SECTION AR = 32/9

TOTAL WING COEFFICIENTS

| YAW | ANG OF ATTACK | MACH NO | CL | CD FORM | CM |
|---|---|---|---|---|---|
| 0.0000 | 0.0300 | .9000 | -.0000 | .0031 | -.0000 |

| CD FRICTION | CD | L/D FORM | L/D |
|---|---|---|---|
| 0.0000 | .0031 | -.0000 | -.0000 |

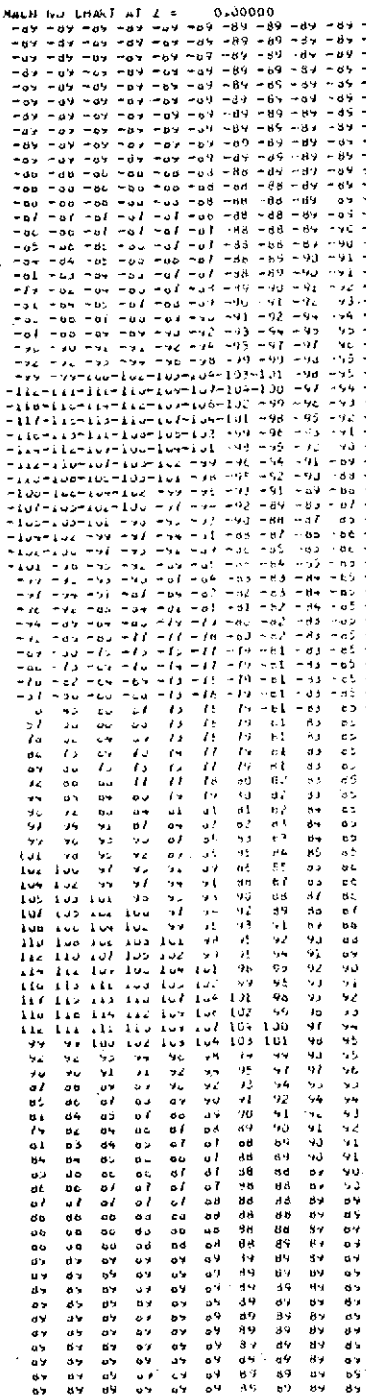


FIGURE 14.- TOTAL AERODYNAMIC COEFFICIENTS AND MACH CHART AT ROOT SECTION IN COMPUTATIONAL PLANE OF JAMESON PROGRAM (SEE APPENDIX FOR COMMENTS).

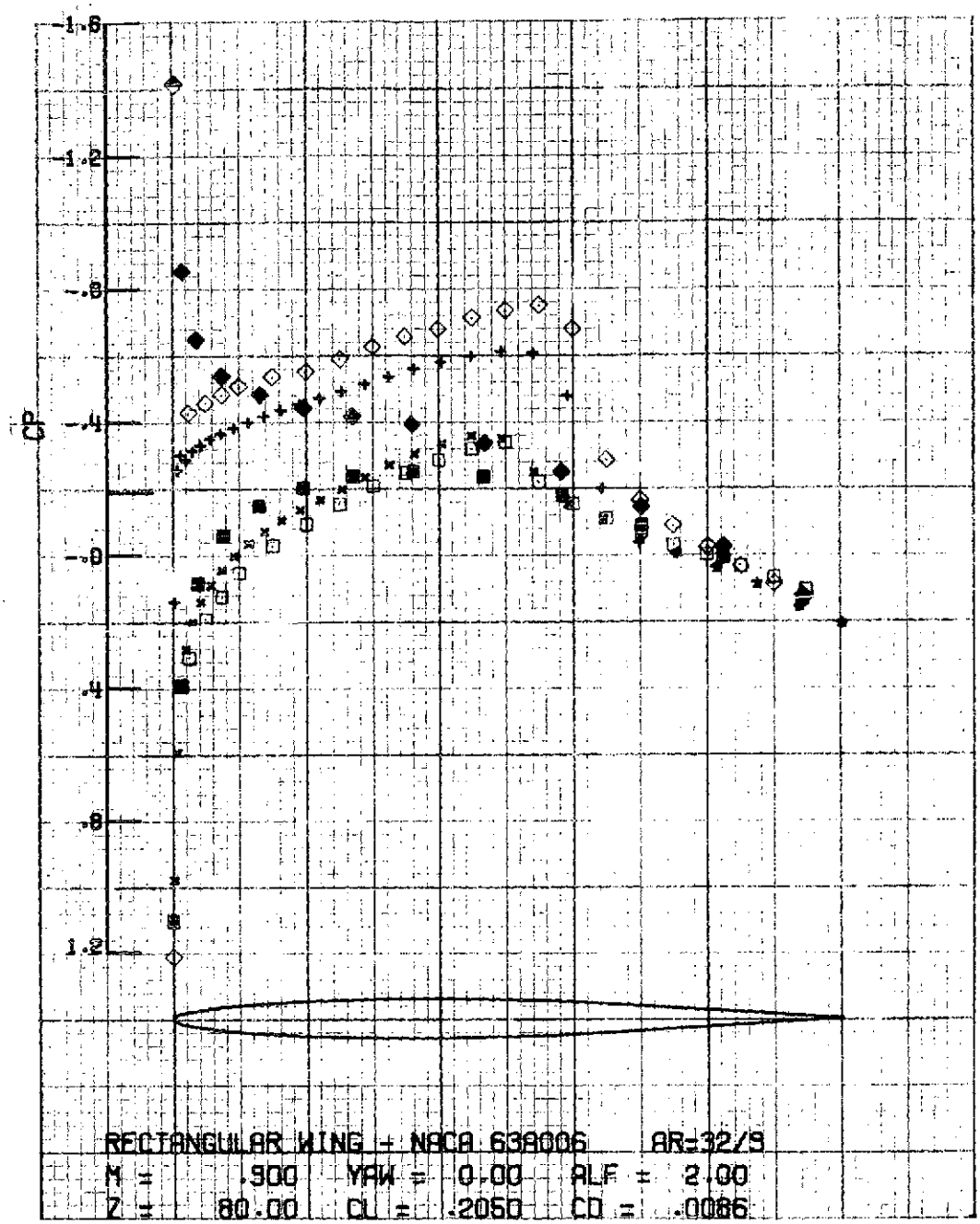


+ Upper surface
× Lower surface
} Nonlinear Theory: Jameson Program

◆ Upper surface
■ Lower surface
} Linear Theory: Woodward Program

◇ Upper surface
□ Lower surface
} Experiment: AEDC (136/8)
M = 0.896 $\alpha$ = 1.97°

Figure 15.- Chordwise distribution of surface pressure coefficients at the 50 percent semispan location.

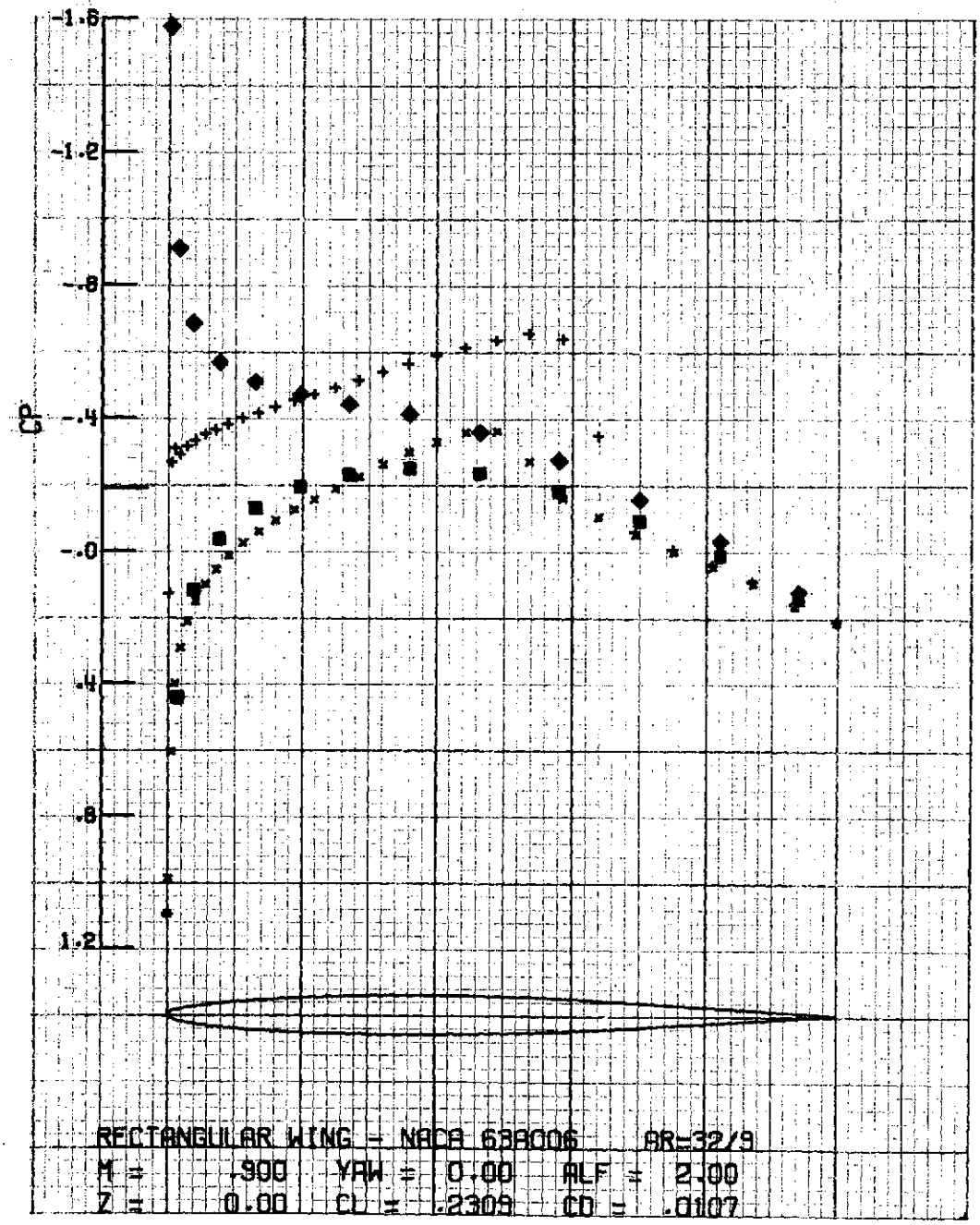


+ Upper surface
× Lower surface
} Nonlinear Theory: *Jameson Program*

◆ Upper surface
■ Lower surface
} Linear Theory: Woodward Program

Figure 16.- Chordwise distribution of surface pressure coefficients at the root section.

TOTAL WING COEFFICIENTS

| YAW | ANG OF ATTACK | MACH NO | CL | CD FUNC | CM |
|---|---|---|---|---|---|
| 0.0000 | 2.0000 | .9000 | .1914 | .0061 | -.0552 |

| CD FRICTION | CD | L/D FORM | L/D |
|---|---|---|---|
| 0.0000 | .0081 | 23.5374 | 23.5374 |

MACH NO CHART AT Z = 0.300000

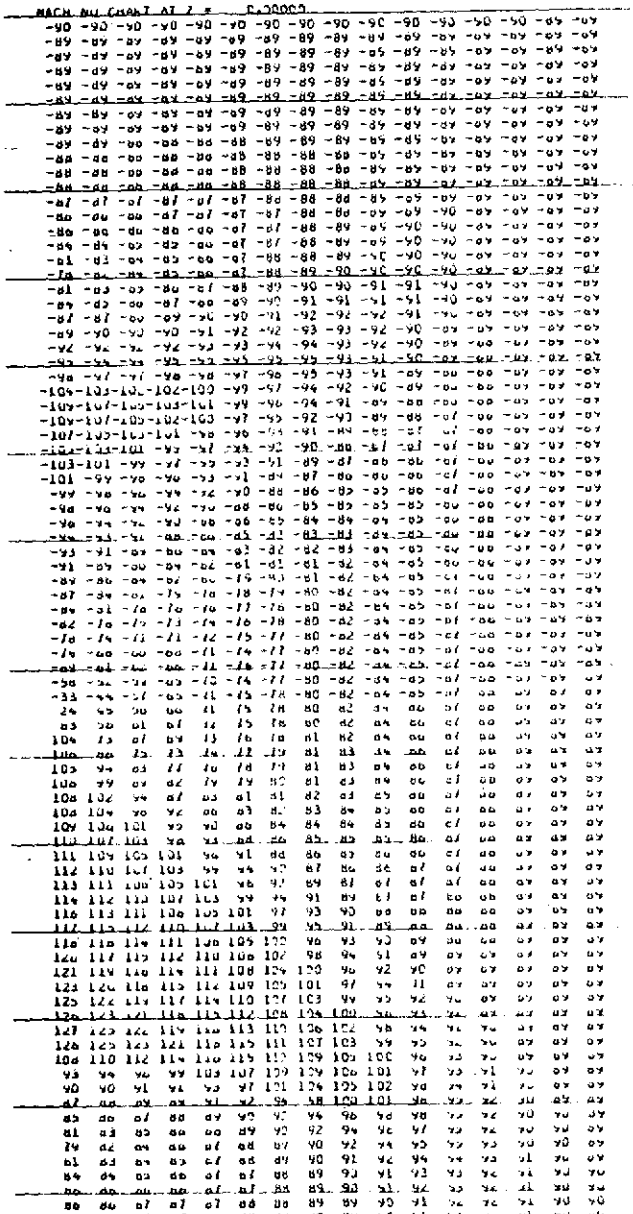

REPRODUCIBILITY OF THE ORIGINAL PAGE IS POOR

FIGURE 17.- TOTAL AERODYNAMIC COEFFICIENTS AND MACH CHART AT ROOT SECTION IN COMPUTATIONAL PLANE OF JAMESON PROGRAM (SEE APPENDIX FOR COMMENTS).

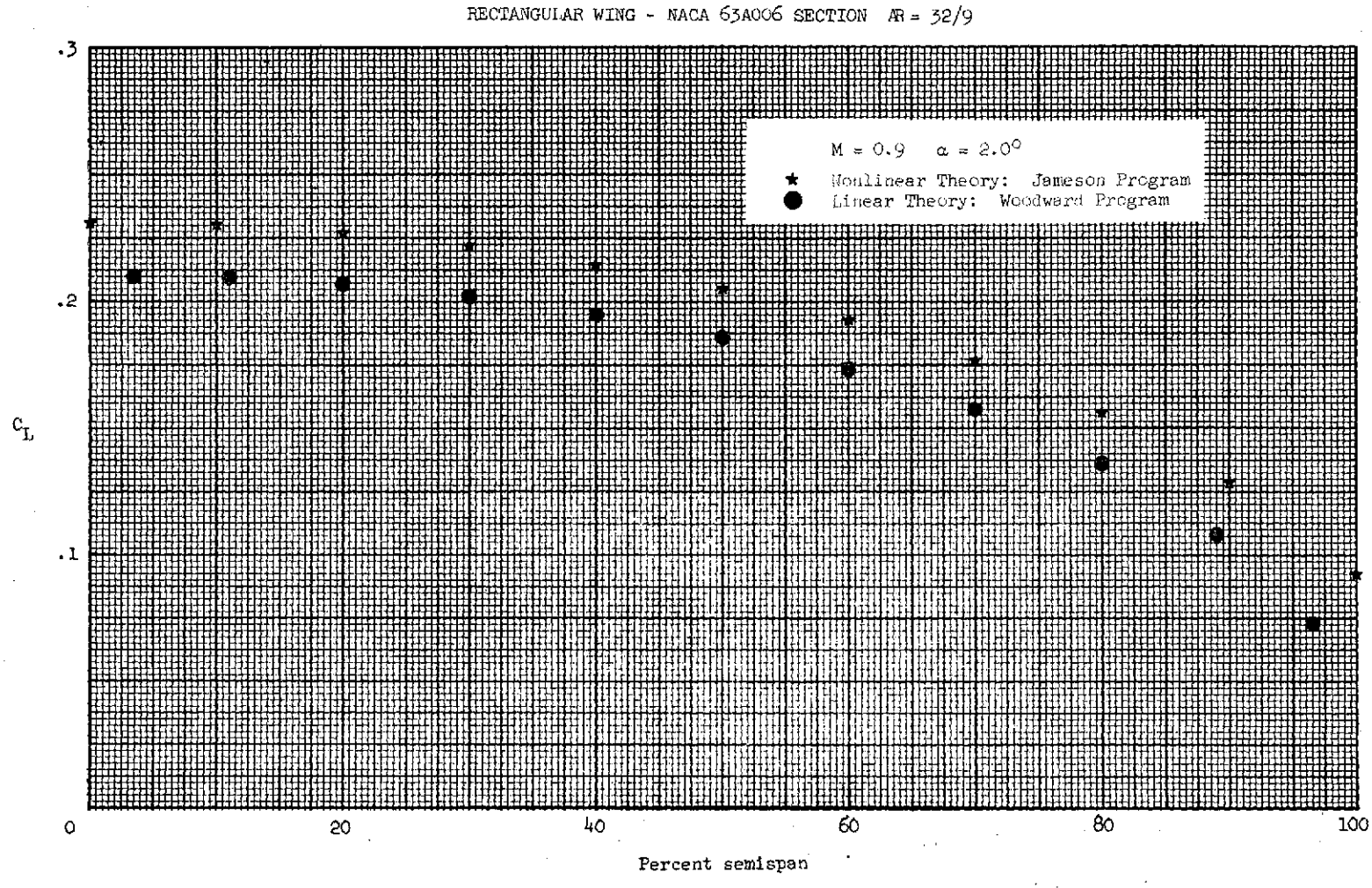


Figure 18.- Spanwise distribution of section lift coefficient.

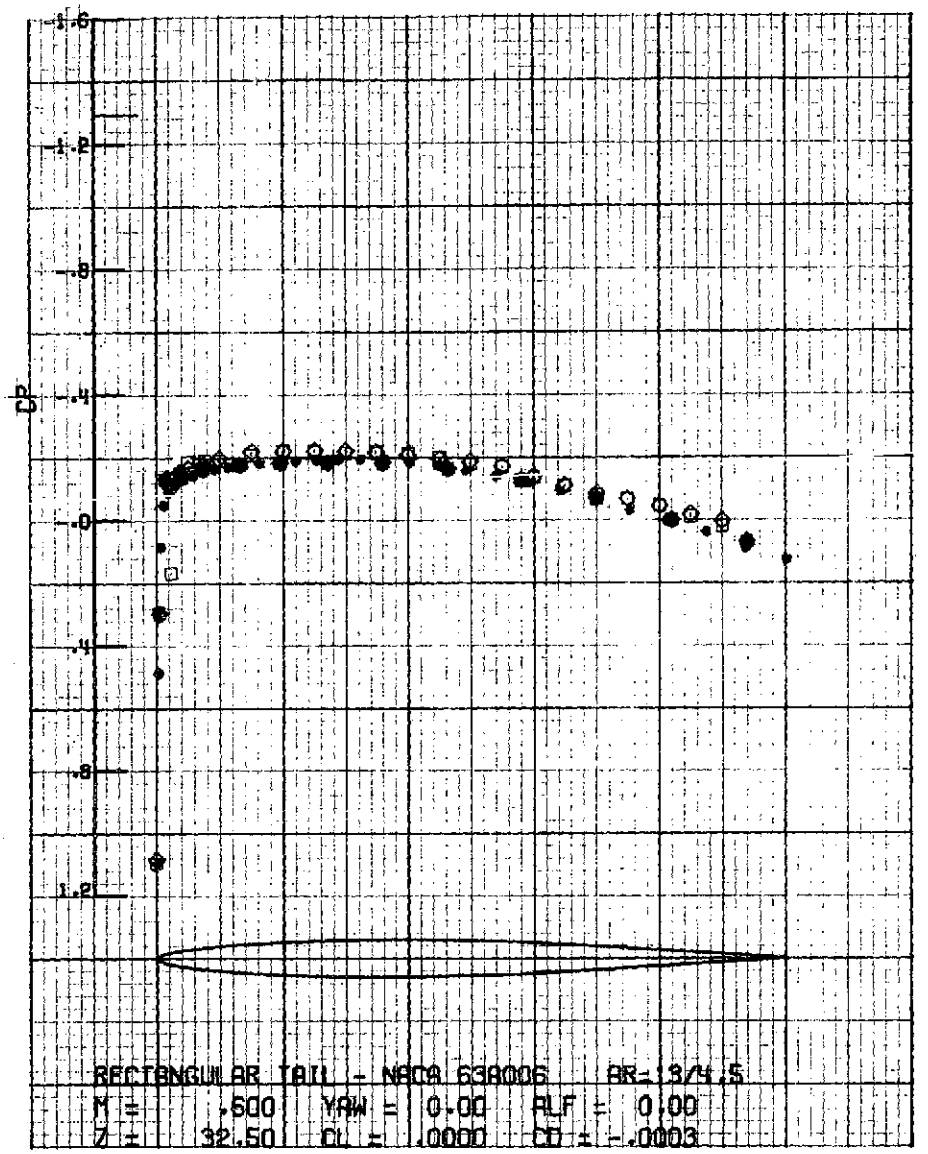


+ Upper surface
× Lower surface
} Nonlinear Theory: Jameson Program

◆ Upper surface
■ Lower surface
} Linear Theory: Woodward Program

◇ Upper surface
□ Lower surface
} Experiment: AEDC (175/4)
M = 0.599 $\alpha$ = -0.02°

Figure 19.- Chordwise distribution of surface pressure coefficients at the 50 percent semispan location.

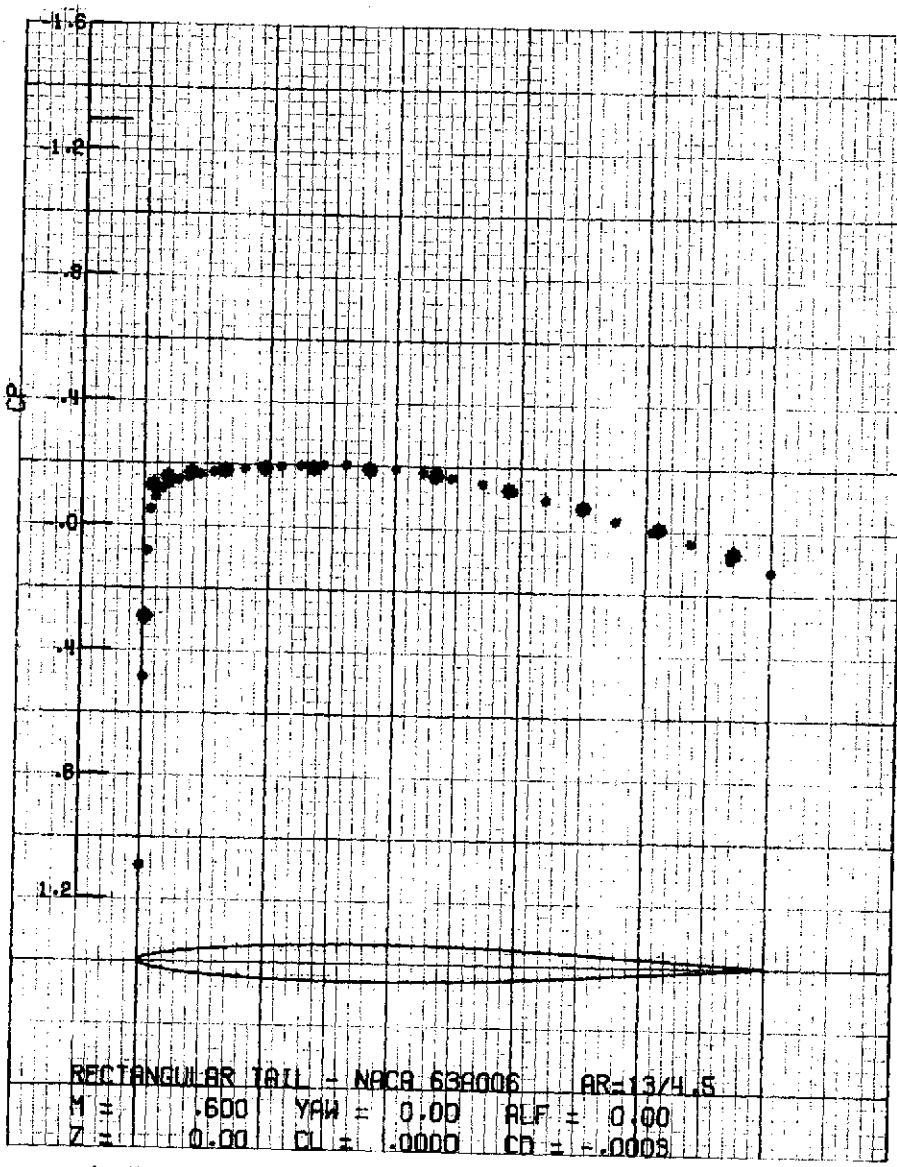


Figure 20.- Chordwise distribution of surface pressure coefficients at the root section.

RECTANGULAR TAIL - NACA 63A006 SECTION AR = 13/4.5

TOTAL TAIL COEFFICIENTS

| YAW | ANGLE OF ATTACK | MACH NO | CL | CD FORM | CM |
|---|---|---|---|---|---|
| 0.0000 | 0.0000 | .6000 | .0000 | -.0003 | -.0022 |

| CD FRICTION | CD | L/D FORM | L/D |
|---|---|---|---|
| .0001 | -.0001 | -.0000 | -.0000 |

MACH NO CHART AT Z = 0.000000

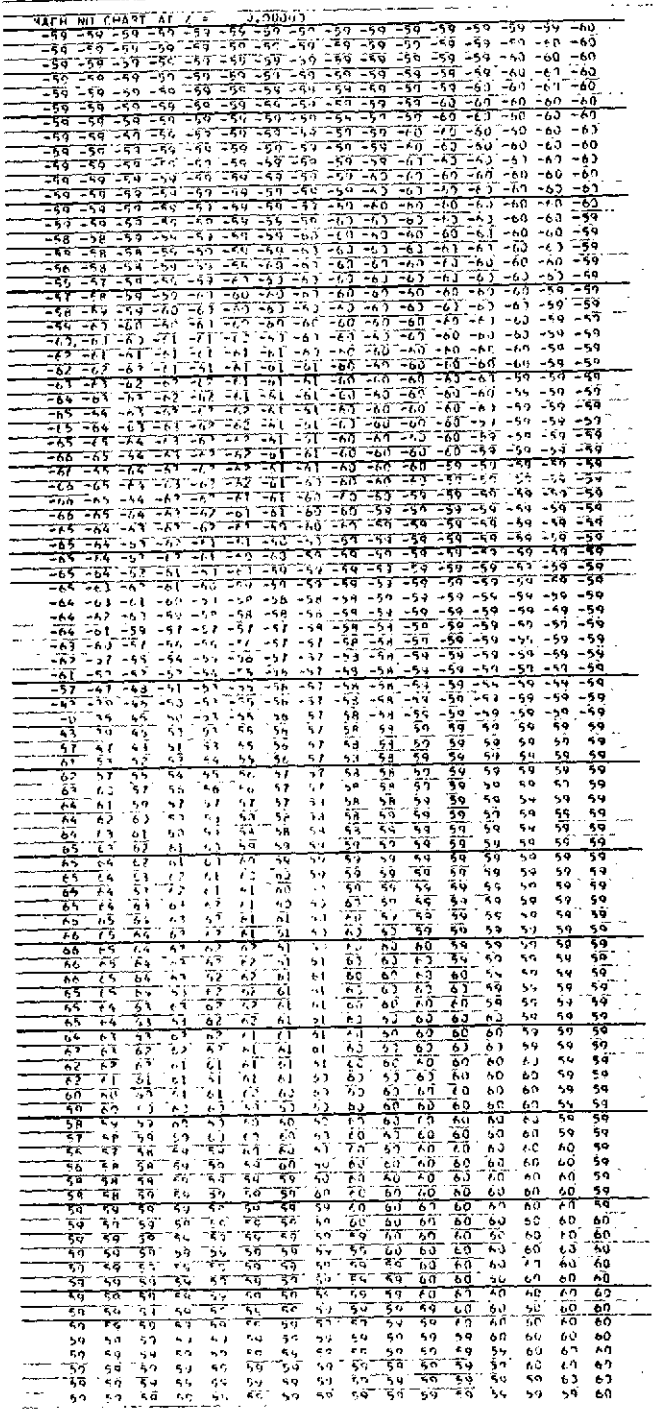

FIGURE 21.- TOTAL AERODYNAMIC COEFFICIENTS AND MACH CHART AT ROOT SECTION IN COMPUTATIONAL PLANE OF JAMESON PROGRAM (SEE APPENDIX FOR COMMENTS).

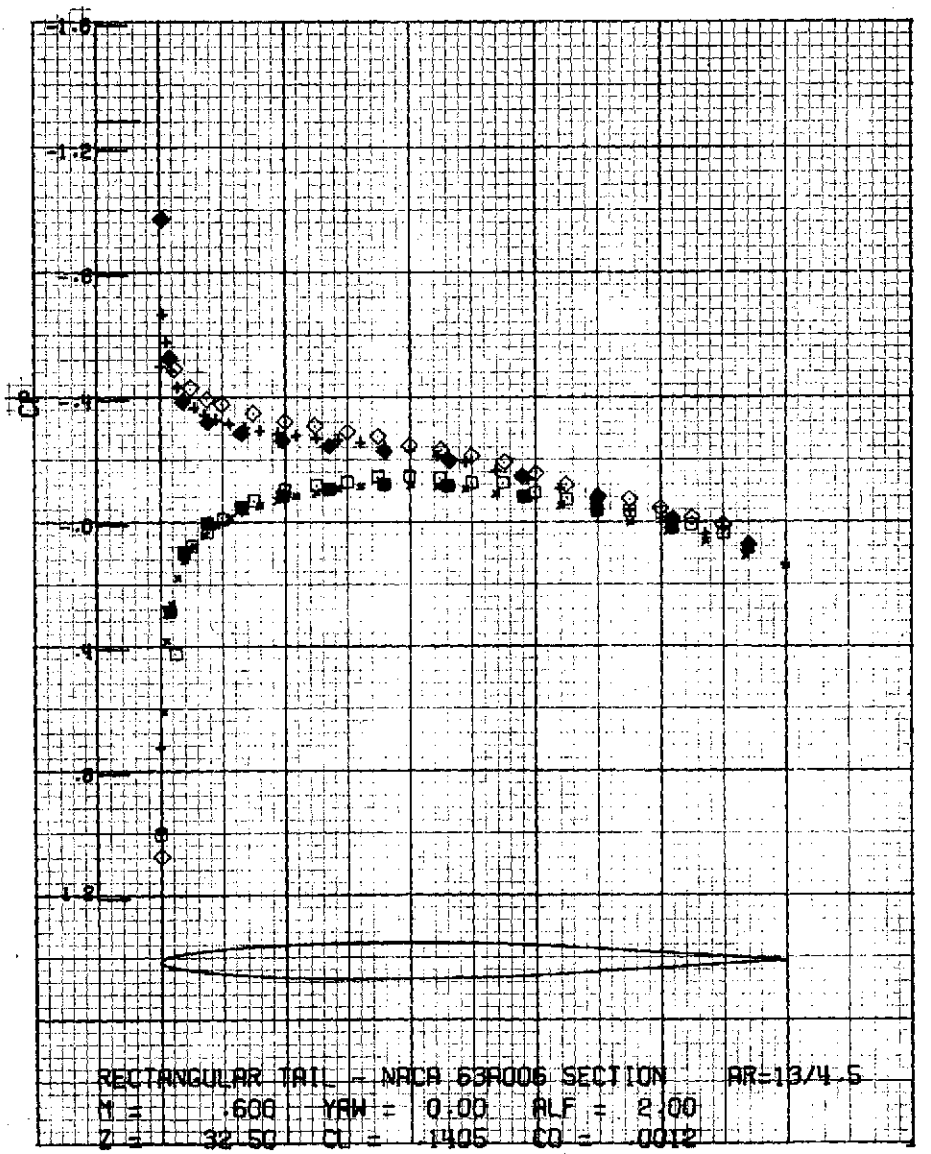


+ Upper surface
× Lower surface
} Nonlinear Theory: Jameson Program

◆ Upper surface
■ Lower surface
} Linear Theory: Woodward Program

◇ Upper surface
□ Lower surface
} Experiment: AEDC (175/5)
M = 0.600 $\alpha$ = 1.99°

Figure 22.- Chordwise distribution of surface pressure coefficients at the 50 percent semispan location.

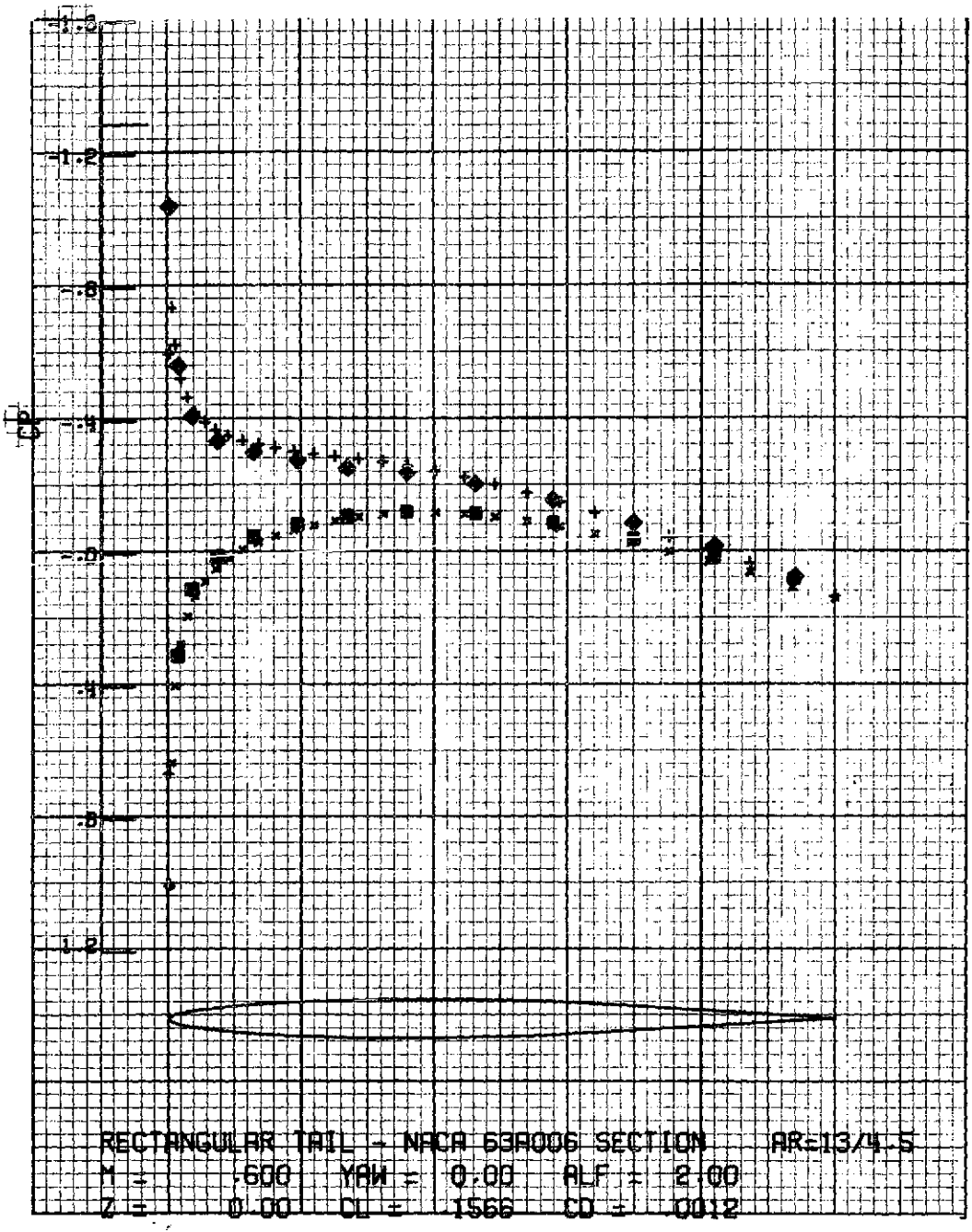


+ Upper surface
× Lower surface
} Nonlinear Theory: Jameson Program

◆ Upper surface
■ Lower surface
} Linear Theory: Woodward Program

Figure 23.- Chordwise distribution of surface pressure coefficients at the root section.

## RECTANGULAR TAIL - NACA 63A006 SECTION AR ≈ 13/4.5

```
TOTAL TAIL COEFFICIENTS

      YAW         ANG OF ATTACK      MACH NO          CL          CD FORM            CM
     0.0000          2.0000           .6000          .1309          .0012          -.0295

   CD FRICTION         CD           L/D FORM         L/D
     0.0000          .0012          107.7688       107.7589

MACH NO CHART AT Z =     0.00000
      -60 -60 -60 -60 -60 -60 -60 -60 -60 -60 -60 -60 -60 -60 -59 -59
      -59 -59 -59 -59 -59 -59 -59 -59 -59 -59 -60 -59 -59 -59 -59 -59
      -59 -59 -59 -59 -59 -59 -59 -59 -59 -59 -59 -59 -59 -59 -59 -59
      -59 -59 -59 -59 -59 -59 -59 -59 -59 -59 -59 -59 -59 -59 -59 -59
      -59 -59 -59 -59 -59 -59 -59 -59 -59 -59 -59 -59 -59 -59 -59 -59
      -59 -59 -59 -59 -59 -59 -59 -59 -59 -59 -59 -59 -59 -59 -59 -59
      -59 -59 -59 -59 -59 -59 -59 -59 -59 -59 -59 -59 -59 -59 -59 -59
      -59 -59 -59 -59 -59 -59 -59 -59 -59 -59 -59 -58 -59 -59 -59 -59
      -59 -59 -59 -59 -59 -59 -59 -59 -59 -59 -59 -59 -59 -59 -59 -59
      -59 -59 -59 -59 -59 -59 -59 -59 -59 -59 -59 -59 -59 -59 -59 -59
      -59 -59 -59 -59 -59 -59 -59 -59 -59 -59 -59 -59 -59 -59 -59 -59
      -59 -59 -59 -59 -59 -59 -59 -59 -59 -59 -59 -59 -59 -59 -59 -59
      -59 -59 -59 -59 -59 -59 -59 -59 -59 -59 -59 -59 -59 -59 -59 -59
      -59 -59 -59 -59 -59 -59 -59 -59 -59 -59 -59 -59 -59 -59 -59 -59
      -58 -58 -58 -59 -59 -59 -59 -59 -59 -59 -59 -59 -59 -59 -59 -59
      -58 -58 -59 -59 -59 -59 -59 -59 -59 -59 -59 -59 -59 -59 -59 -59
      -56 -57 -58 -58 -59 -59 -59 -59 -59 -59 -59 -59 -59 -59 -59 -59
      -55 -57 -58 -59 -59 -59 -59 -59 -59 -59 -59 -59 -59 -59 -59 -59
      -56 -58 -58 -59 -59 -59 -59 -59 -59 -59 -59 -59 -59 -59 -59 -59
      -58 -59 -59 -59 -59 -59 -59 -59 -59 -59 -59 -59 -59 -59 -59 -59
      -59 -59 -59 -59 -59 -60 -60 -59 -59 -59 -59 -59 -59 -59 -59 -59
      -60 -60 -60 -60 -60 -60 -60 -60 -59 -59 -59 -59 -59 -59 -59 -59
      -61 -60 -60 -60 -60 -60 -60 -60 -59 -59 -59 -59 -59 -59 -59 -59
      -61 -61 -61 -60 -60 -60 -60 -60 -59 -59 -59 -59 -59 -59 -59 -59
      -62 -62 -61 -61 -60 -60 -60 -60 -59 -59 -59 -59 -59 -59 -59 -59
      -63 -62 -61 -61 -61 -60 -60 -60 -59 -59 -59 -59 -59 -59 -59 -59
      -63 -62 -62 -61 -61 -60 -60 -60 -59 -59 -59 -59 -59 -59 -59 -59
      -63 -62 -62 -61 -61 -60 -60 -59 -59 -59 -59 -59 -59 -59 -59 -59
      -63 -63 -62 -61 -61 -60 -60 -60 -59 -59 -59 -59 -59 -59 -59 -59
      -63 -61 -62 -61 -60 -60 -59 -59 -59 -59 -59 -59 -59 -59 -59 -59
      -63 -62 -62 -61 -60 -60 -59 -59 -59 -59 -59 -59 -60 -59 -59 -59
      -63 -62 -61 -61 -60 -59 -59 -59 -59 -59 -59 -59 -59 -59 -59 -59
      -63 -62 -61 -60 -60 -59 -59 -59 -59 -58 -59 -59 -59 -59 -59 -59
      -62 -61 -61 -60 -59 -59 -58 -58 -58 -58 -59 -59 -59 -59 -59 -59
      -62 -61 -60 -59 -59 -58 -58 -58 -58 -58 -58 -59 -59 -59 -59 -59
      -61 -60 -59 -58 -59 -58 -58 -58 -58 -58 -58 -59 -59 -59 -59 -59
      -61 -60 -59 -58 -58 -57 -57 -57 -58 -58 -58 -59 -59 -59 -59 -59
      -60 -59 -58 -57 -57 -57 -57 -57 -58 -58 -58 -59 -59 -59 -59 -59
      -59 -58 -57 -56 -56 -56 -56 -57 -57 -58 -58 -59 -59 -59 -59 -59
      -58 -57 -56 -55 -55 -55 -56 -57 -57 -58 -58 -59 -59 -59 -59 -59
      -57 -55 -54 -54 -54 -55 -56 -57 -57 -58 -58 -59 -59 -59 -59 -59
      -55 -53 -52 -53 -53 -54 -55 -56 -57 -58 -58 -59 -59 -59 -59 -59
      -53 -51 -50 -51 -53 -54 -55 -56 -57 -58 -58 -59 -59 -59 -59 -59
      -50 -47 -48 -50 -52 -54 -55 -56 -57 -58 -58 -59 -59 -59 -59 -59
      -46 -43 -45 -49 -52 -54 -55 -56 -57 -58 -58 -59 -59 -59 -59 -59
      -37 -37 -44 -49 -52 -54 -55 -57 -57 -58 -58 -59 -59 -59 -59  59
      -36 -33 -44 -49 -52 -54 -56 -57 -57 -58 -58 -59  59  59  59  59
       36  37  46  50  53  45  56  57  58  58  59  59  59  59  59  59
       78  49  49  52  54  55  56  57  58  58  59  59  59  59  59  59
       82  61  55  56  55  56  57  57  58  58  59  59  59  59  59  59
       79  67  59  57  57  57  57  58  58  59  59  59  59  59  59  59
       76  69  63  59  58  58  58  58  58  59  59  59  59  59  59  59
       74  70  65  62  60  59  59  59  59  59  59  59  59  59  59  59
       73  70  66  63  61  60  59  59  59  59  59  59  59  59  59  59
       72  69  67  64  62  61  60  60  59  59  59  59  59  59  59  59
       71  69  67  65  63  62  61  60  60  59  59  59  59  59  59  59
       71  69  67  66  64  62  61  60  60  60  60  59  59  59  59  59
       70  69  67  65  64  63  62  61  60  60  60  60  59  59  59  59
       70  69  67  66  65  63  62  61  61  60  60  60  60  59  59  59
       70  68  67  66  65  64  62  62  61  60  60  60  60  60  59  59
       69  68  67  66  65  64  63  62  61  60  60  60  60  60  60  60
       69  69  67  66  65  64  63  62  61  61  60  60  60  60  60  60
       69  69  67  66  65  64  63  62  61  61  60  60  60  60  60  60
       68  67  67  66  65  64  63  62  62  61  60  60  60  60  60  60
       68  67  66  65  65  64  63  62  62  61  60  60  60  60  60  60
       68  67  66  65  64  64  63  62  62  61  61  60  60  60  60  60
       67  66  66  65  64  64  63  62  62  61  61  60  60  60  60  60
       67  66  65  64  64  63  63  62  62  61  61  60  60  60  60  60
       66  65  65  64  64  63  63  62  62  61  61  60  60  60  60  60
       65  65  64  64  63  63  62  62  61  61  61  60  60  60  60  60
       64  64  63  63  63  62  62  62  61  61  61  60  60  60  60  60
       63  63  63  62  62  62  62  62  61  61  61  60  60  60  60  60
       62  62  62  62  62  62  61  61  61  61  61  60  60  60  60  60
       61  61  61  61  61  61  61  61  61  61  60  60  60  60  60  60
       60  60  60  61  61  61  61  61  61  61  60  60  60  60  60  60
       59  59  60  60  60  61  61  61  61  61  60  60  60  60  60  60
       57  59  59  60  60  60  60  60  60  60  60  60  60  60  60  60
       55  58  59  59  60  60  60  60  60  60  60  60  60  60  60  60
       56  58  58  59  59  60  60  60  60  60  60  60  60  60  60  60
       58  58  59  59  59  60  60  60  60  60  60  60  60  60  60  60
       58  58  59  59  59  59  60  60  60  60  60  60  60  60  60  60
       59  59  59  59  59  59  60  60  60  60  60  60  60  60  60  60
       59  59  59  59  59  59  60  60  60  60  60  60  60  60  60  60
       59  59  59  59  59  59  59  60  60  60  60  60  60  60  60  60
       59  59  59  59  59  59  59  60  60  60  60  60  60  60  60  60
       59  59  59  59  59  59  59  60  60  60  60  60  60  60  60  60
       59  59  59  59  59  59  59  59  60  60  60  60  60  60  60  60
       59  59  59  59  59  59  59  59  60  60  60  60  60  60  60  60
       59  59  59  59  59  59  59  59  60  60  60  60  60  60  60  60
       59  59  59  59  59  59  59  59  59  60  60  60  60  60  60  60
       59  59  59  59  59  59  59  59  59  59  60  60  60  60  60  60
       59  59  59  59  59  59  59  59  59  59  59  60  60  60  60  60
       59  59  59  59  59  59  59  59  59  59  59  59  59  59  60  60
       59  59  59  59  59  59  59  59  59  59  59  59  59  59  59  60
```

REPRODUCIBILITY OF THE ORIGINAL PAGE IS POOR

FIGURE 24.- TOTAL AERODYNAMIC COEFFICIENTS AND MACH CHART AT ROOT SECTION IN COMPUTATIONAL PLANE OF JAMESON PROGRAM (SEE APPENDIX FOR COMMENTS).

RECTANGULAR TAIL - NACA 63A006 SECTION AR = 13/4.5

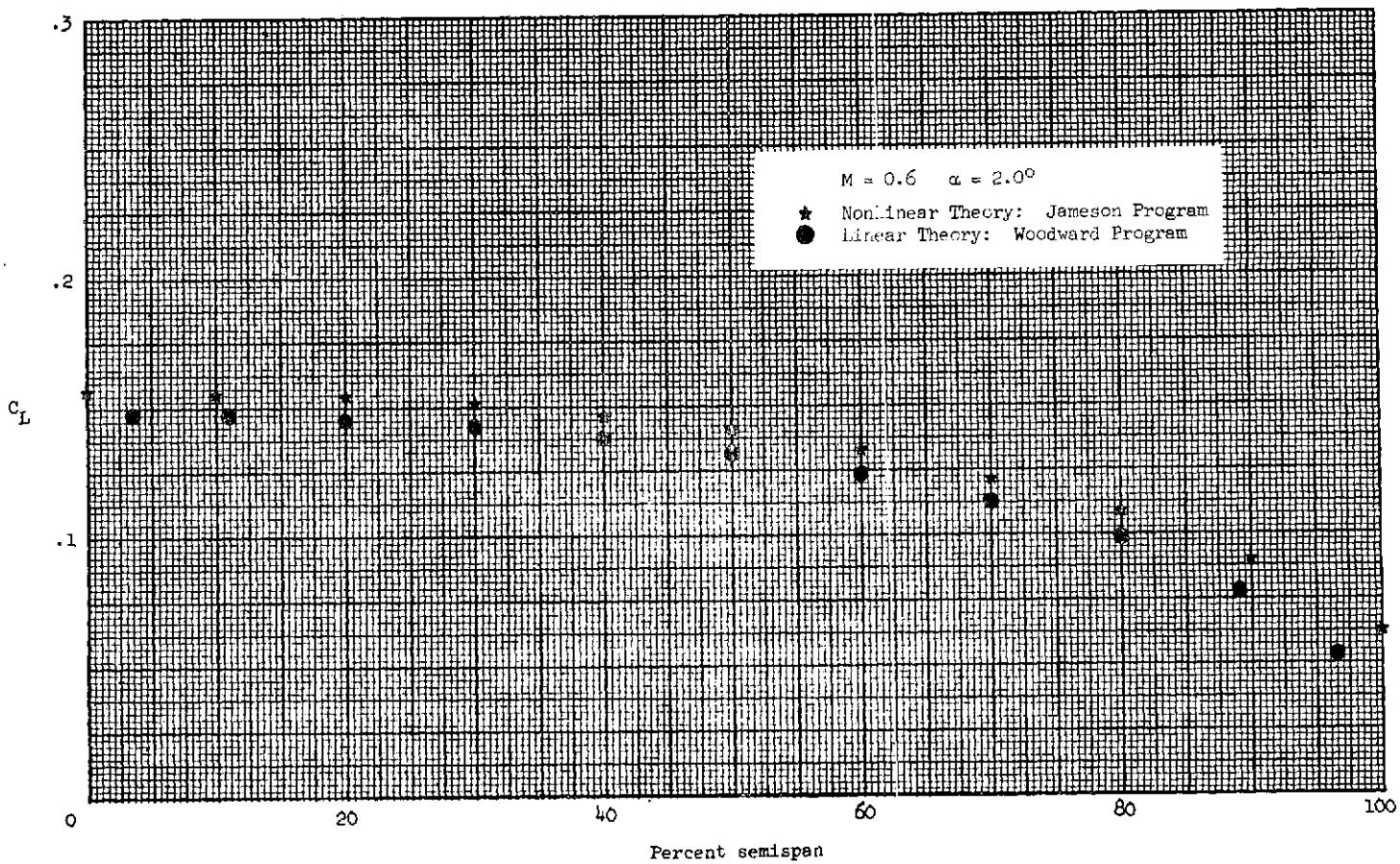


Figure 25.- Spanwise distribution of section lift coefficient.

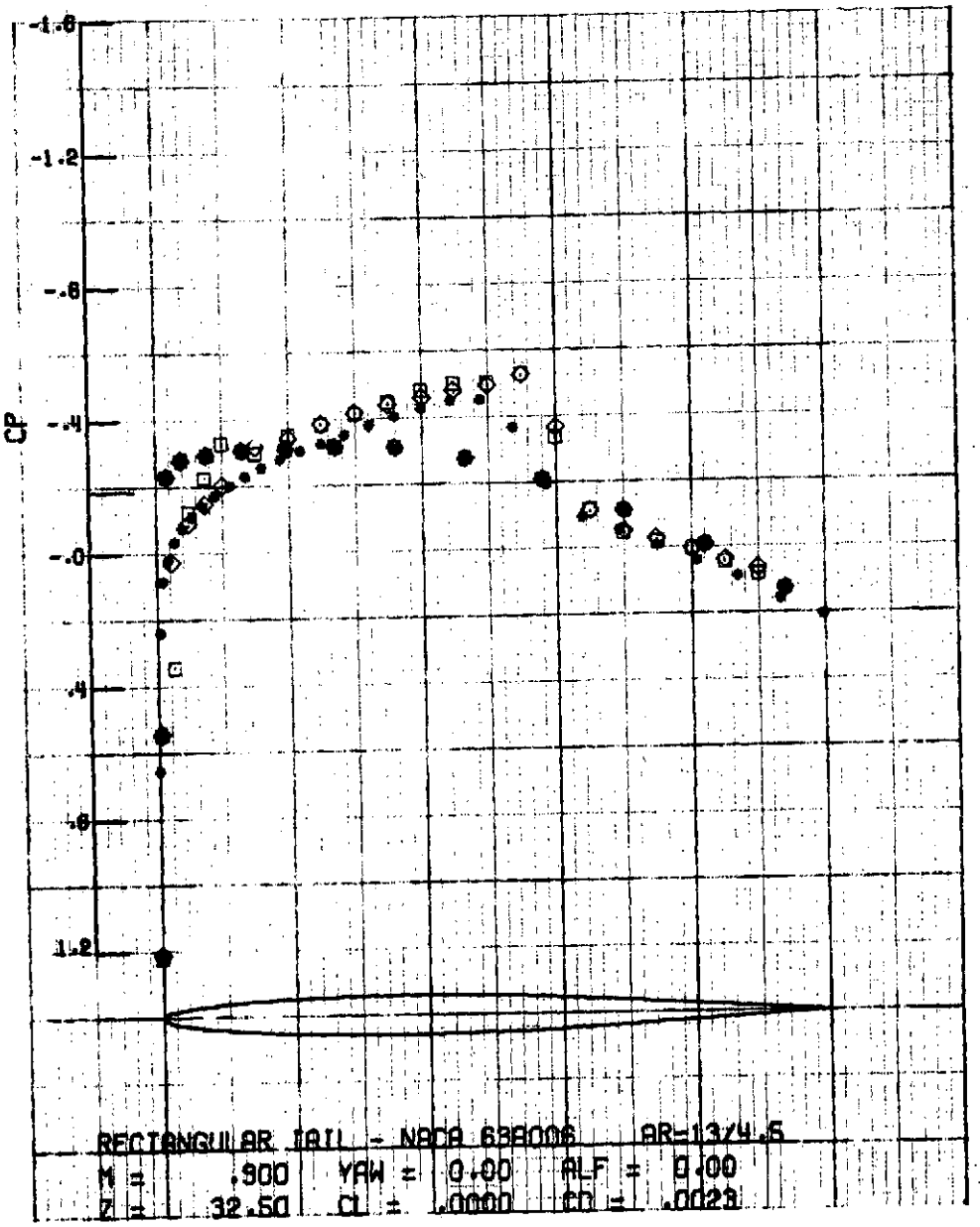


Figure 26.- Chordwise distribution of surface pressure coefficients at the 50 percent semispan location.

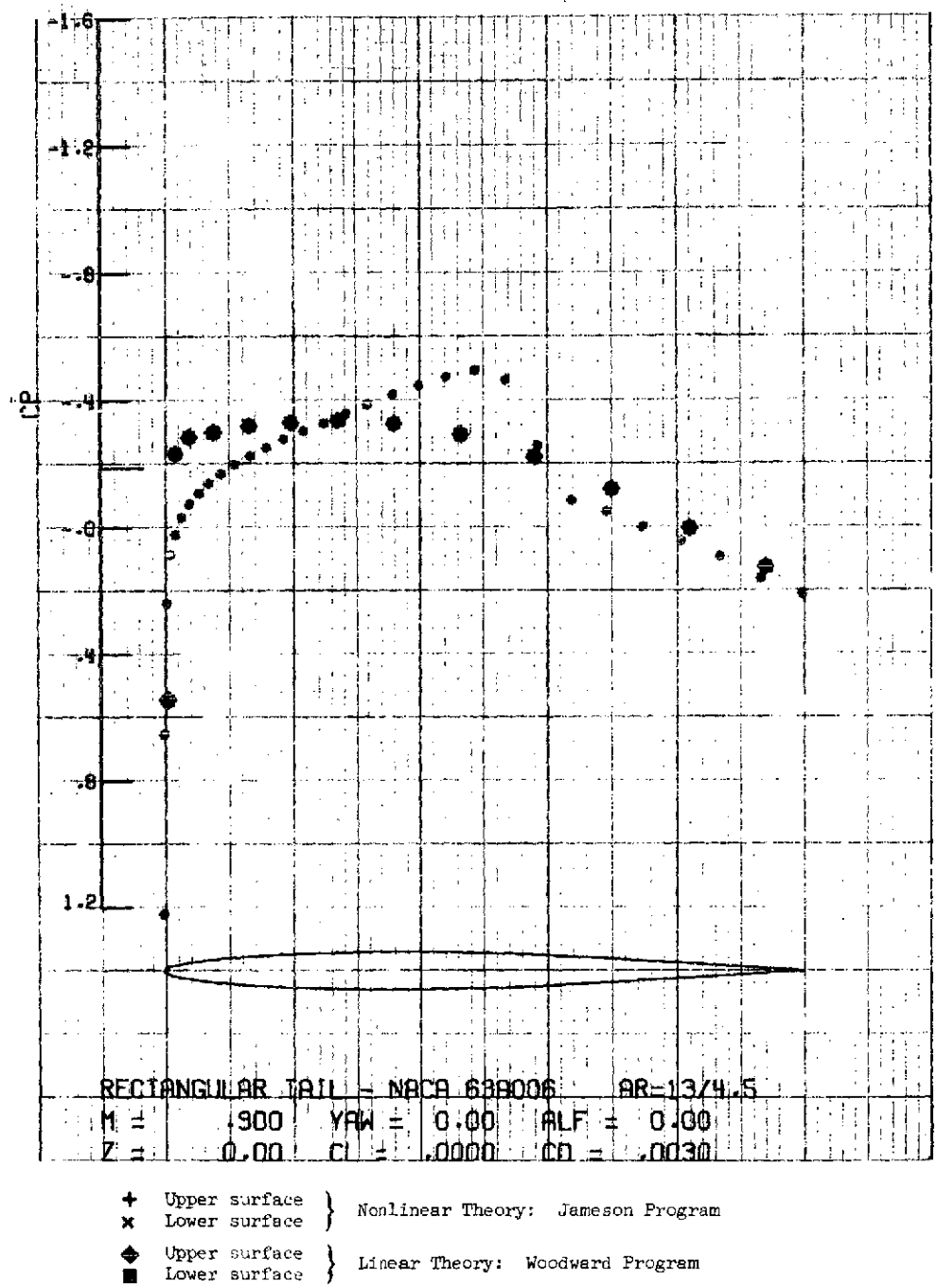


Figure 27.- Chordwise distribution of surface pressure coefficients at the root section.

TOTAL TAIL COEFFICIENTS

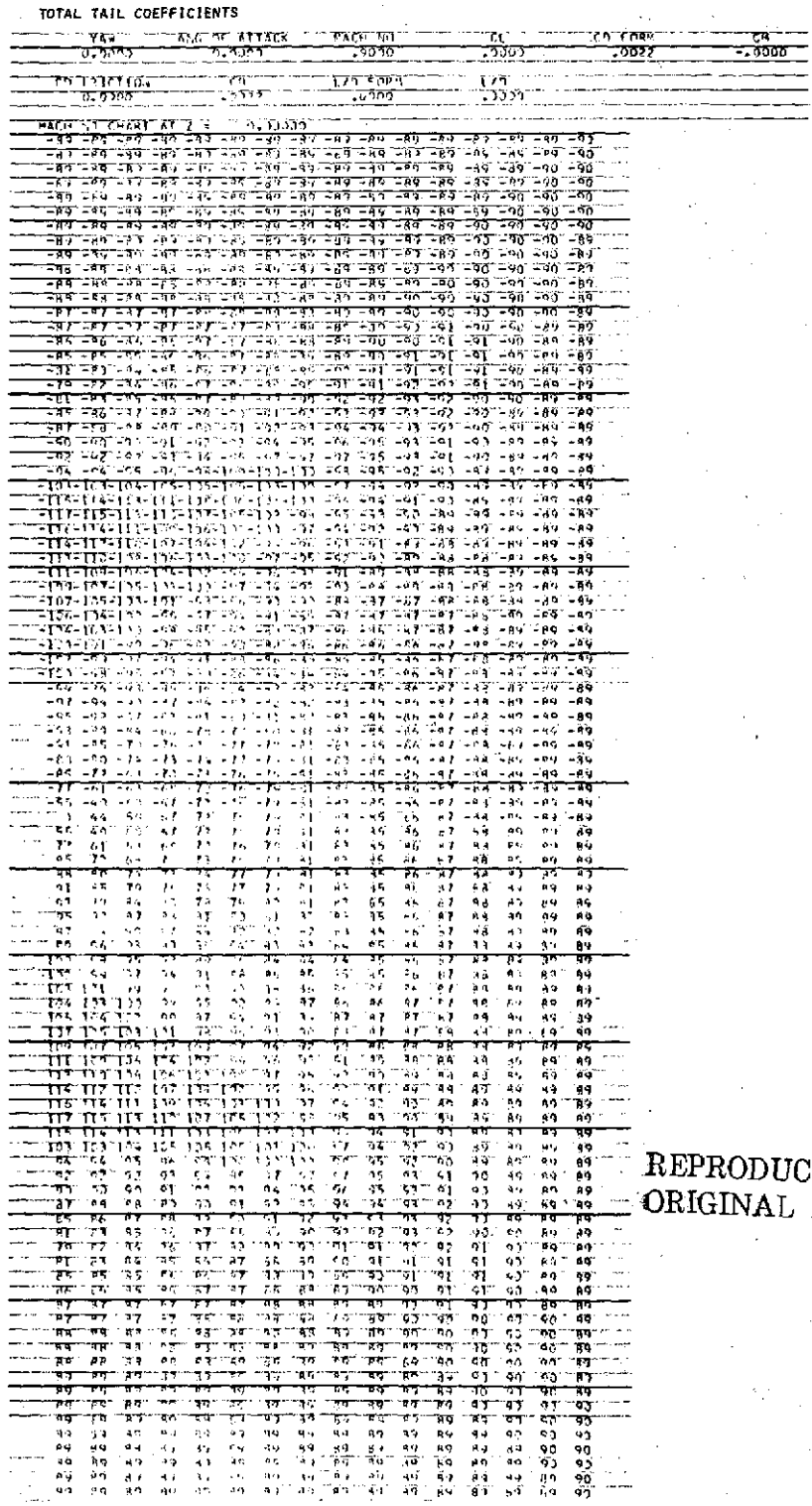



FIGURE 28.- TOTAL AERODYNAMIC COEFFICIENTS AND MACH CHART AT ROOT SECTION IN COMPUTATIONAL PLANE OF JAMESON PROGRAM (SEE APPENDIX FOR COMMENTS).

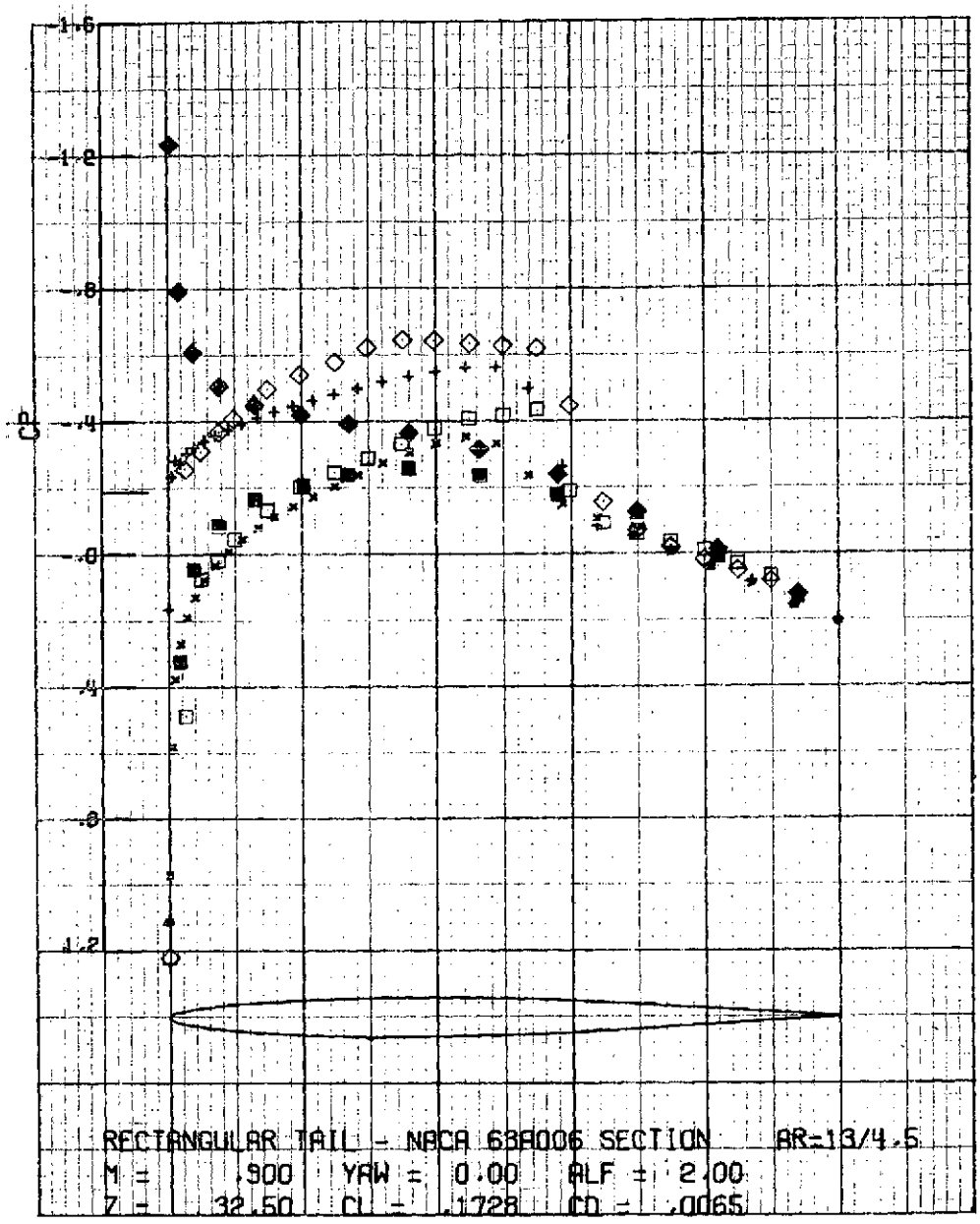


+ Upper surface
× Lower surface
} Nonlinear Theory: Jameson Program

◆ Upper surface
■ Lower surface
} Linear Theory: Woodward Program

◇ Upper surface
□ Lower surface
} Experiment: AEDC (167/7)
M = 0.895 $\alpha$ = 1.91°

Figure 29.- Chordwise distribution of surface pressure coefficients at the 50 percent semispan location.

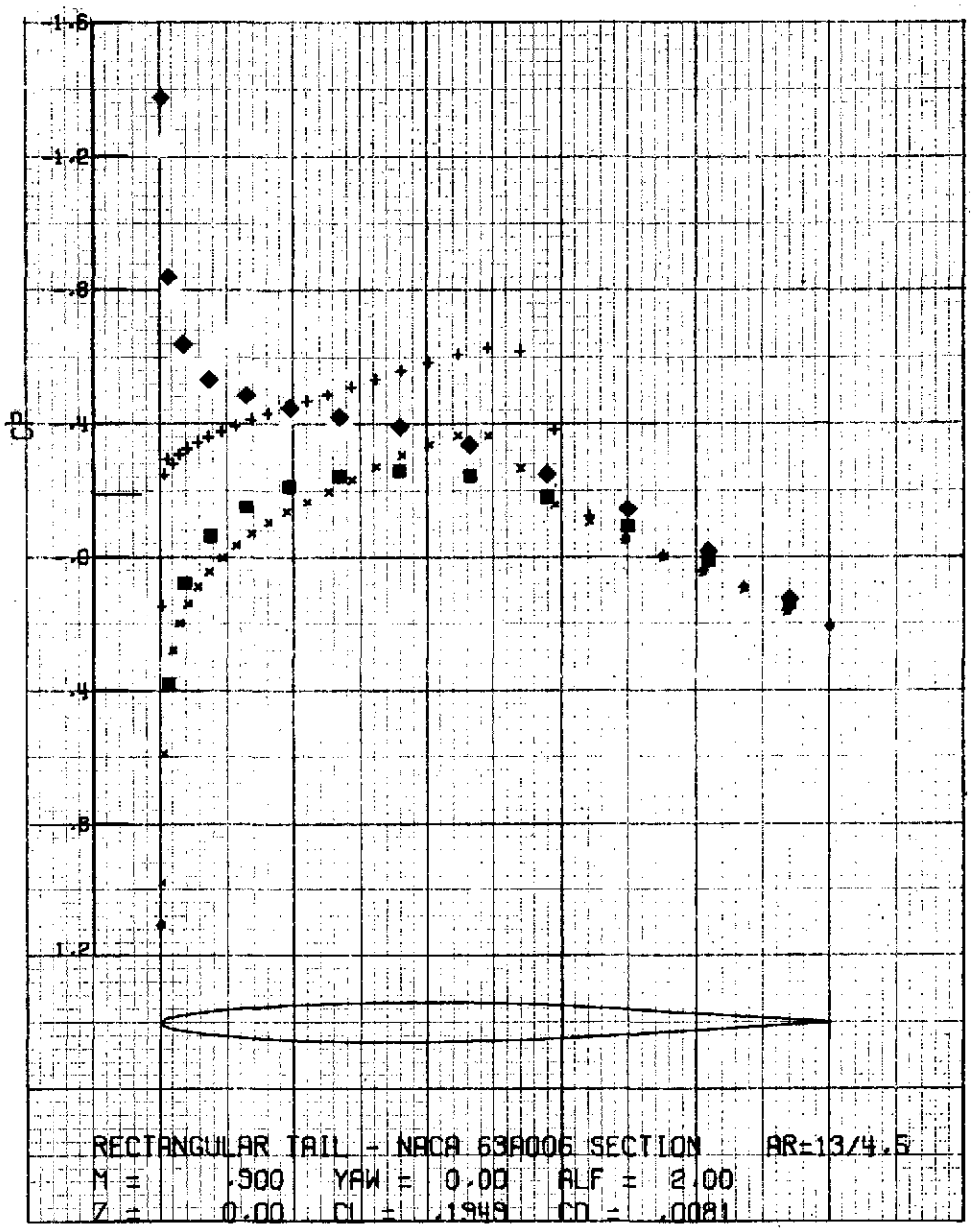


+ Upper surface
× Lower surface
} Nonlinear Theory: Jameson Program

◆ Upper surface
■ Lower surface
} Linear Theory: Woodward Program

Figure 30.- Chordwise distribution of surface pressure coefficients at the root section.

RECTANGULAR TAIL - NACA 63A006 SECTION AR = 13/4.5

TOTAL TAIL COEFFICIENTS

| YAW | ANG OF ATTACK | MACH NO | CL | CD FORM | CM |
|---|---|---|---|---|---|
| 0.0000 | 2.0000 | .9000 | .1614 | .0062 | -.0409 |

| CD FRICTION | CD | L/D FORM | L/D |
|---|---|---|---|
| 0.0000 | .0062 | 25.9257 | 25.9257 |

MACH NO CHART AT Z = 0.00000

| | | | | | | | | | | | | | | | |
|---|---|---|---|---|---|---|---|---|---|---|---|---|---|---|---|
| -90 | -90 | -90 | -90 | -90 | -90 | -90 | -90 | -90 | -90 | -90 | -90 | -90 | -90 | -89 | -89 |
| -89 | -89 | -89 | -89 | -89 | -89 | -89 | -89 | -89 | -89 | -90 | -89 | -89 | -89 | -89 | -89 |
| -89 | -89 | -89 | -89 | -89 | -89 | -89 | -89 | -89 | -89 | -89 | -89 | -89 | -89 | -89 | -89 |
| -89 | -89 | -89 | -89 | -89 | -89 | -89 | -89 | -89 | -89 | -89 | -89 | -89 | -89 | -89 | -89 |
| -89 | -89 | -89 | -89 | -89 | -89 | -89 | -89 | -89 | -89 | -89 | -89 | -89 | -89 | -89 | -89 |
| -89 | -89 | -89 | -89 | -89 | -89 | -89 | -89 | -89 | -89 | -89 | -89 | -89 | -89 | -89 | -89 |
| -89 | -89 | -89 | -89 | -89 | -89 | -89 | -89 | -89 | -89 | -89 | -89 | -89 | -89 | -89 | -89 |
| -89 | -89 | -89 | -89 | -89 | -89 | -89 | -89 | -89 | -89 | -89 | -89 | -89 | -89 | -89 | -89 |
| -89 | -89 | -89 | -89 | -89 | -89 | -89 | -89 | -89 | -89 | -89 | -89 | -89 | -89 | -89 | -89 |
| -88 | -88 | -88 | -88 | -88 | -88 | -88 | -88 | -89 | -89 | -89 | -89 | -89 | -89 | -89 | -89 |
| -88 | -88 | -88 | -88 | -88 | -88 | -88 | -88 | -88 | -89 | -89 | -89 | -89 | -89 | -89 | -89 |
| -88 | -88 | -88 | -88 | -88 | -88 | -88 | -88 | -88 | -89 | -89 | -89 | -90 | -89 | -89 | -89 |
| -87 | -87 | -87 | -87 | -87 | -88 | -88 | -88 | -88 | -89 | -89 | -90 | -90 | -89 | -89 | -89 |
| -87 | -86 | -87 | -87 | -87 | -87 | -88 | -88 | -88 | -89 | -89 | -90 | -90 | -89 | -89 | -89 |
| -86 | -86 | -86 | -86 | -87 | -87 | -88 | -88 | -89 | -89 | -90 | -90 | -90 | -89 | -89 | -89 |
| -84 | -84 | -85 | -86 | -86 | -87 | -88 | -88 | -89 | -90 | -90 | -90 | -90 | -89 | -89 | -89 |
| -81 | -83 | -84 | -85 | -86 | -87 | -88 | -89 | -89 | -90 | -90 | -90 | -90 | -89 | -89 | -89 |
| -79 | -82 | -84 | -85 | -86 | -87 | -88 | -89 | -90 | -90 | -90 | -90 | -89 | -89 | -89 | -89 |
| -81 | -83 | -85 | -86 | -87 | -88 | -89 | -90 | -90 | -91 | -91 | -90 | -89 | -89 | -89 | -89 |
| -85 | -85 | -86 | -87 | -88 | -89 | -90 | -91 | -91 | -91 | -91 | -90 | -89 | -89 | -89 | -89 |
| -87 | -88 | -88 | -89 | -90 | -90 | -91 | -92 | -92 | -92 | -91 | -90 | -89 | -89 | -89 | -89 |
| -90 | -90 | -90 | -91 | -91 | -92 | -92 | -93 | -93 | -92 | -91 | -89 | -89 | -89 | -89 | -89 |
| -92 | -92 | -92 | -92 | -93 | -93 | -94 | -94 | -93 | -92 | -90 | -89 | -89 | -89 | -89 | -89 |
| -95 | -94 | -94 | -95 | -95 | -95 | -95 | -95 | -93 | -92 | -90 | -89 | -88 | -89 | -89 | -89 |
| -98 | -97 | -97 | -97 | -98 | -97 | -97 | -95 | -93 | -91 | -89 | -88 | -88 | -89 | -89 | -89 |
| -104 | -103 | -102 | -102 | -101 | -99 | -97 | -95 | -92 | -90 | -89 | -88 | -88 | -89 | -89 | -89 |
| -109 | -108 | -106 | -104 | -101 | -99 | -96 | -94 | -91 | -90 | -88 | -88 | -88 | -89 | -89 | -89 |
| -109 | -107 | -105 | -103 | -100 | -98 | -95 | -93 | -91 | -89 | -88 | -88 | -88 | -89 | -89 | -89 |
| -108 | -106 | -103 | -101 | -99 | -96 | -94 | -91 | -89 | -88 | -87 | -87 | -88 | -89 | -89 | -89 |
| -106 | -104 | -102 | -99 | -97 | -95 | -92 | -90 | -88 | -87 | -87 | -87 | -88 | -89 | -89 | -89 |
| -104 | -102 | -100 | -98 | -95 | -93 | -91 | -89 | -87 | -87 | -87 | -87 | -88 | -89 | -89 | -89 |
| -102 | -100 | -98 | -96 | -94 | -92 | -90 | -88 | -87 | -86 | -86 | -87 | -88 | -89 | -89 | -89 |
| -100 | -98 | -96 | -94 | -92 | -90 | -88 | -87 | -86 | -85 | -86 | -87 | -88 | -89 | -89 | -89 |
| -98 | -96 | -95 | -93 | -90 | -88 | -87 | -85 | -85 | -85 | -86 | -87 | -88 | -89 | -89 | -89 |
| -97 | -95 | -93 | -91 | -89 | -87 | -85 | -84 | -84 | -85 | -86 | -87 | -88 | -89 | -89 | -89 |
| -95 | -93 | -91 | -89 | -87 | -85 | -84 | -83 | -83 | -84 | -85 | -87 | -88 | -89 | -89 | -89 |
| -93 | -91 | -89 | -87 | -85 | -83 | -82 | -82 | -83 | -84 | -85 | -87 | -88 | -89 | -89 | -89 |
| -91 | -89 | -87 | -85 | -83 | -81 | -81 | -82 | -83 | -84 | -85 | -87 | -88 | -89 | -89 | -89 |
| -89 | -87 | -85 | -82 | -80 | -80 | -80 | -81 | -82 | -84 | -85 | -87 | -88 | -89 | -89 | -89 |
| -87 | -85 | -82 | -80 | -78 | -78 | -79 | -80 | -82 | -84 | -85 | -87 | -88 | -89 | -89 | -89 |
| -85 | -82 | -79 | -77 | -76 | -77 | -78 | -80 | -82 | -84 | -85 | -87 | -88 | -89 | -89 | -89 |
| -82 | -78 | -75 | -74 | -74 | -76 | -78 | -80 | -82 | -84 | -86 | -87 | -88 | -89 | -89 | -89 |
| -79 | -74 | -71 | -71 | -73 | -75 | -78 | -80 | -82 | -84 | -86 | -87 | -88 | -89 | -89 | -89 |
| -75 | -69 | -67 | -68 | -71 | -75 | -77 | -80 | -82 | -84 | -86 | -87 | -88 | -89 | -89 | -89 |
| -69 | -61 | -62 | -66 | -71 | -74 | -78 | -80 | -82 | -84 | -86 | -87 | -88 | -89 | -89 | -89 |
| -59 | -52 | -59 | -66 | -71 | -75 | -78 | -80 | -82 | -84 | -86 | -87 | -88 | -89 | -89 | 89 |
| -34 | -44 | -57 | -65 | -71 | -75 | -78 | -80 | -82 | -84 | -86 | -87 | 88 | 89 | 89 | 89 |
| 23 | 45 | 58 | 66 | 71 | 75 | 78 | 80 | 83 | 84 | 86 | 87 | 88 | 89 | 89 | 89 |
| 82 | 56 | 61 | 67 | 72 | 75 | 78 | 81 | 83 | 84 | 86 | 87 | 88 | 89 | 89 | 89 |
| 103 | 72 | 67 | 69 | 73 | 76 | 79 | 81 | 83 | 84 | 86 | 87 | 88 | 89 | 89 | 89 |
| 105 | 86 | 75 | 73 | 74 | 77 | 79 | 81 | 83 | 84 | 86 | 87 | 88 | 89 | 89 | 89 |
| 105 | 94 | 82 | 77 | 76 | 78 | 79 | 81 | 83 | 85 | 86 | 87 | 88 | 89 | 89 | 89 |
| 106 | 98 | 89 | 82 | 79 | 79 | 80 | 82 | 83 | 85 | 86 | 87 | 88 | 89 | 89 | 89 |
| 107 | 101 | 94 | 87 | 82 | 81 | 81 | 82 | 83 | 85 | 86 | 87 | 88 | 89 | 89 | 89 |
| 108 | 104 | 98 | 91 | 86 | 83 | 82 | 83 | 84 | 85 | 86 | 87 | 88 | 89 | 89 | 89 |
| 109 | 105 | 101 | 95 | 89 | 86 | 84 | 84 | 84 | 85 | 86 | 87 | 88 | 89 | 89 | 89 |
| 110 | 107 | 103 | 96 | 93 | 88 | 86 | 85 | 85 | 85 | 86 | 87 | 88 | 89 | 89 | 89 |
| 111 | 108 | 105 | 101 | 96 | 91 | 88 | 86 | 85 | 86 | 86 | 87 | 88 | 89 | 89 | 89 |
| 112 | 110 | 107 | 103 | 98 | 94 | 90 | 87 | 86 | 86 | 87 | 87 | 88 | 89 | 89 | 89 |
| 113 | 111 | 108 | 105 | 101 | 96 | 92 | 89 | 87 | 87 | 87 | 88 | 88 | 89 | 89 | 89 |
| 114 | 112 | 110 | 107 | 103 | 99 | 94 | 91 | 88 | 87 | 87 | 88 | 88 | 89 | 89 | 89 |
| 115 | 113 | 111 | 108 | 105 | 101 | 96 | 93 | 90 | 88 | 88 | 88 | 88 | 89 | 89 | 89 |
| 116 | 114 | 112 | 109 | 106 | 103 | 98 | 94 | 91 | 89 | 88 | 88 | 88 | 89 | 89 | 89 |
| 118 | 116 | 113 | 111 | 108 | 104 | 100 | 96 | 93 | 90 | 89 | 88 | 89 | 89 | 89 | 89 |
| 119 | 117 | 115 | 112 | 109 | 106 | 102 | 98 | 94 | 91 | 89 | 89 | 89 | 89 | 89 | 89 |
| 121 | 119 | 116 | 113 | 111 | 107 | 104 | 100 | 96 | 92 | 90 | 89 | 89 | 89 | 89 | 89 |
| 123 | 120 | 117 | 115 | 112 | 109 | 105 | 101 | 97 | 94 | 91 | 89 | 89 | 89 | 89 | 89 |
| 124 | 121 | 119 | 116 | 113 | 110 | 107 | 103 | 99 | 95 | 92 | 90 | 89 | 89 | 89 | 89 |
| 125 | 123 | 120 | 117 | 115 | 111 | 108 | 104 | 100 | 96 | 93 | 90 | 89 | 89 | 89 | 89 |
| 125 | 123 | 121 | 119 | 116 | 113 | 109 | 105 | 101 | 97 | 94 | 91 | 90 | 89 | 89 | 89 |
| 110 | 111 | 112 | 114 | 114 | 113 | 111 | 107 | 103 | 98 | 95 | 92 | 90 | 89 | 89 | 89 |
| 96 | 96 | 98 | 101 | 104 | 107 | 108 | 107 | 104 | 100 | 96 | 92 | 90 | 89 | 89 | 89 |
| 92 | 92 | 92 | 93 | 95 | 98 | 101 | 103 | 103 | 100 | 96 | 93 | 91 | 90 | 89 | 89 |
| 90 | 90 | 90 | 91 | 92 | 93 | 95 | 98 | 100 | 99 | 97 | 93 | 91 | 90 | 89 | 89 |
| 87 | 88 | 88 | 89 | 90 | 91 | 92 | 94 | 96 | 97 | 96 | 94 | 91 | 90 | 89 | 89 |
| 85 | 86 | 87 | 88 | 89 | 90 | 91 | 92 | 94 | 95 | 96 | 96 | 92 | 90 | 90 | 89 |
| 81 | 83 | 85 | 86 | 88 | 89 | 90 | 91 | 92 | 94 | 95 | 94 | 92 | 90 | 90 | 89 |
| 79 | 82 | 84 | 86 | 87 | 88 | 89 | 90 | 91 | 92 | 94 | 93 | 92 | 90 | 90 | 89 |
| 81 | 83 | 84 | 85 | 86 | 87 | 88 | 89 | 90 | 91 | 93 | 93 | 92 | 90 | 90 | 90 |
| 84 | 85 | 85 | 86 | 87 | 87 | 88 | 89 | 90 | 91 | 92 | 92 | 92 | 90 | 90 | 90 |
| 86 | 86 | 86 | 86 | 87 | 87 | 88 | 89 | 89 | 90 | 91 | 92 | 92 | 90 | 90 | 90 |
| 87 | 87 | 87 | 87 | 87 | 88 | 88 | 88 | 89 | 90 | 91 | 91 | 91 | 91 | 90 | 90 |
| 87 | 87 | 87 | 87 | 88 | 88 | 88 | 88 | 89 | 89 | 90 | 91 | 91 | 91 | 90 | 90 |
| 88 | 88 | 88 | 88 | 88 | 88 | 88 | 88 | 89 | 89 | 90 | 90 | 91 | 90 | 90 | 90 |
| 88 | 88 | 88 | 88 | 88 | 88 | 88 | 89 | 89 | 89 | 90 | 90 | 91 | 90 | 90 | 90 |
| 88 | 88 | 88 | 88 | 88 | 89 | 89 | 89 | 89 | 89 | 89 | 90 | 90 | 90 | 90 | 90 |
| 89 | 89 | 89 | 89 | 89 | 89 | 89 | 89 | 89 | 89 | 89 | 90 | 90 | 90 | 90 | 90 |
| 89 | 89 | 89 | 89 | 89 | 89 | 89 | 89 | 89 | 89 | 89 | 90 | 90 | 90 | 90 | 90 |
| 89 | 89 | 89 | 89 | 89 | 89 | 89 | 89 | 89 | 89 | 89 | 89 | 90 | 90 | 90 | 90 |
| 89 | 89 | 89 | 89 | 89 | 89 | 89 | 89 | 89 | 89 | 89 | 89 | 89 | 90 | 90 | 90 |
| 89 | 89 | 89 | 89 | 89 | 89 | 89 | 89 | 89 | 89 | 89 | 89 | 89 | 89 | 90 | 90 |
| 89 | 89 | 89 | 89 | 89 | 89 | 89 | 89 | 89 | 89 | 89 | 89 | 89 | 89 | 89 | 90 |

FIGURE 31.- TOTAL AERODYNAMIC COEFFICIENTS AND MACH CHART AT ROOT SECTION IN COMPUTATIONAL PLANE OF JAMESON PROGRAM (SEE APPENDIX FOR COMMENTS).

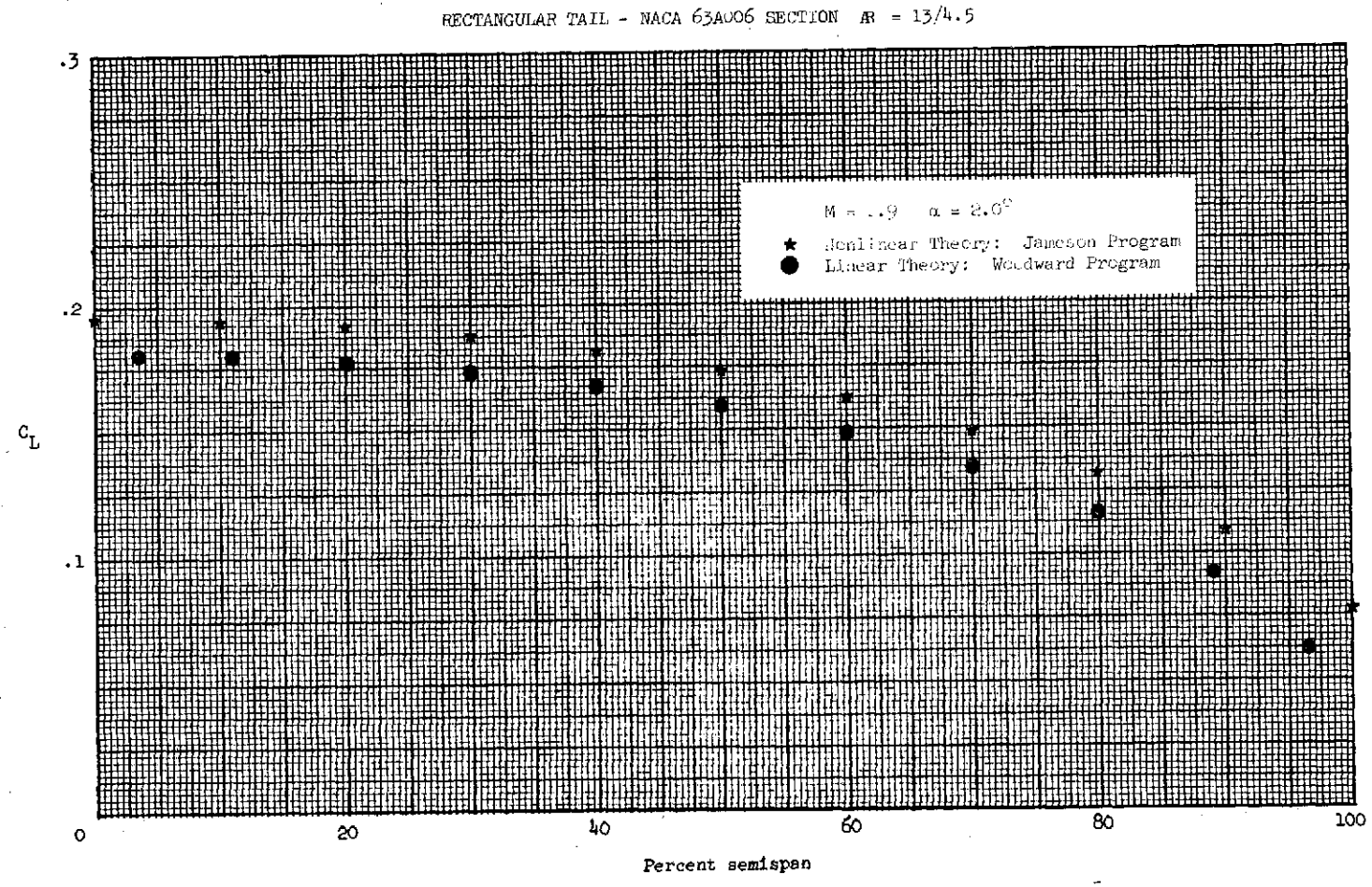


Figure 32.- Spanwise distribution of section lift coefficient.

RECTANGULAR WING NACA 63A006 SECTION AR = 32/9
WITH EXPERIMENTAL STING-BODY

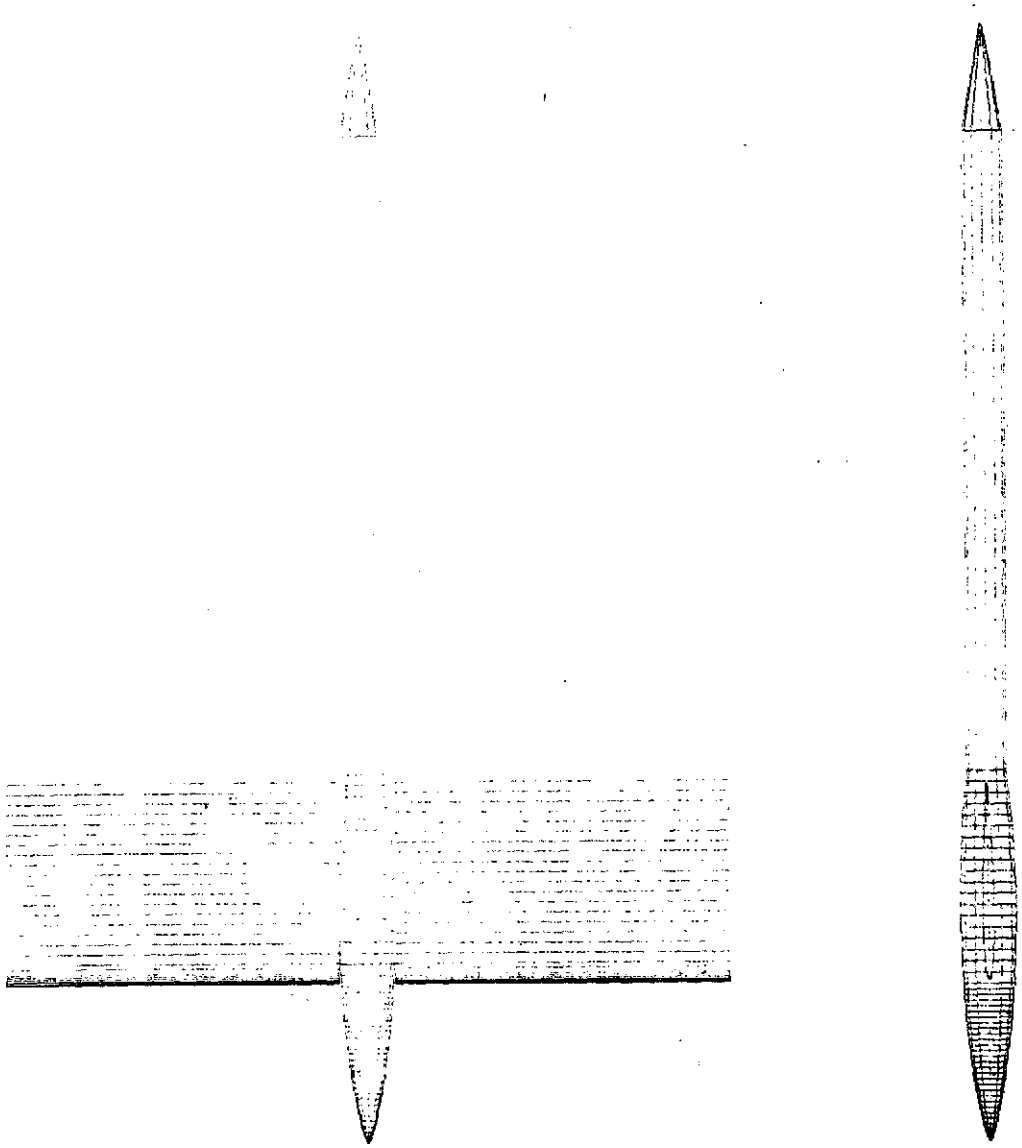

FIGURE 33.- RECTANGULAR WING PLUS EXPERIMENTAL STING-BODY CONFIGURATION USED IN CALCULATIONS.

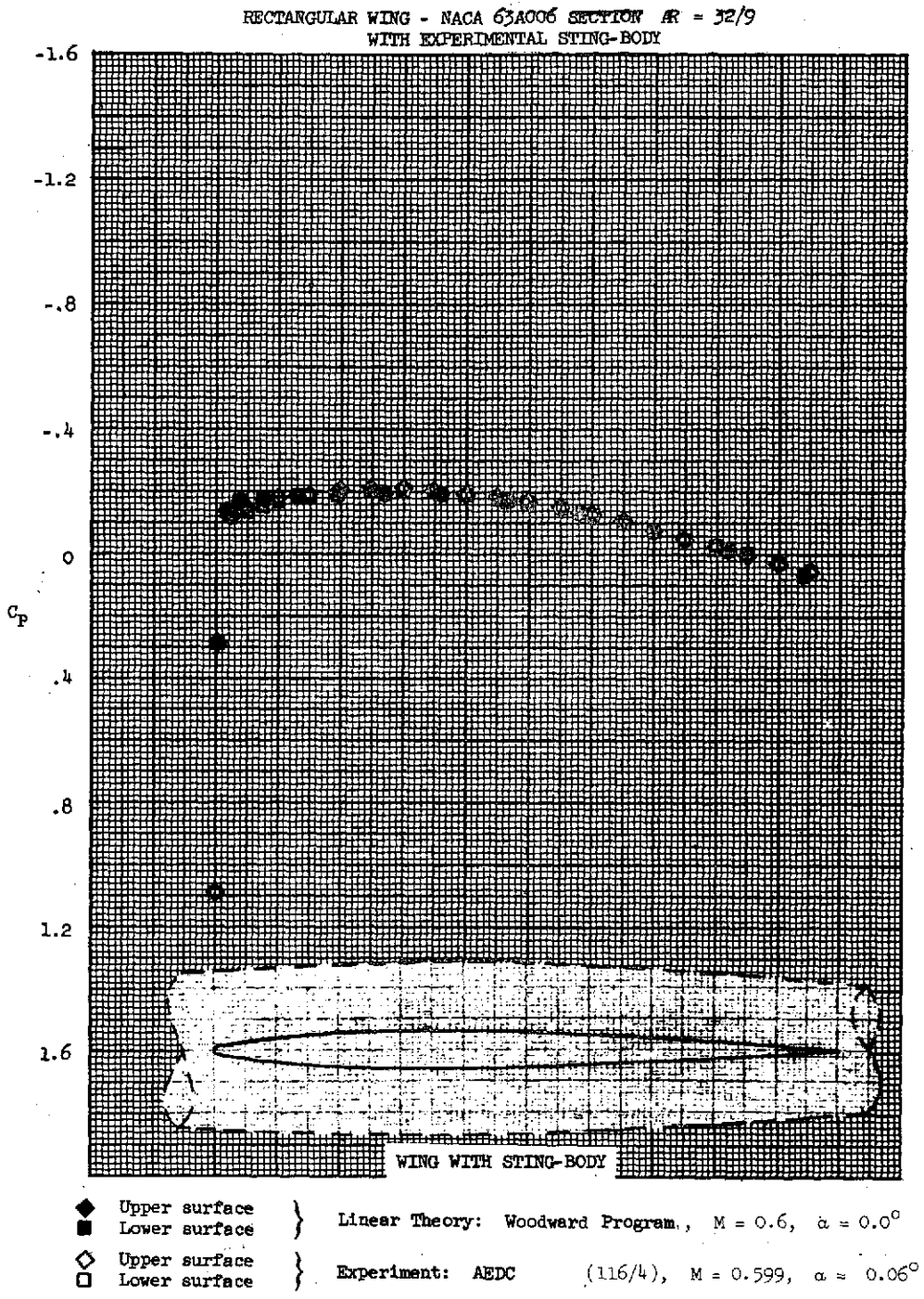


Figure 34.- Chordwise distribution of surface pressure coefficients at the 50 percent semispan location on the wing.

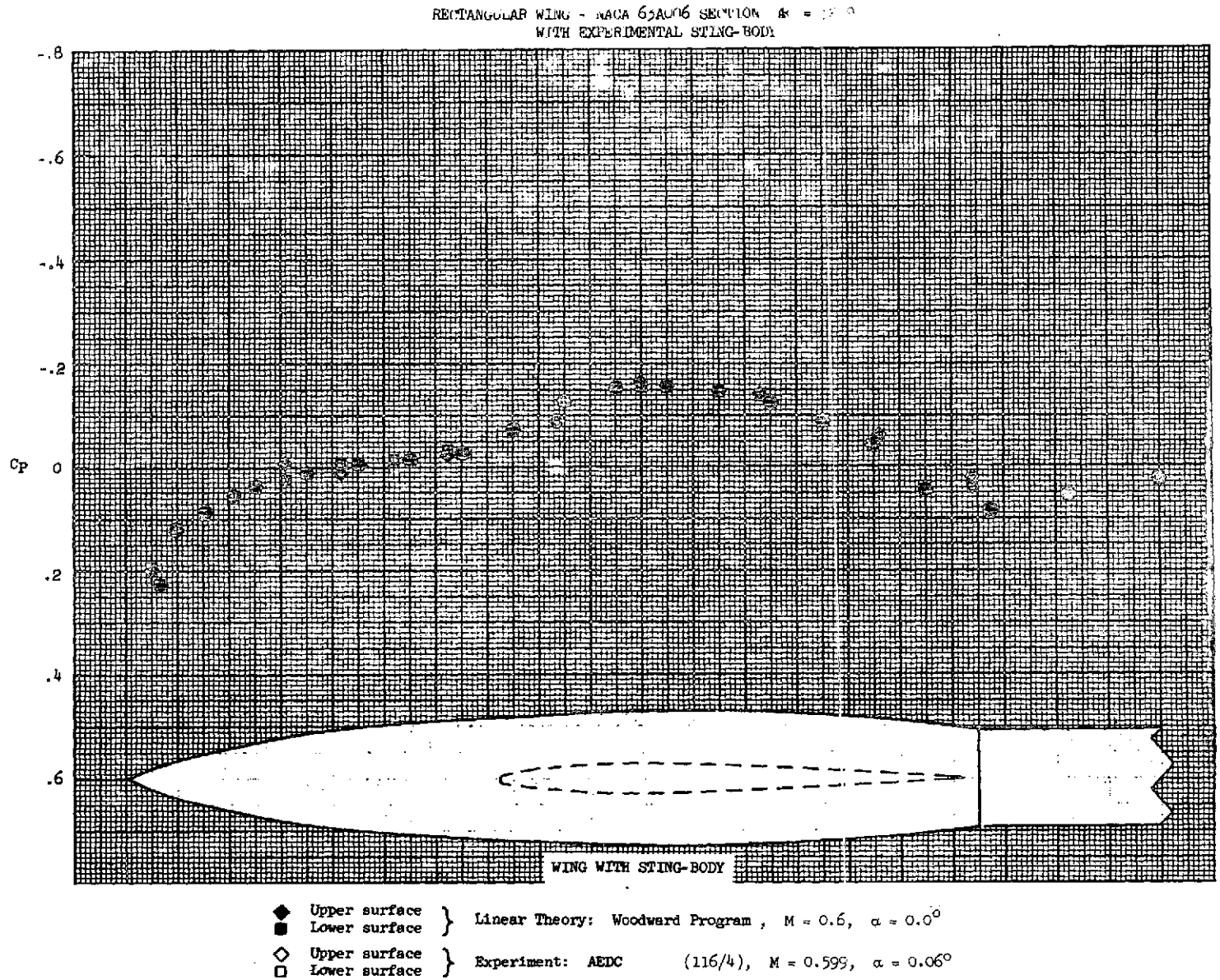


Figure 35.- Axial distribution of surface pressure coefficients on the sting-body of the wing.

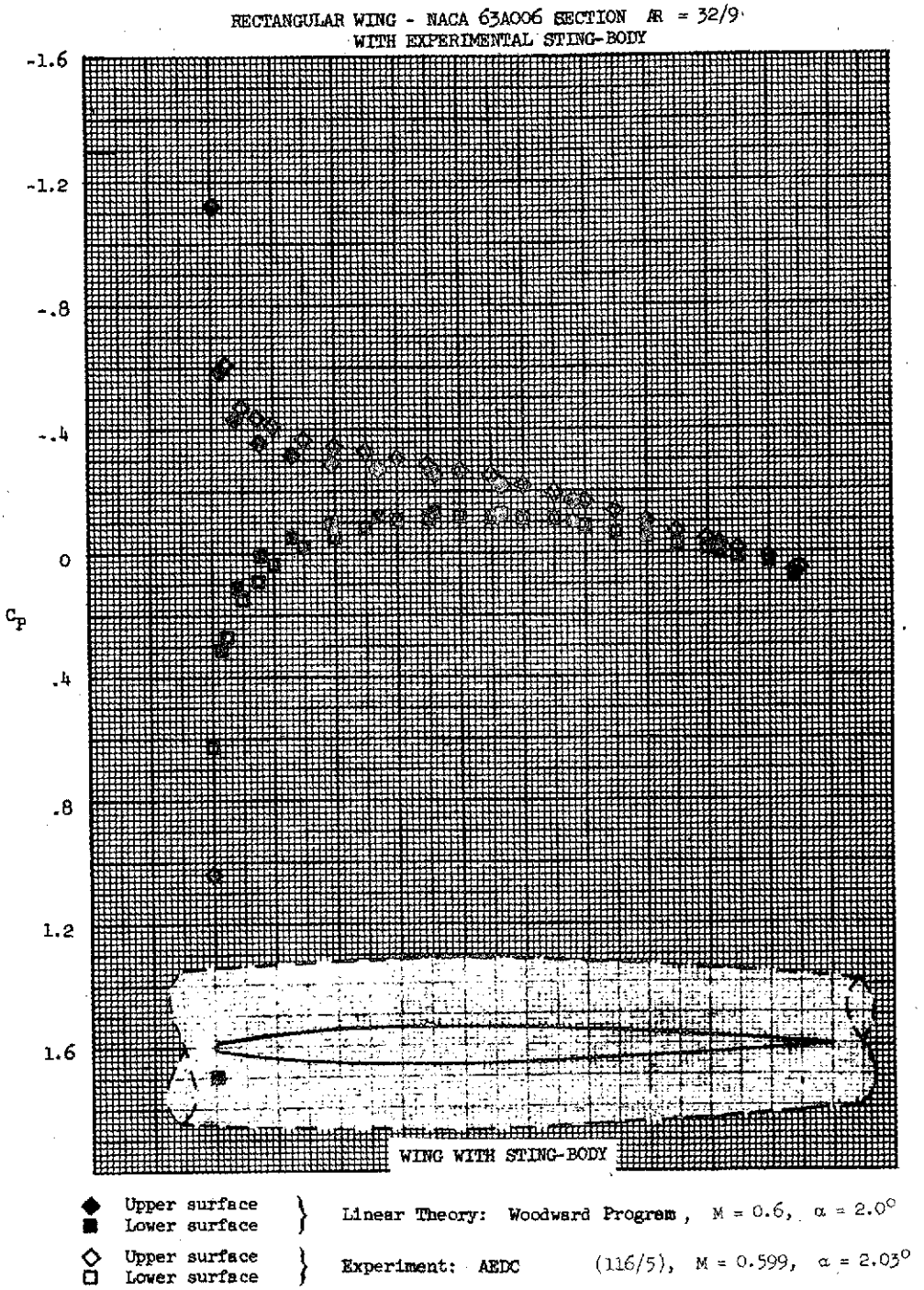


Figure 36.- Chordwise distribution of surface pressure coefficients at the 50 percent semispan location on the wing.

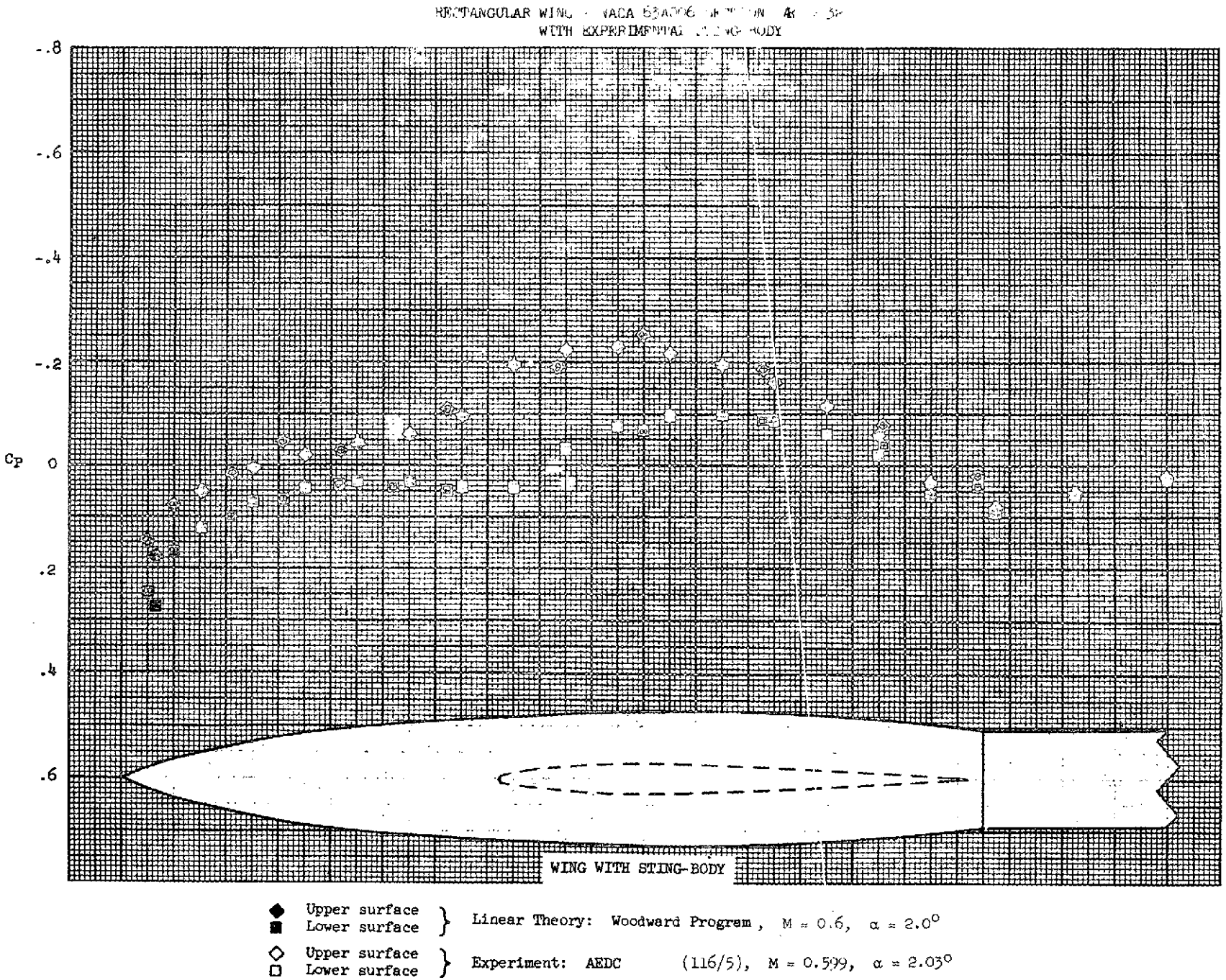


Figure 37.- Axial distribution of surface pressure coefficients on the sting-body of the wing.

RECTANGULAR WING - NACA 63A006 SECTION AR = 32/9
WITH EXPERIMENTAL STING-BODY

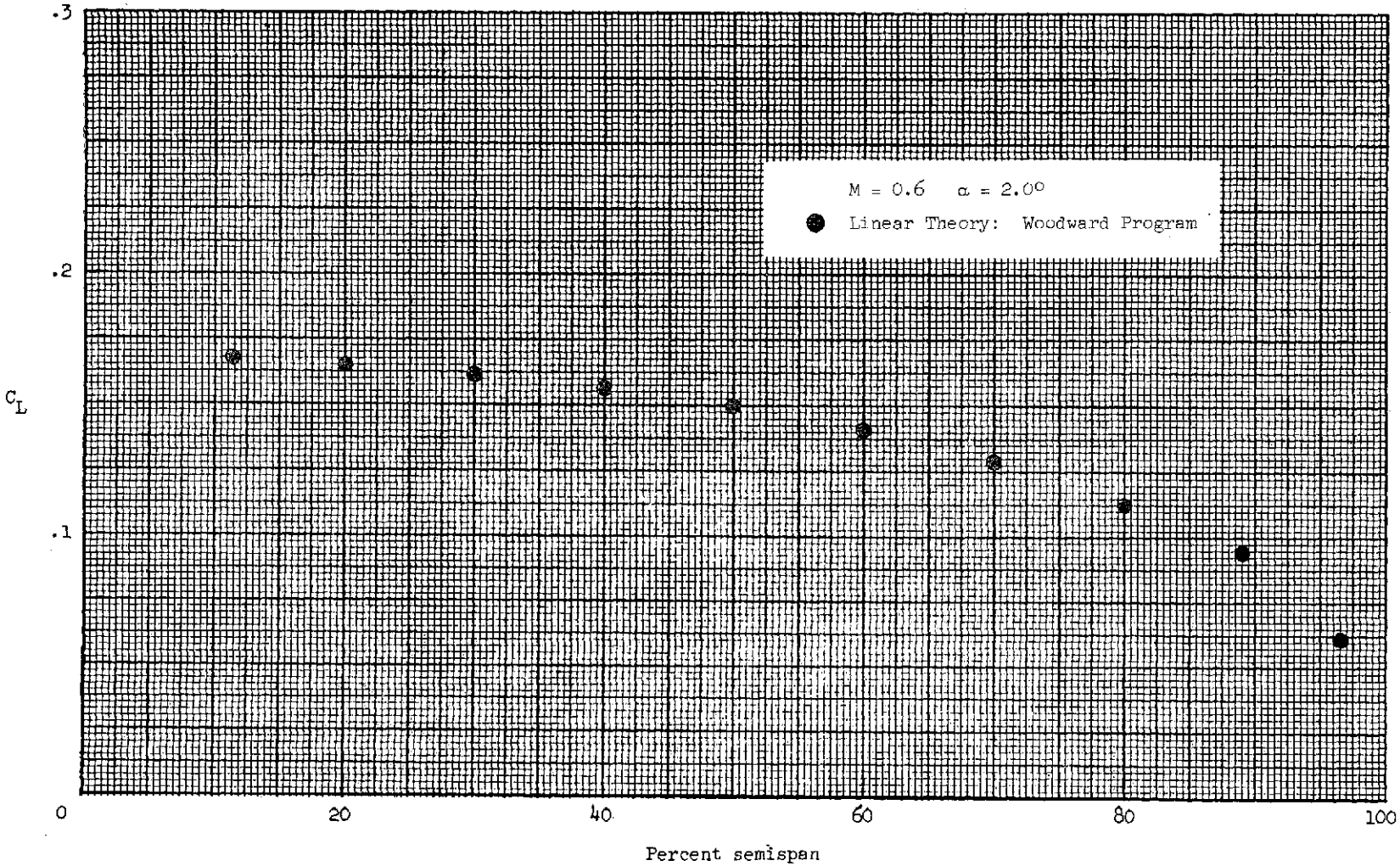


Figure 38.- Spanwise distribution of section lift coefficient.

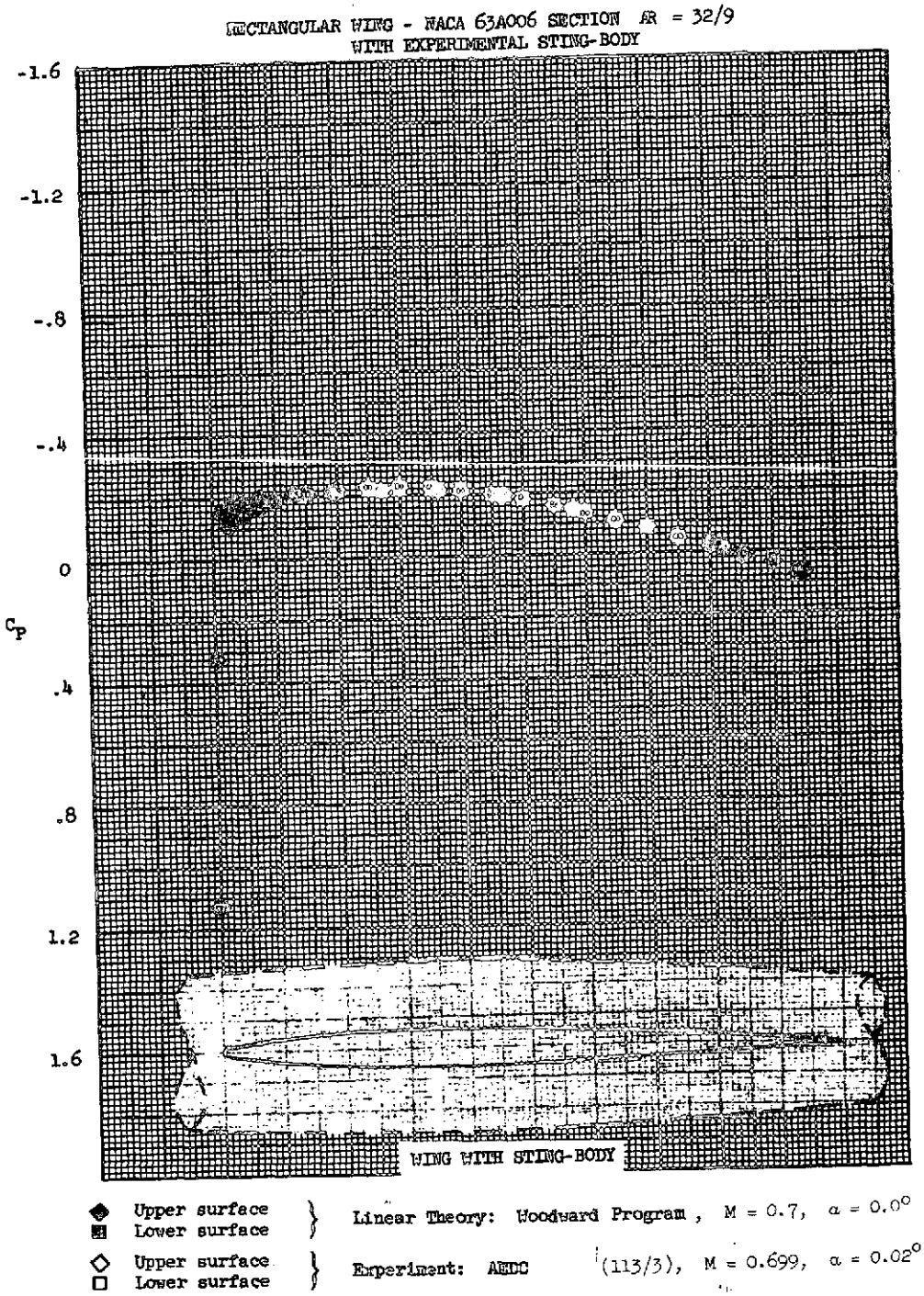


Figure 39.- Chordwise distribution of surface pressure coefficients at the 50 percent semispan location on the wing.

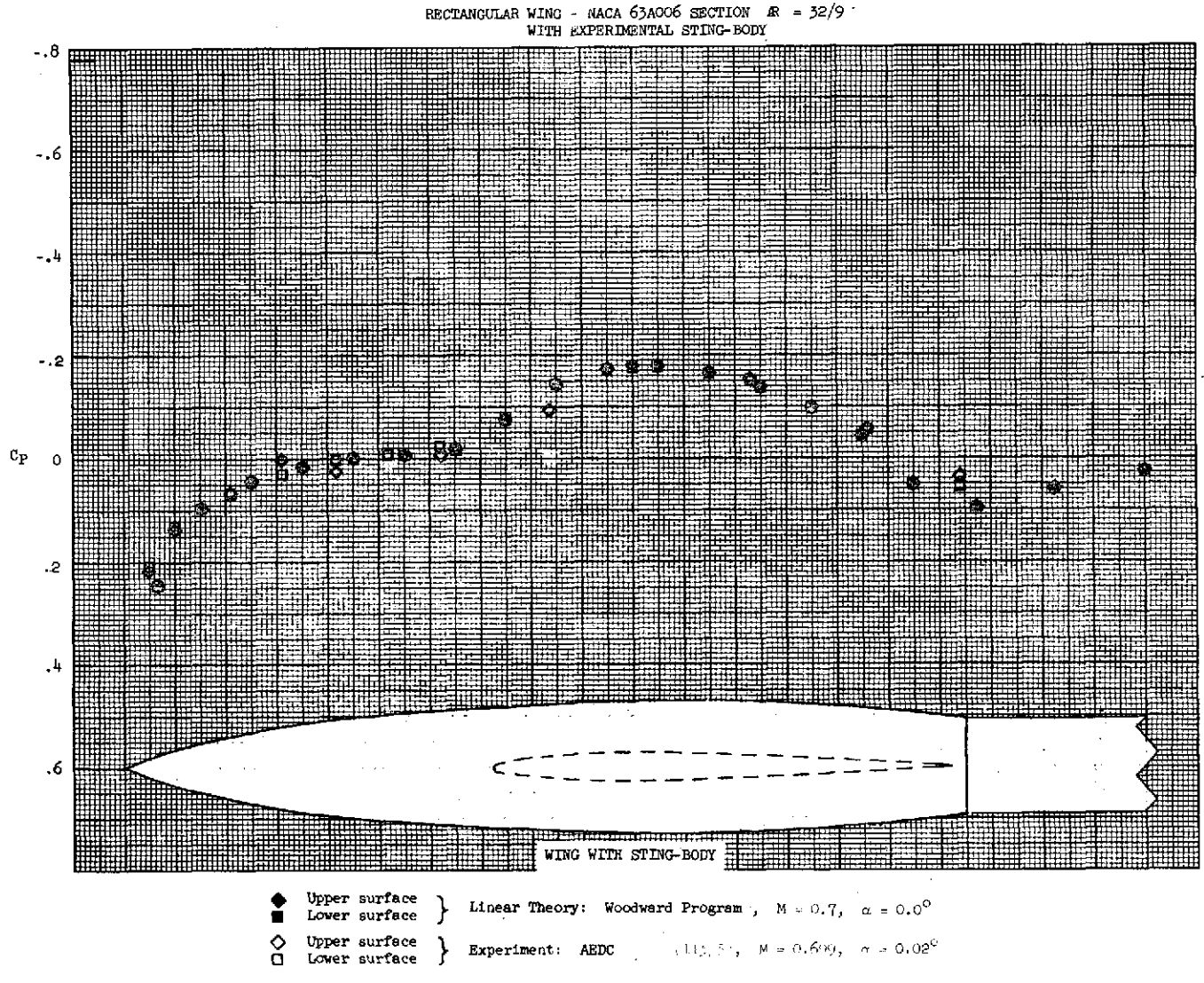


Figure 4. - Axial distribution of surface pressure coefficients on the sting-body of the wing.

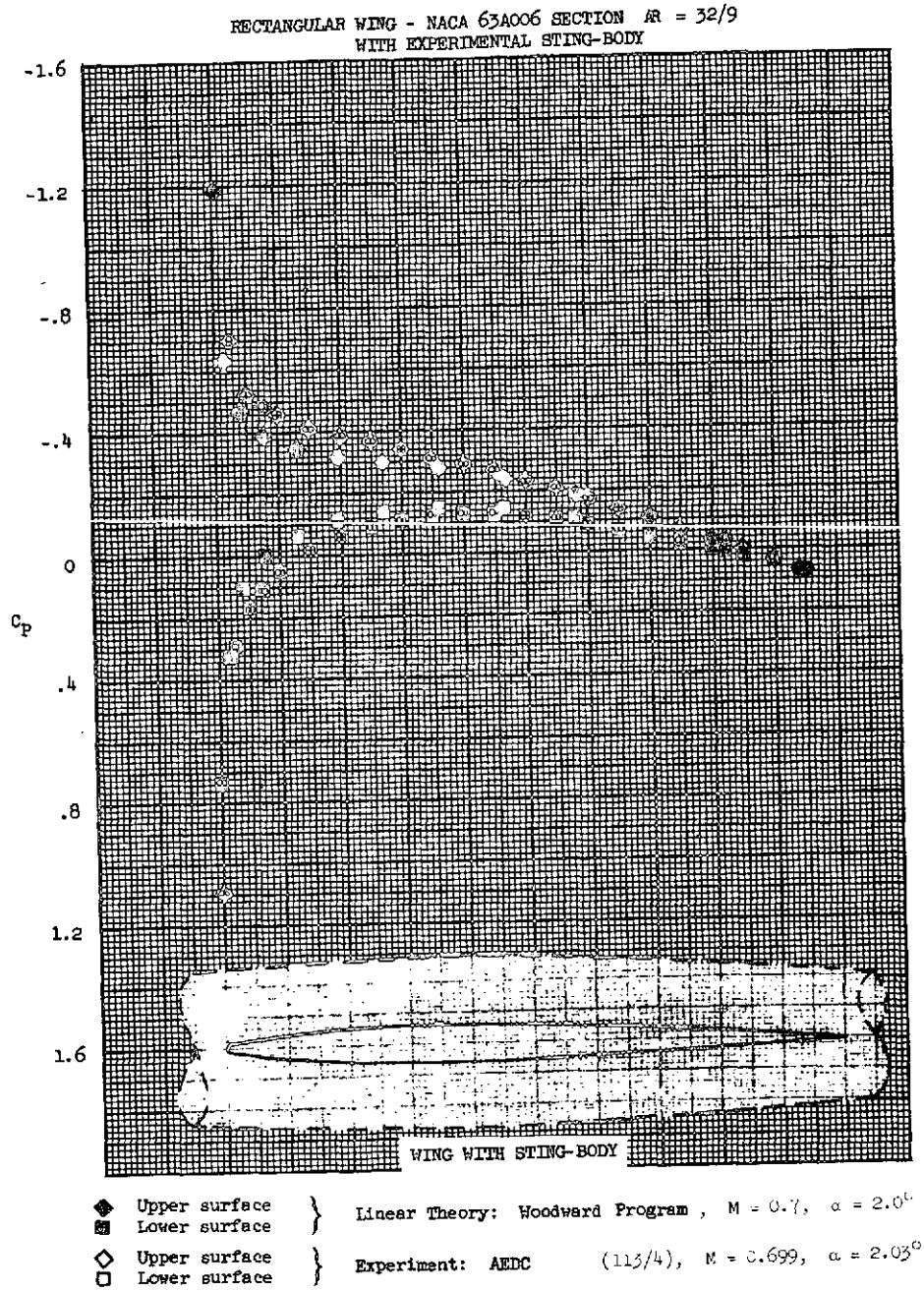


Figure 41.- Chordwise distribution of surface pressure coefficients at the 50 percent semispan location on the wing.

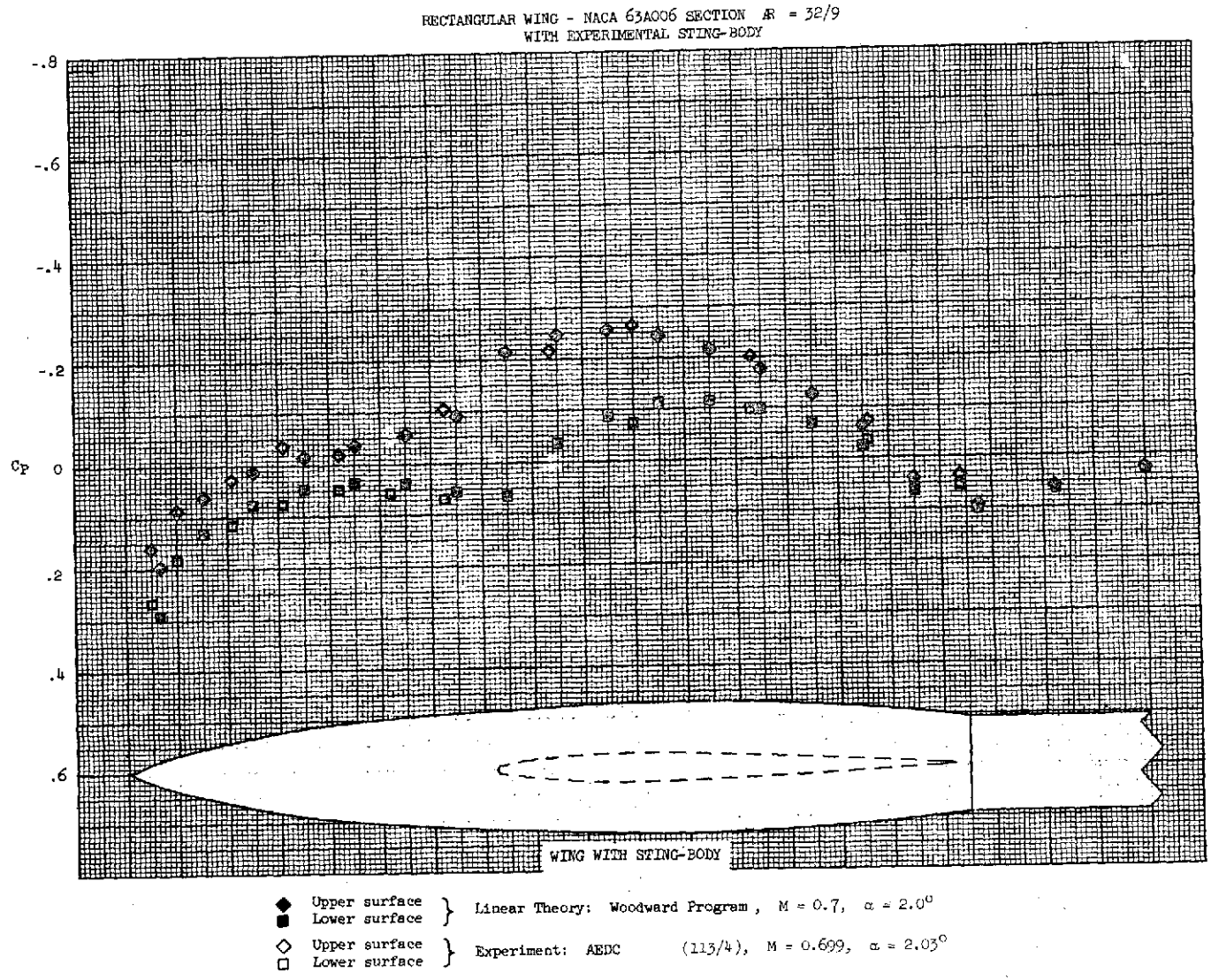


Figure 42.- Axial distribution of surface pressure coefficients on the sting-body of the wing.

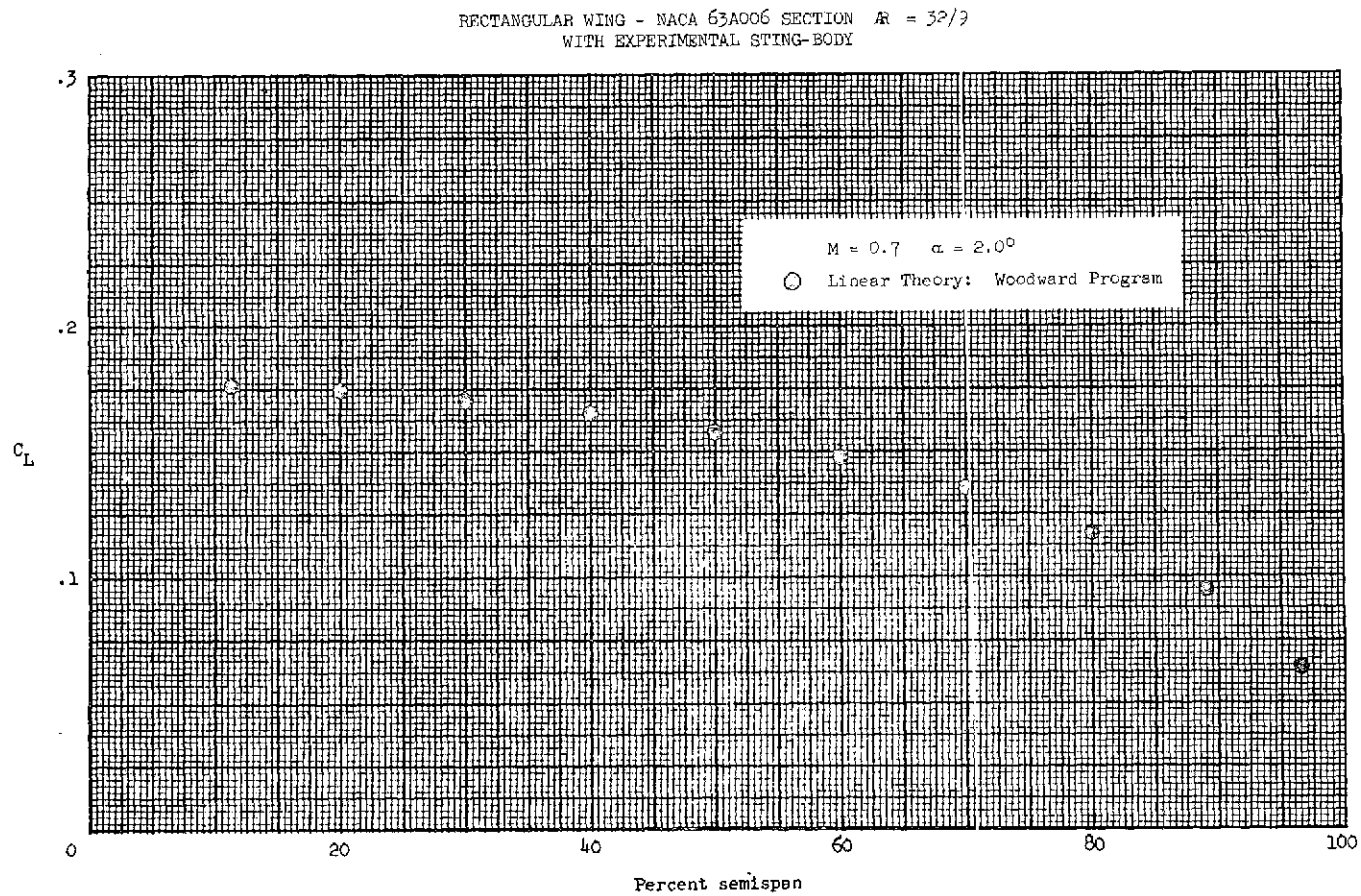


Figure 43.- Spanwise distribution of section lift coefficient.

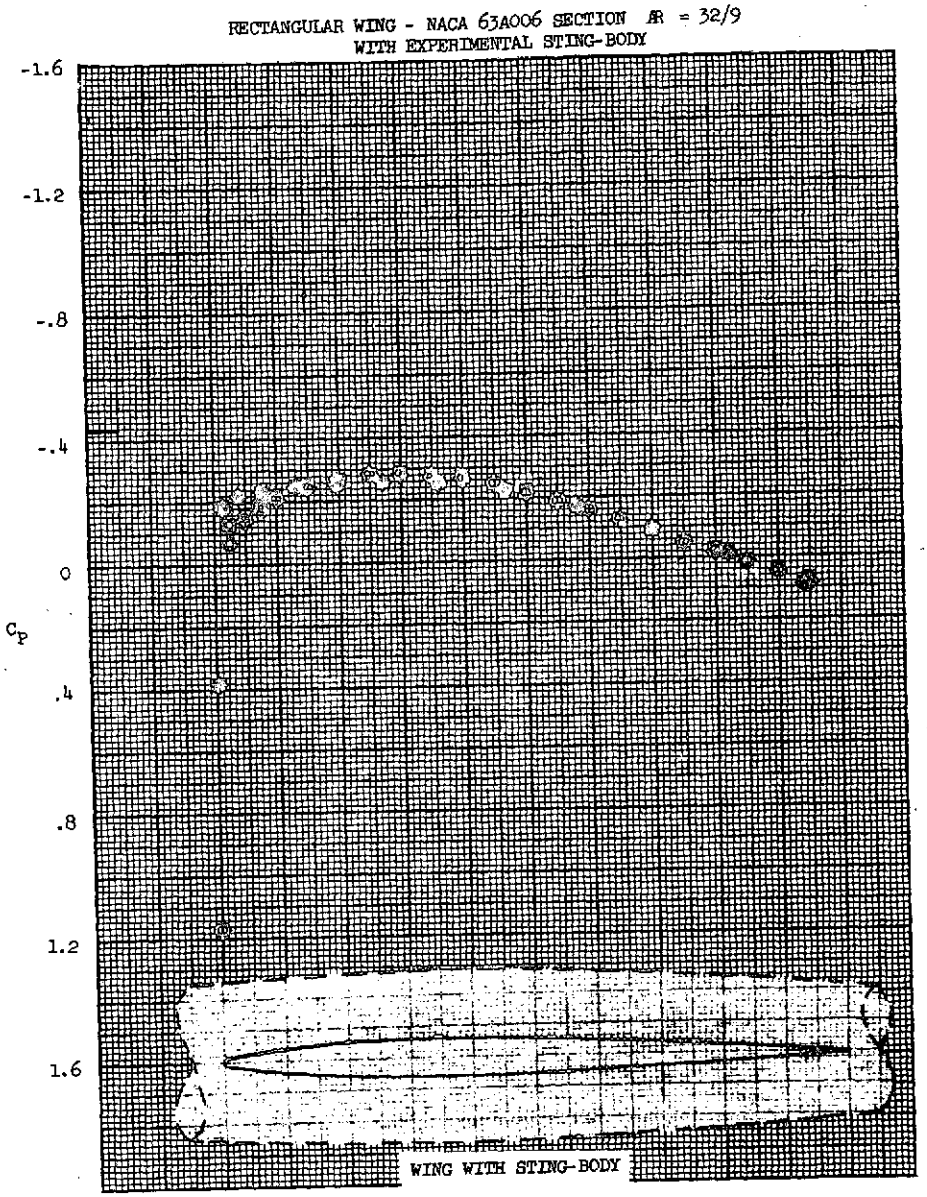


Figure 44.- Chordwise distribution of surface pressure coefficients at the 50 percent semispan location on the wing.

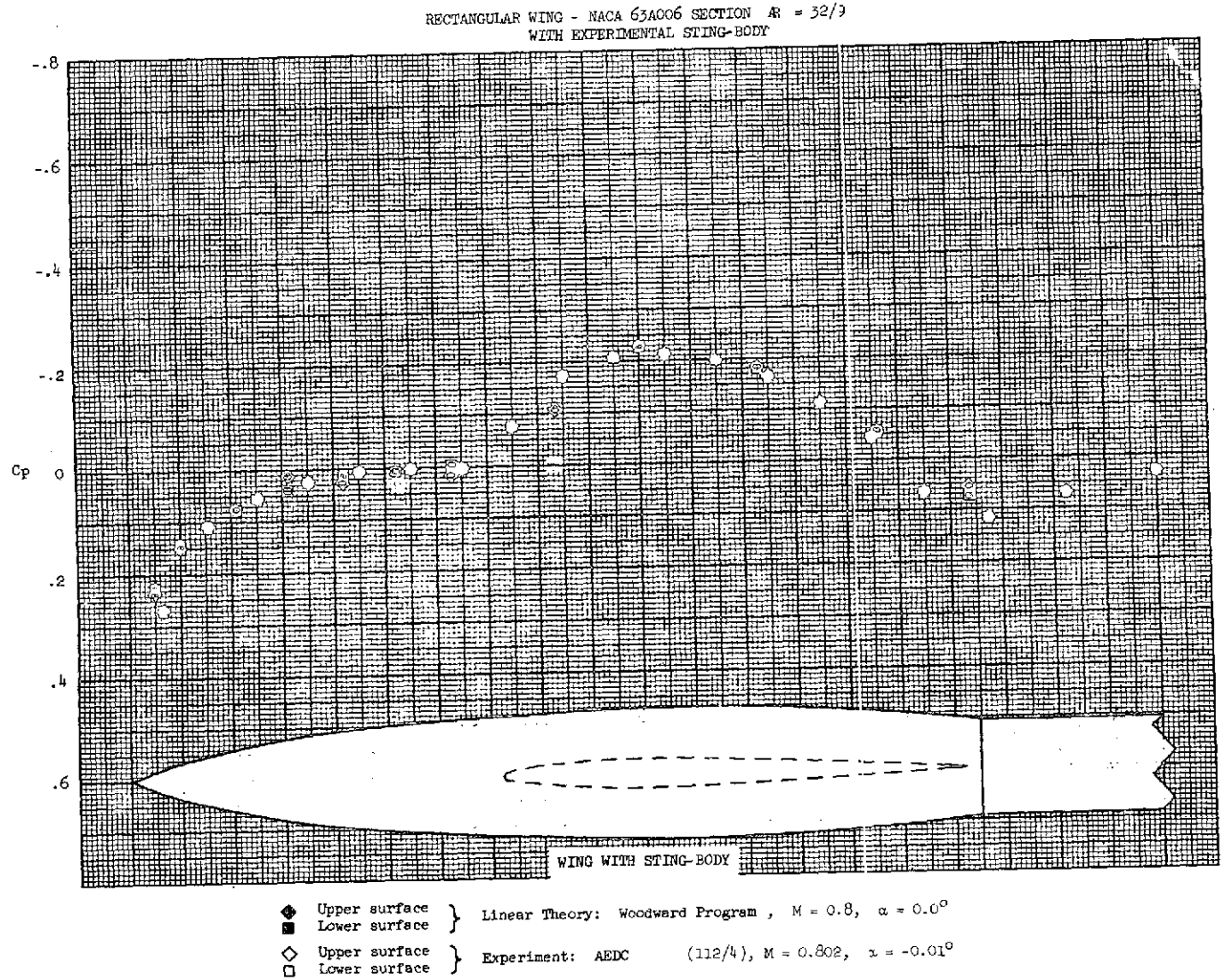


Figure 45.- Axial distribution of surface pressure coefficients on the sting-body of the wing.

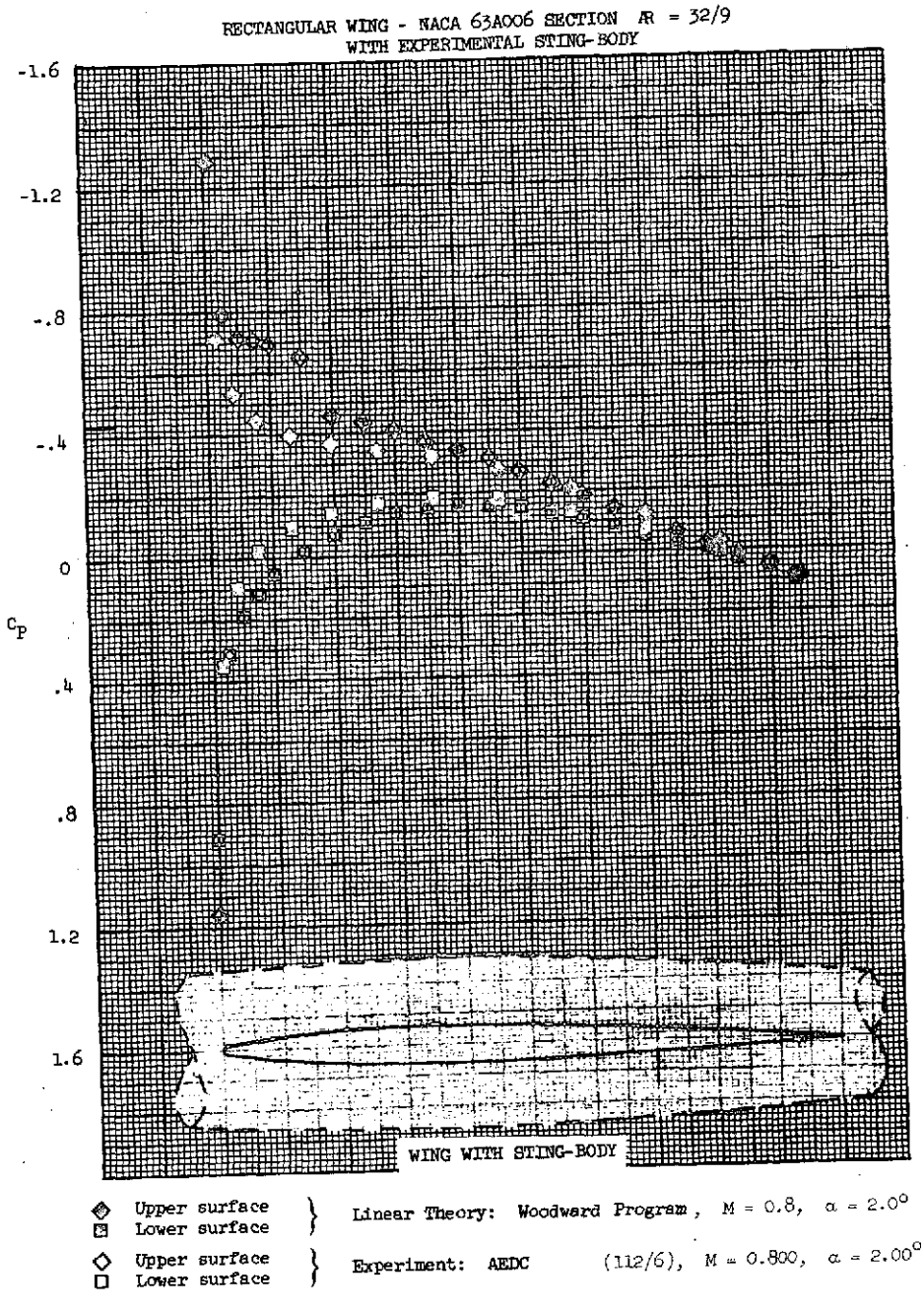


Figure 46.- Chordwise distribution of surface pressure coefficients at the 50 percent semispan location on the wing.

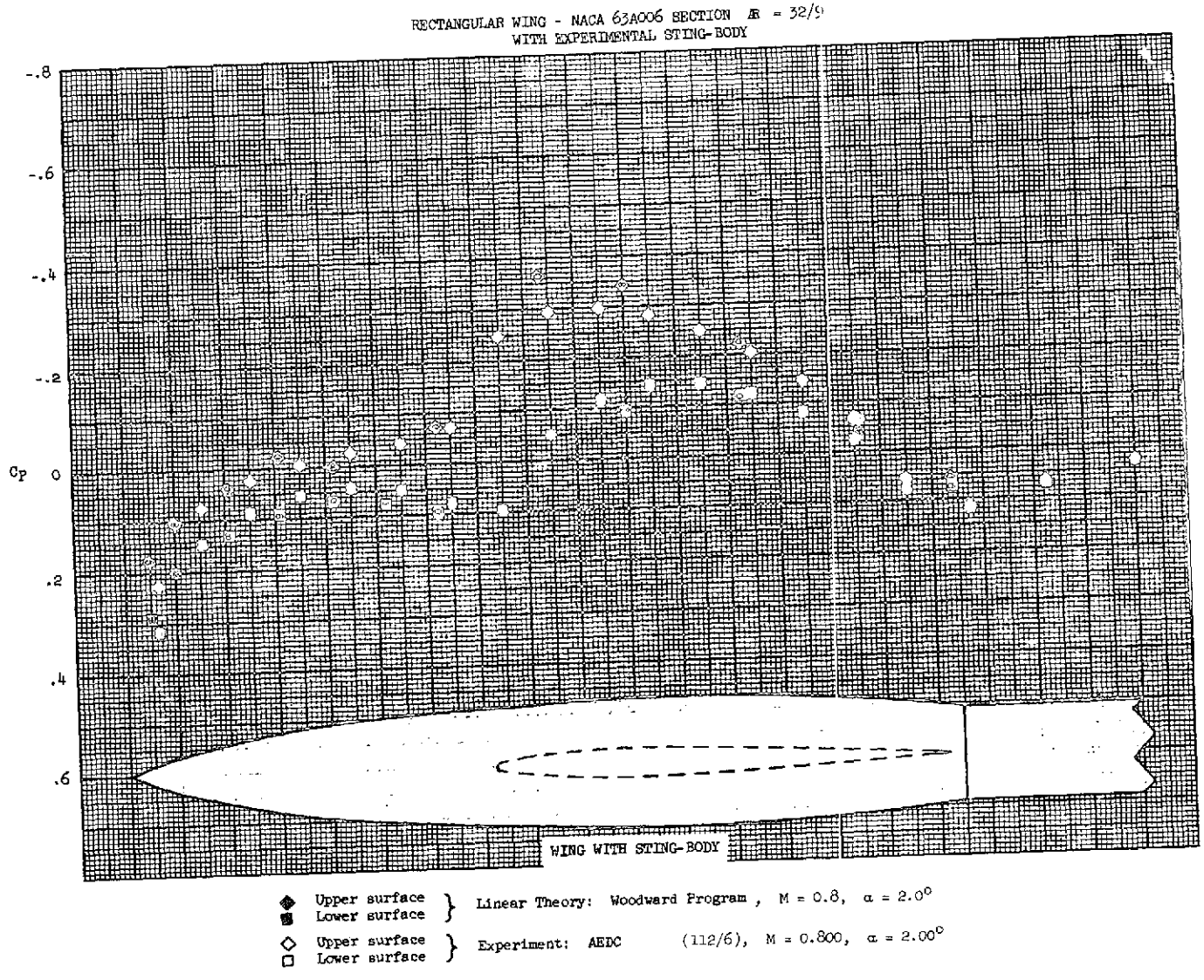


Figure 47.- Axial distribution of surface pressure coefficients on the sting-body of the wing.

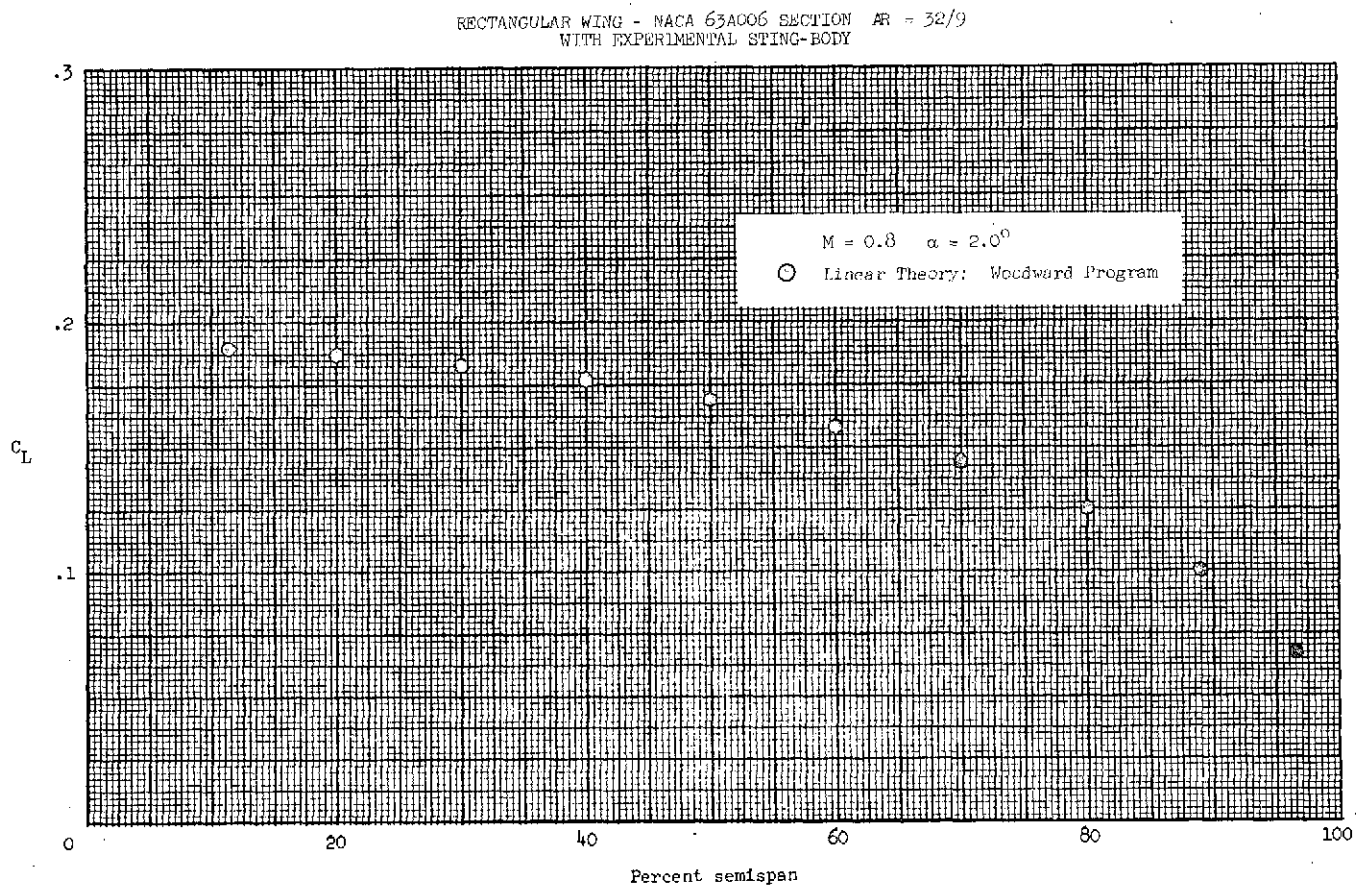


Figure 48.- Spanwise distribution of section lift coefficient.

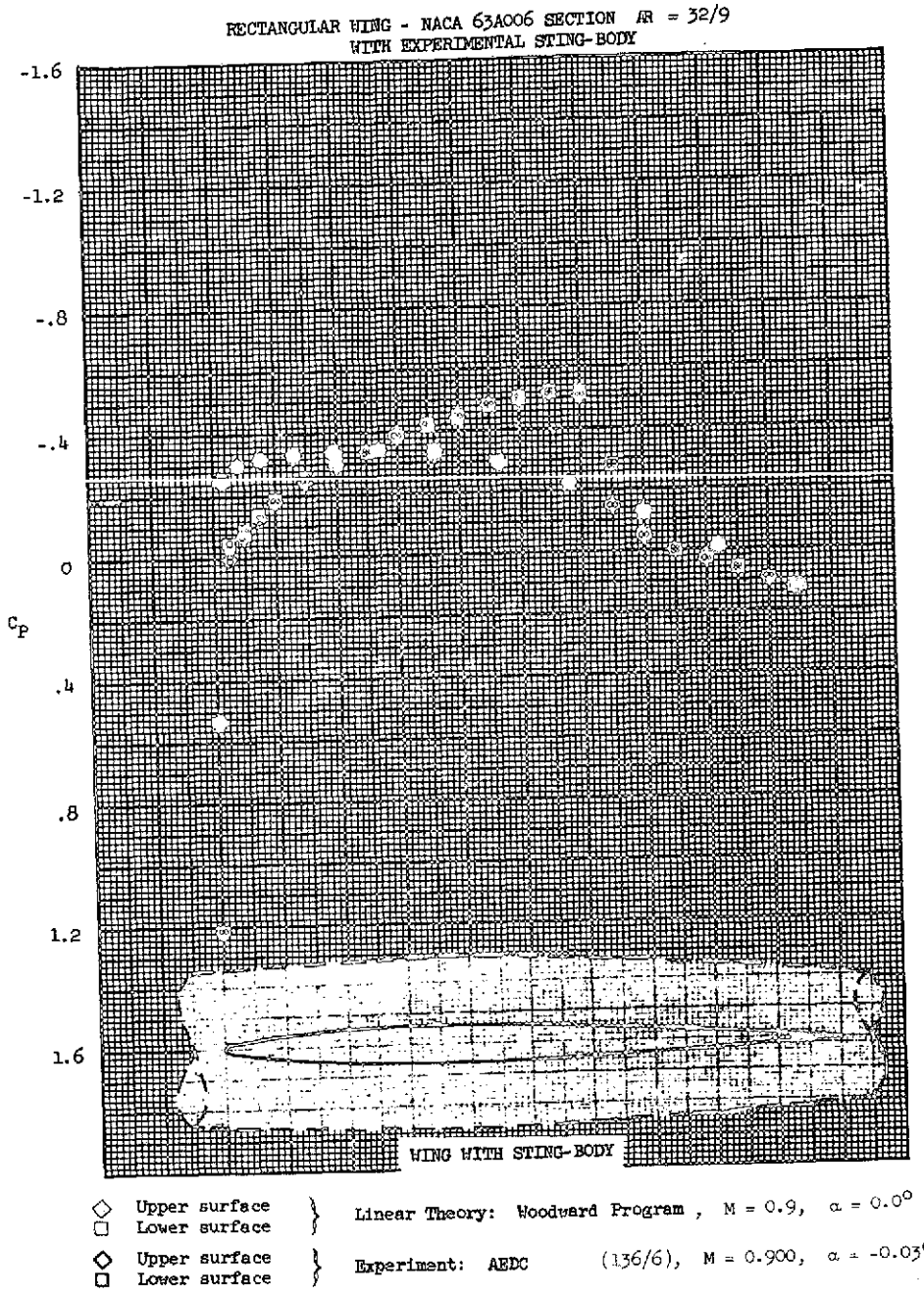


Figure 49.- Chordwise distribution of surface pressure coefficients at the 50 percent semispan location on the wing.

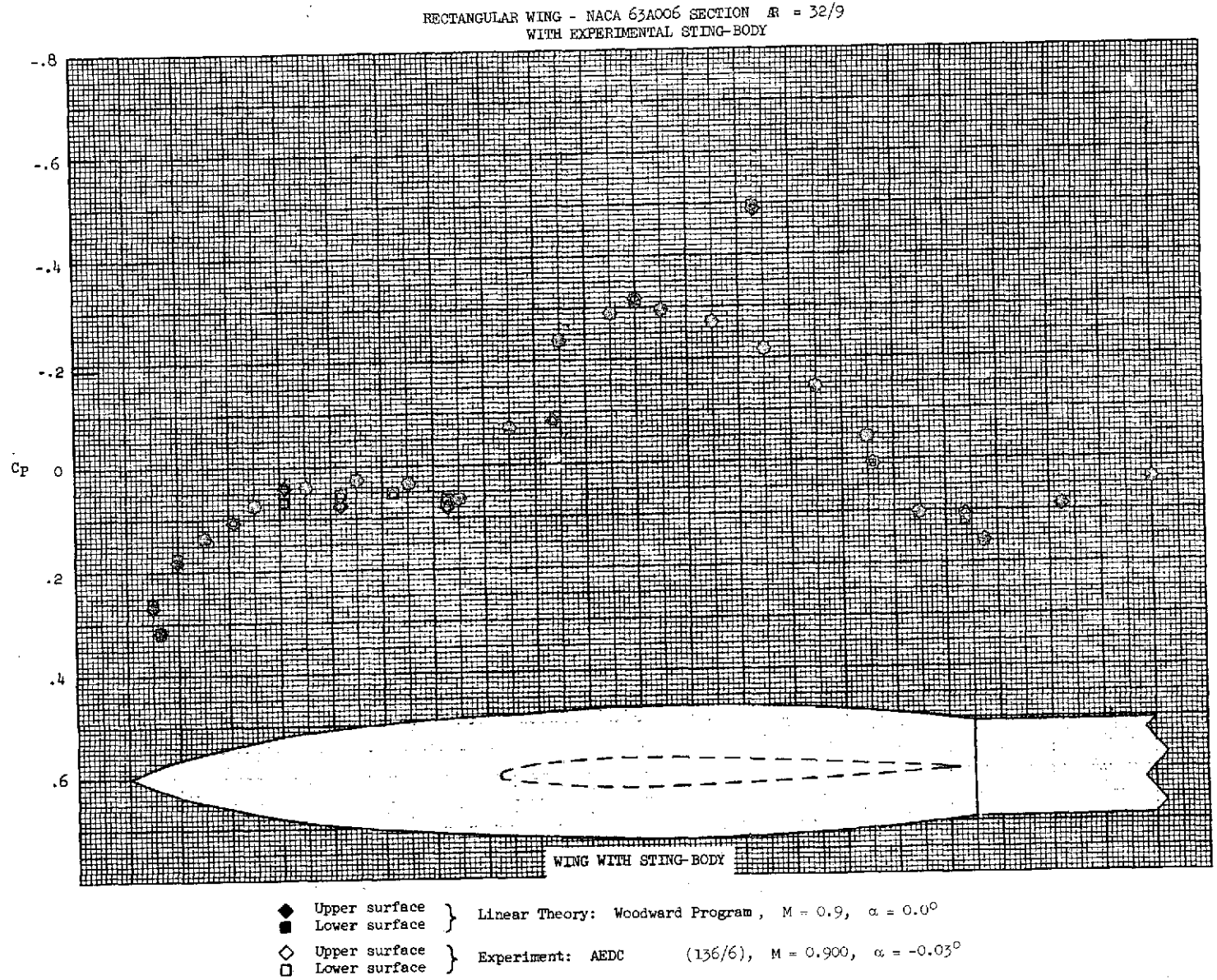


Figure 50.- Axial distribution of surface pressure coefficients on the sting-body of the wing.

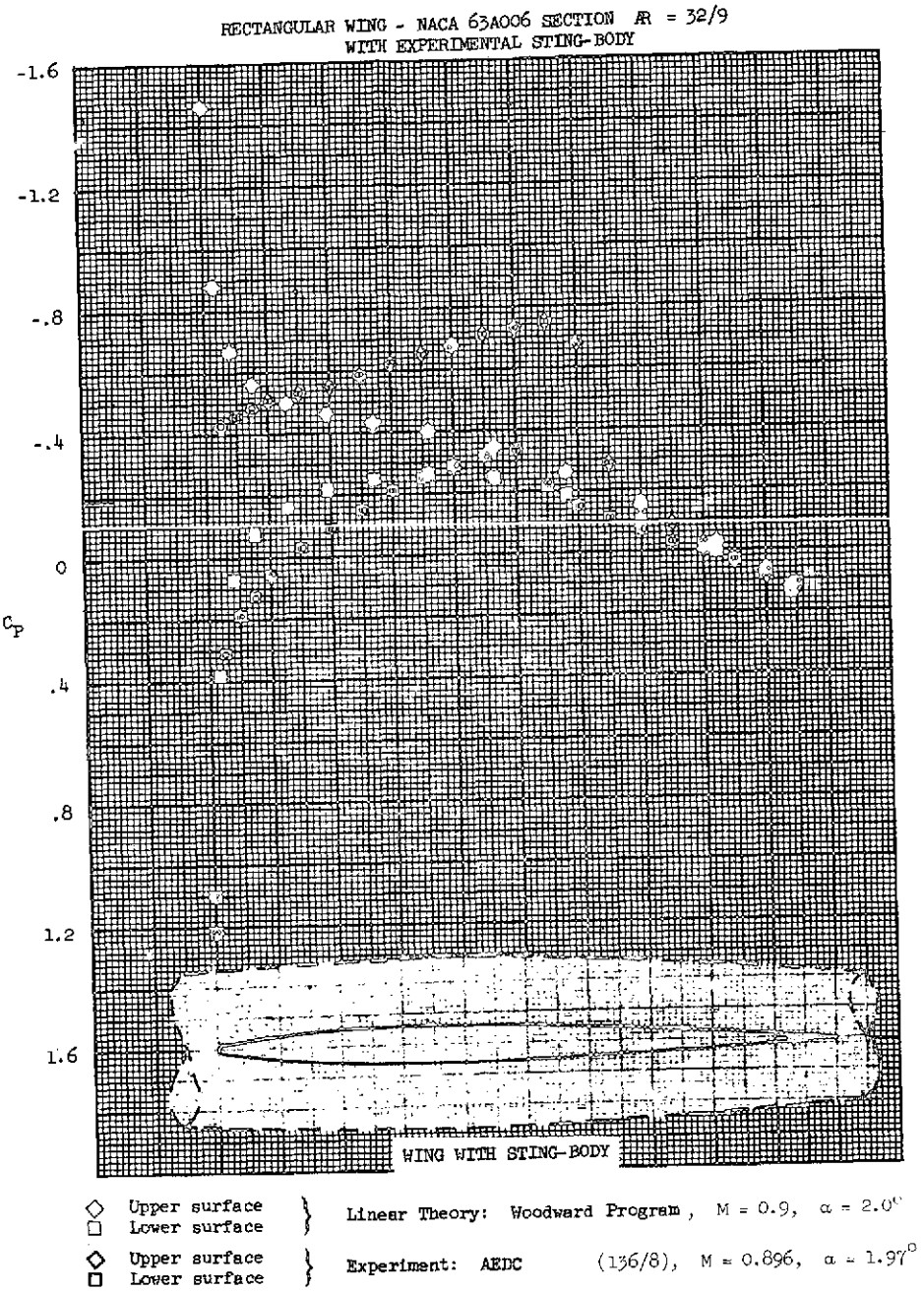


Figure 51.- Chordwise distribution of surface pressure coefficients at the 50 percent semispan location on the wing.

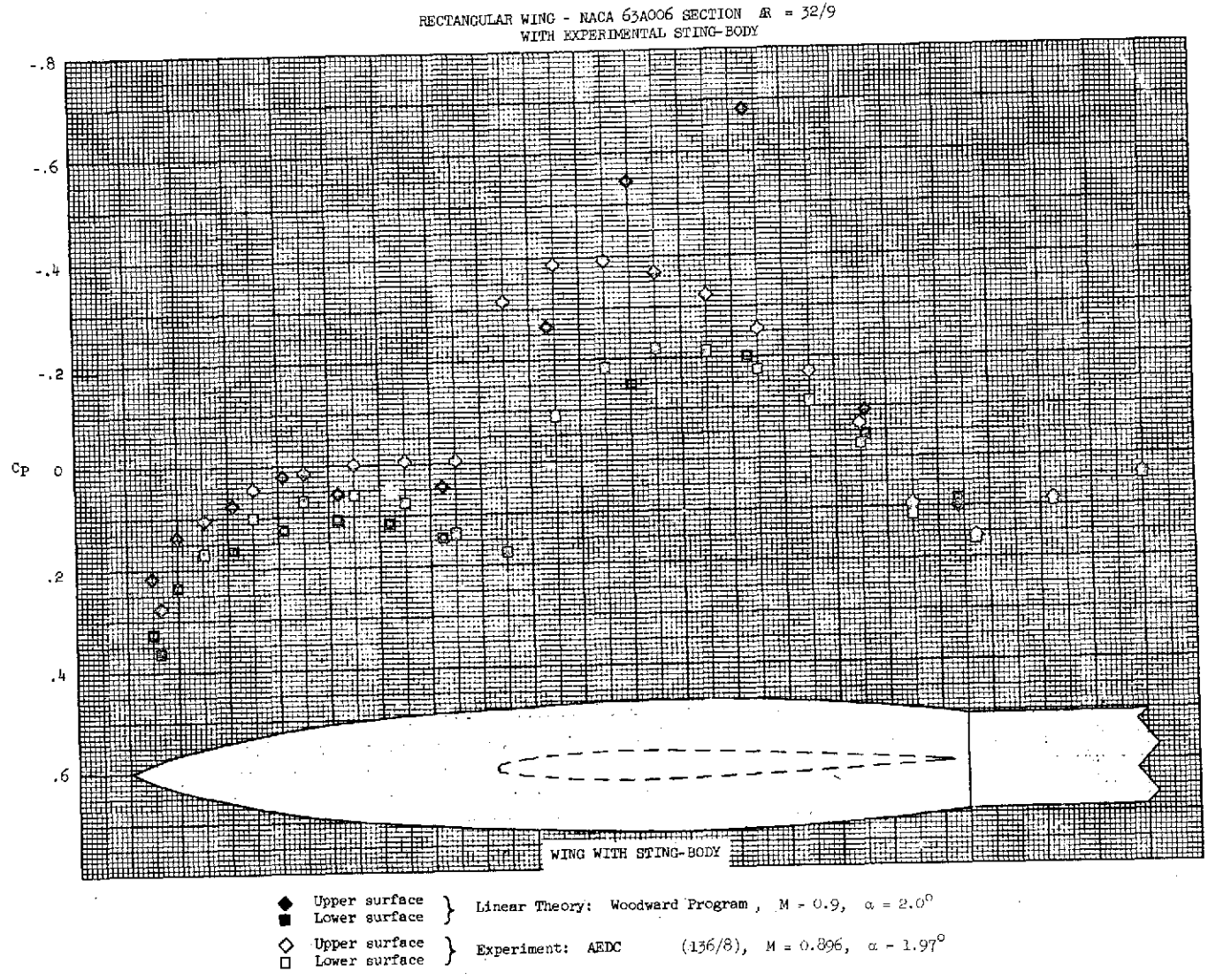


Figure 52.- Axial distribution of surface pressure coefficients on the sting-body of the wing.

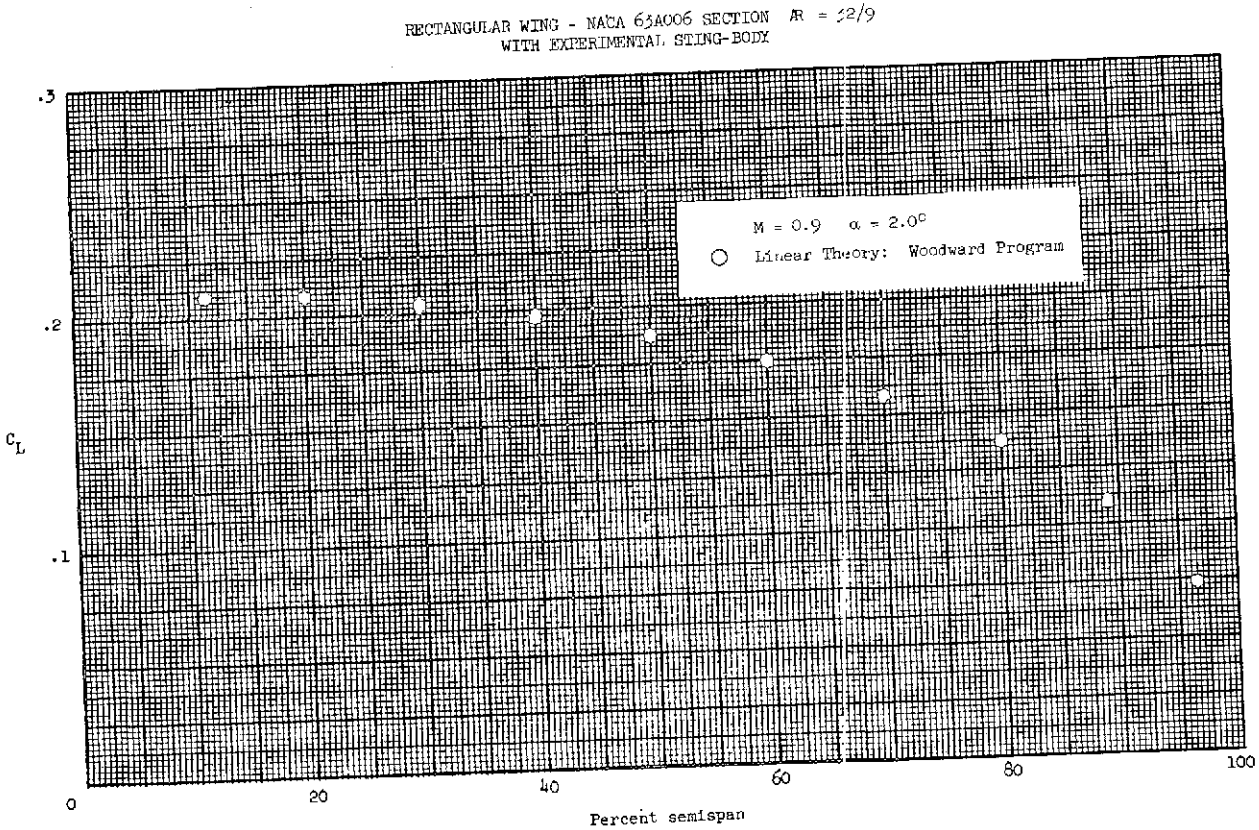


Figure 53.- Spanwise distribution of section lift coefficient.

RECTANGULAR TAIL NACA 63A006 SECTION AR = 13/4.5
WITH EXPERIMENTAL STING-BODY

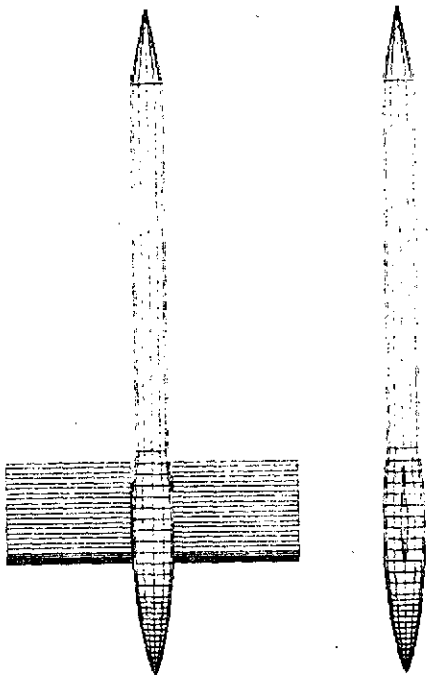

FIGURE 54.- RECTANGULAR TAIL PLUS EXPERIMENTAL STING-BODY CONFIGURATION USED IN CALCULATIONS.

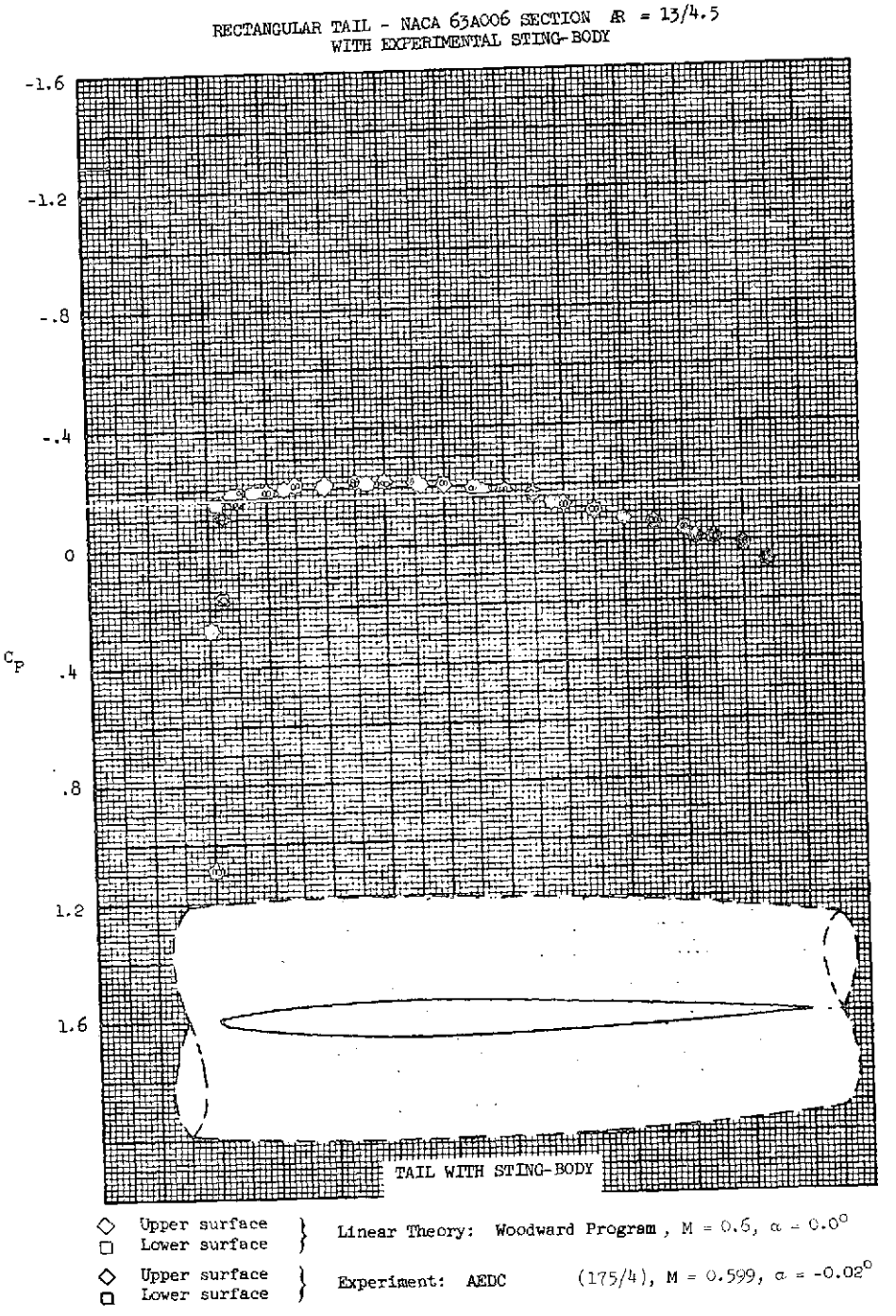


Figure 55.- Chordwise distribution of surface pressure coefficients at the 50 percent semispan location on the tail.

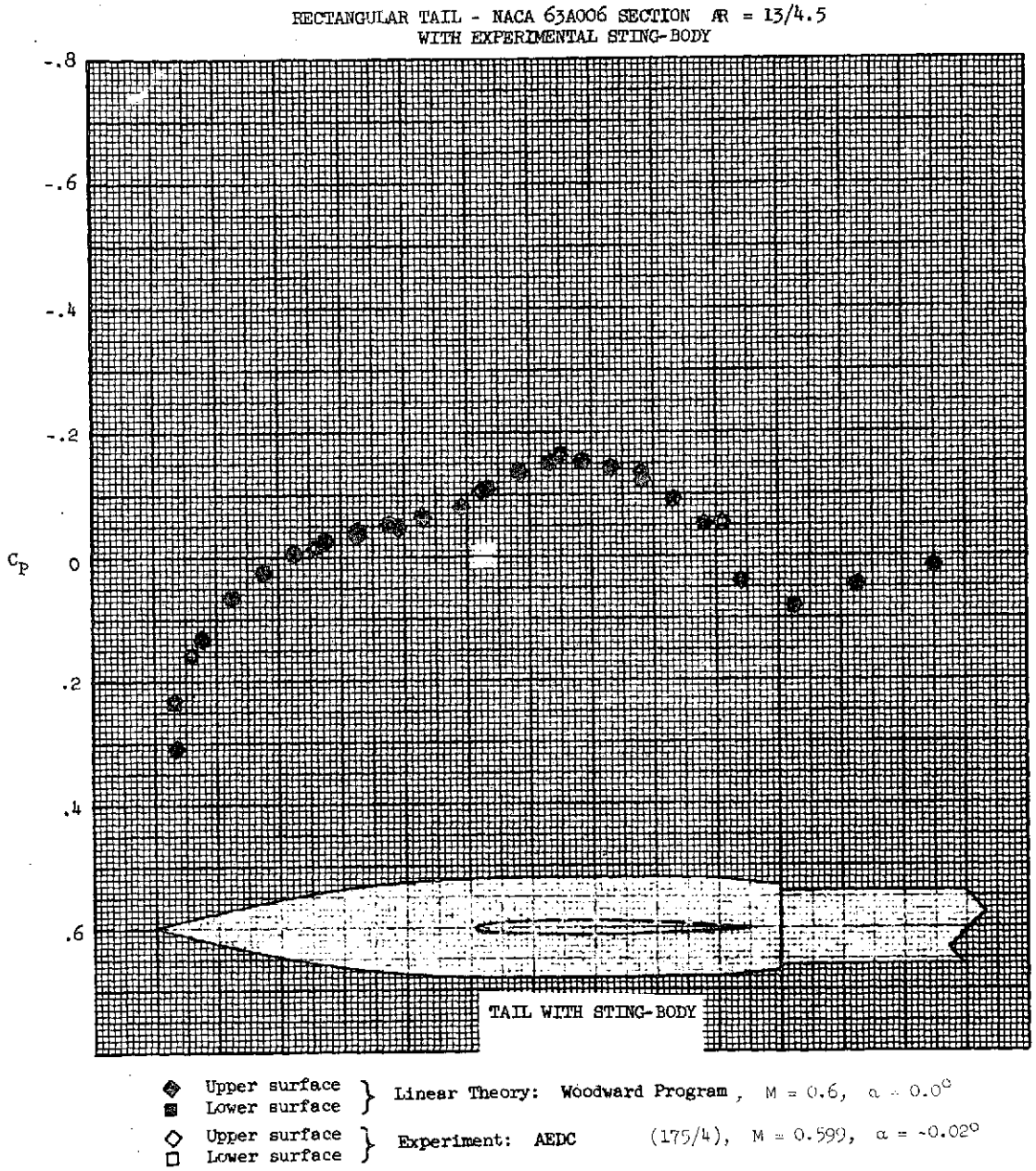


Figure 56.- Axial distribution of surface pressure coefficients on the sting-body of the tail.

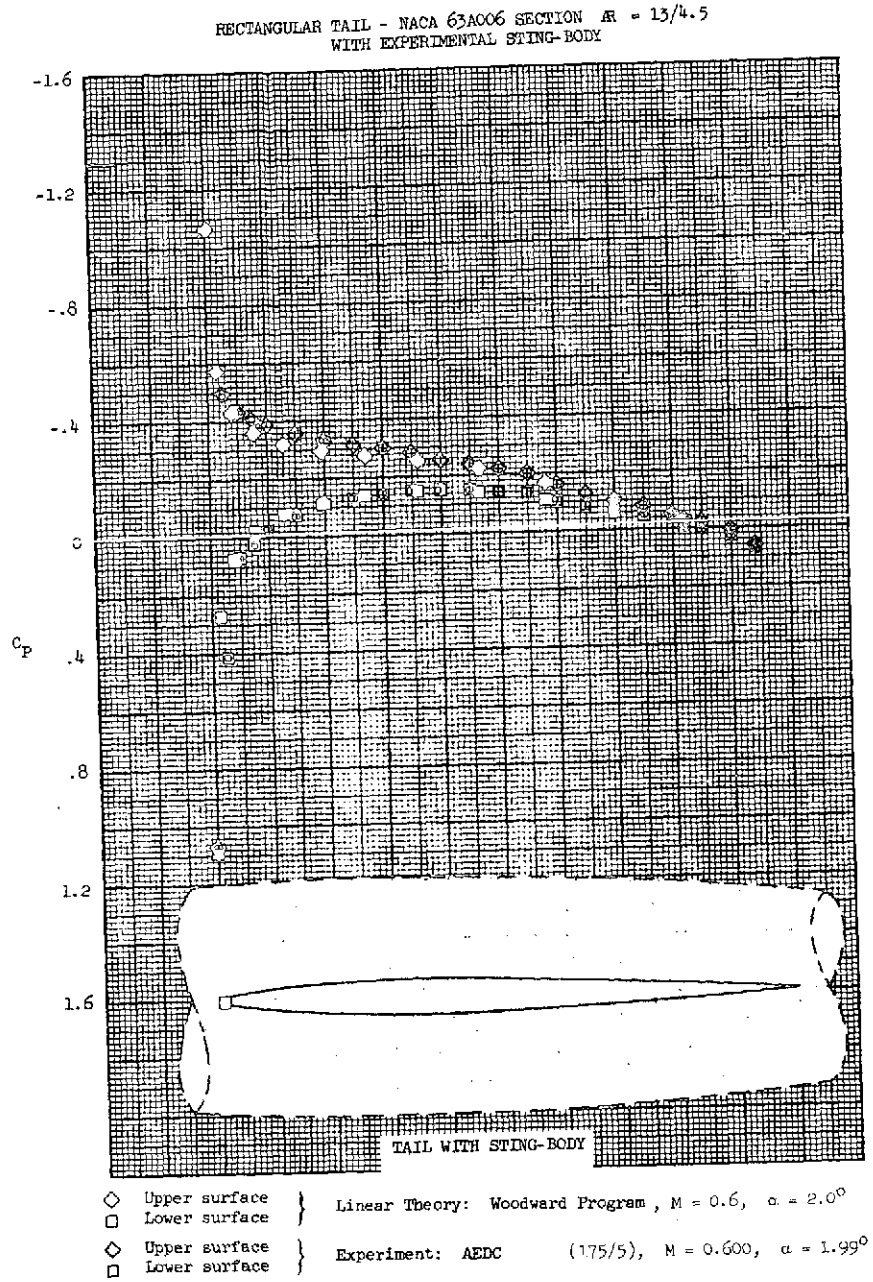


Figure 57.- Chordwise distribution of surface pressure coefficients at the 50 percent semispan location on the tail.

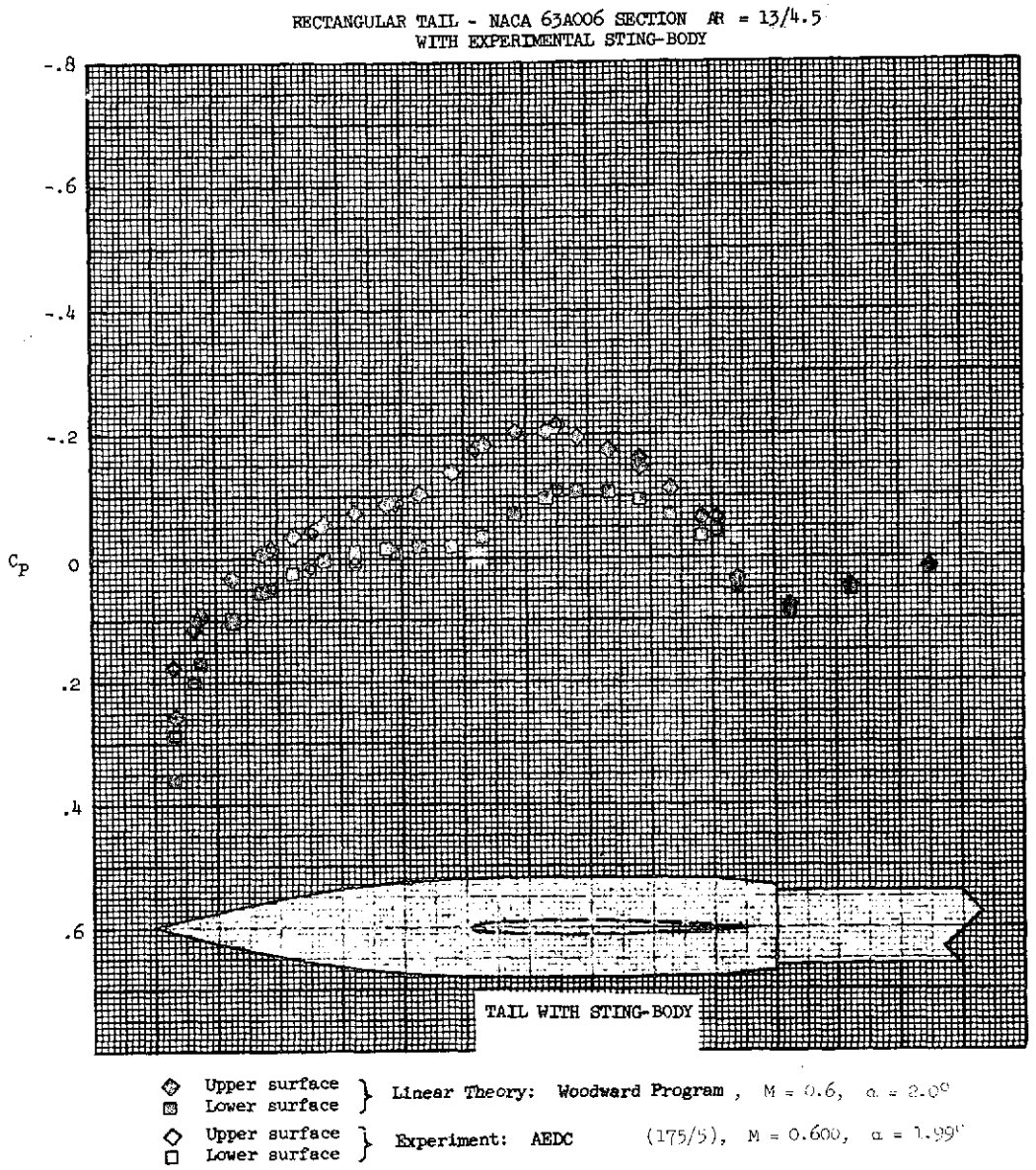


Figure 58.- Axial distribution of surface pressure coefficients on the sting-body of the tail.

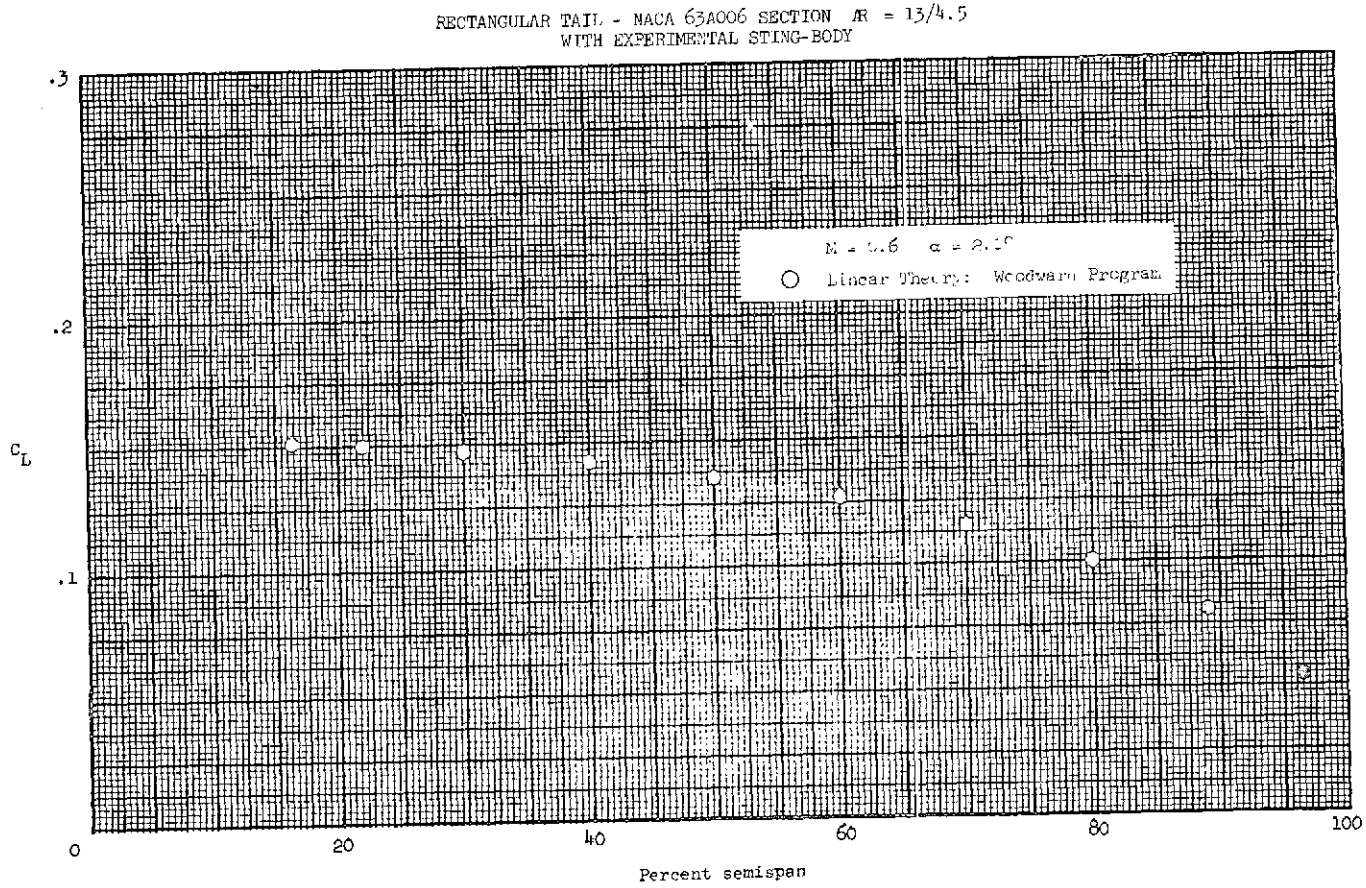


Figure 59.- Spanwise distribution of section lift coefficient.

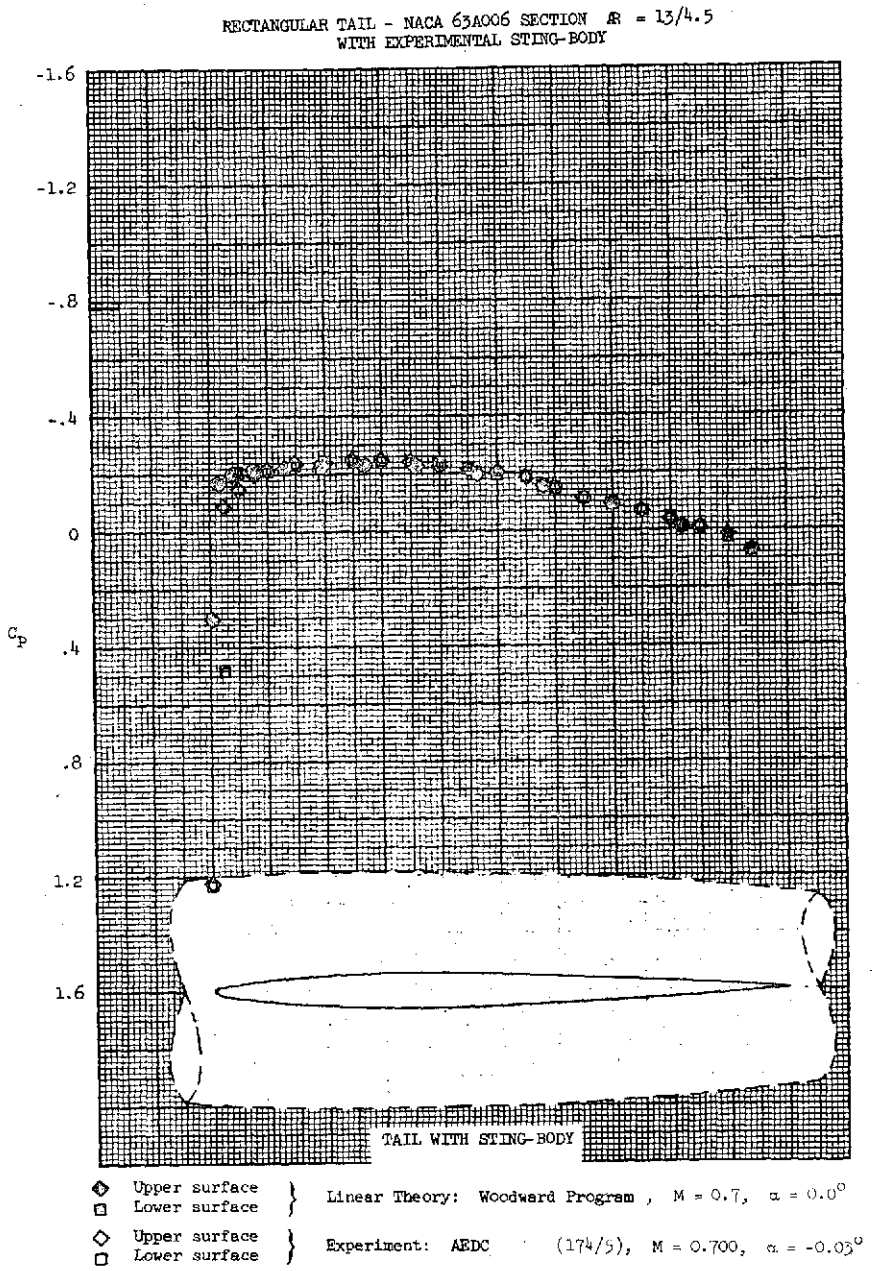


Figure 60.- Chordwise distribution of surface pressure coefficients at the 50 percent semispan location on the tail.

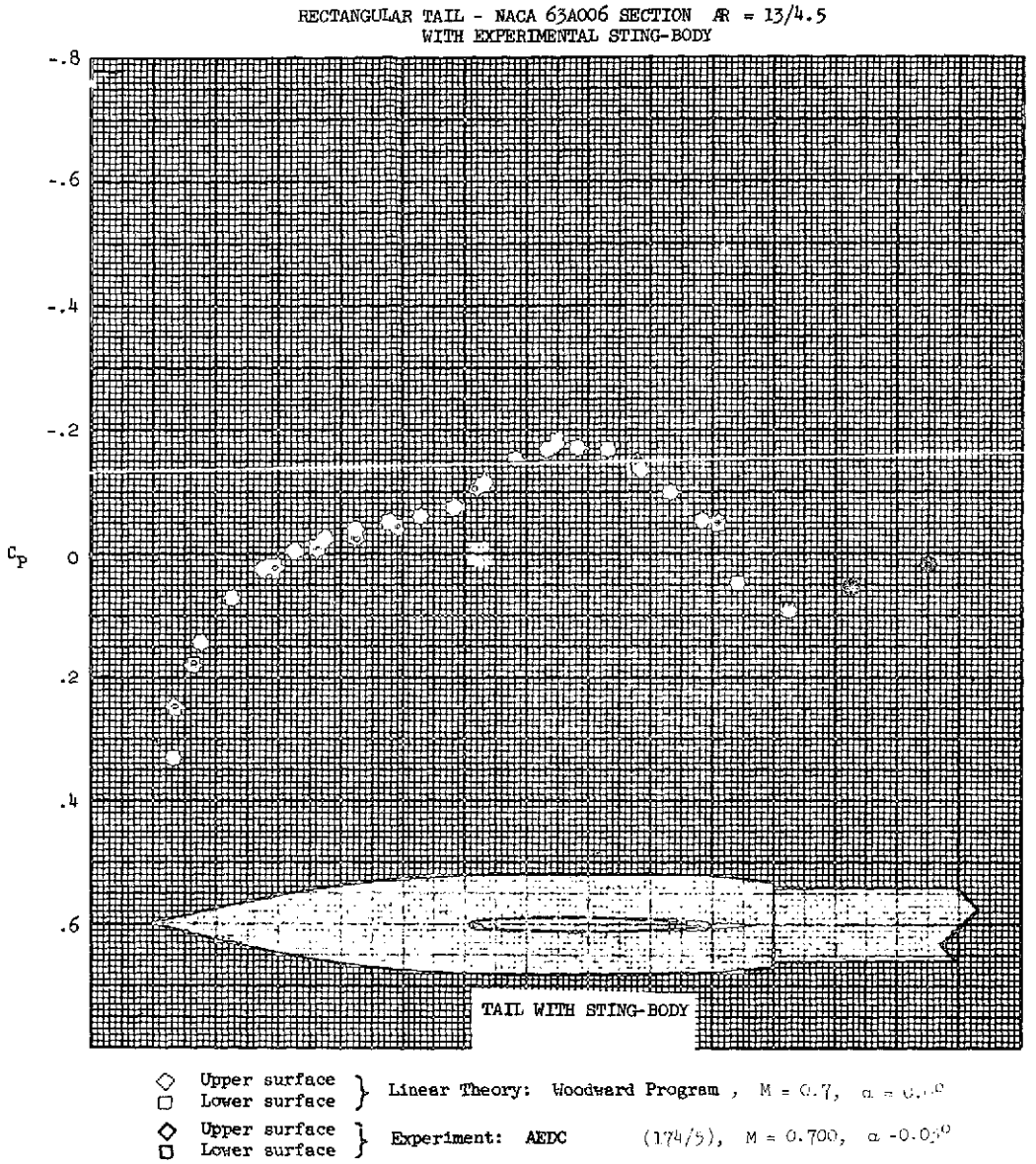


Figure 61.- Axial distribution of surface pressure coefficients on the sting-body of the tail.

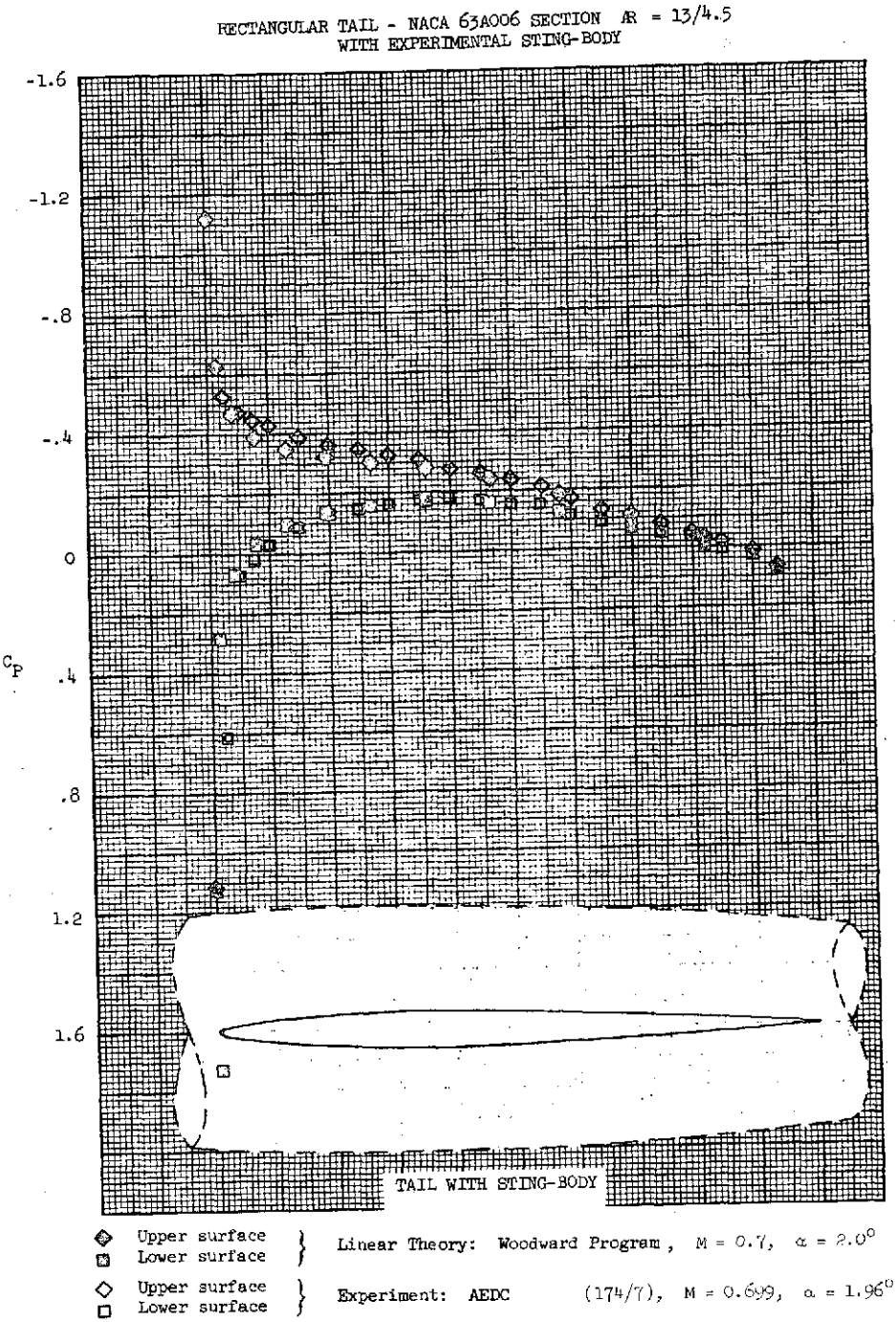


Figure 62.- Chordwise distribution of surface pressure coefficients at the 50 percent semispan location on the tail.

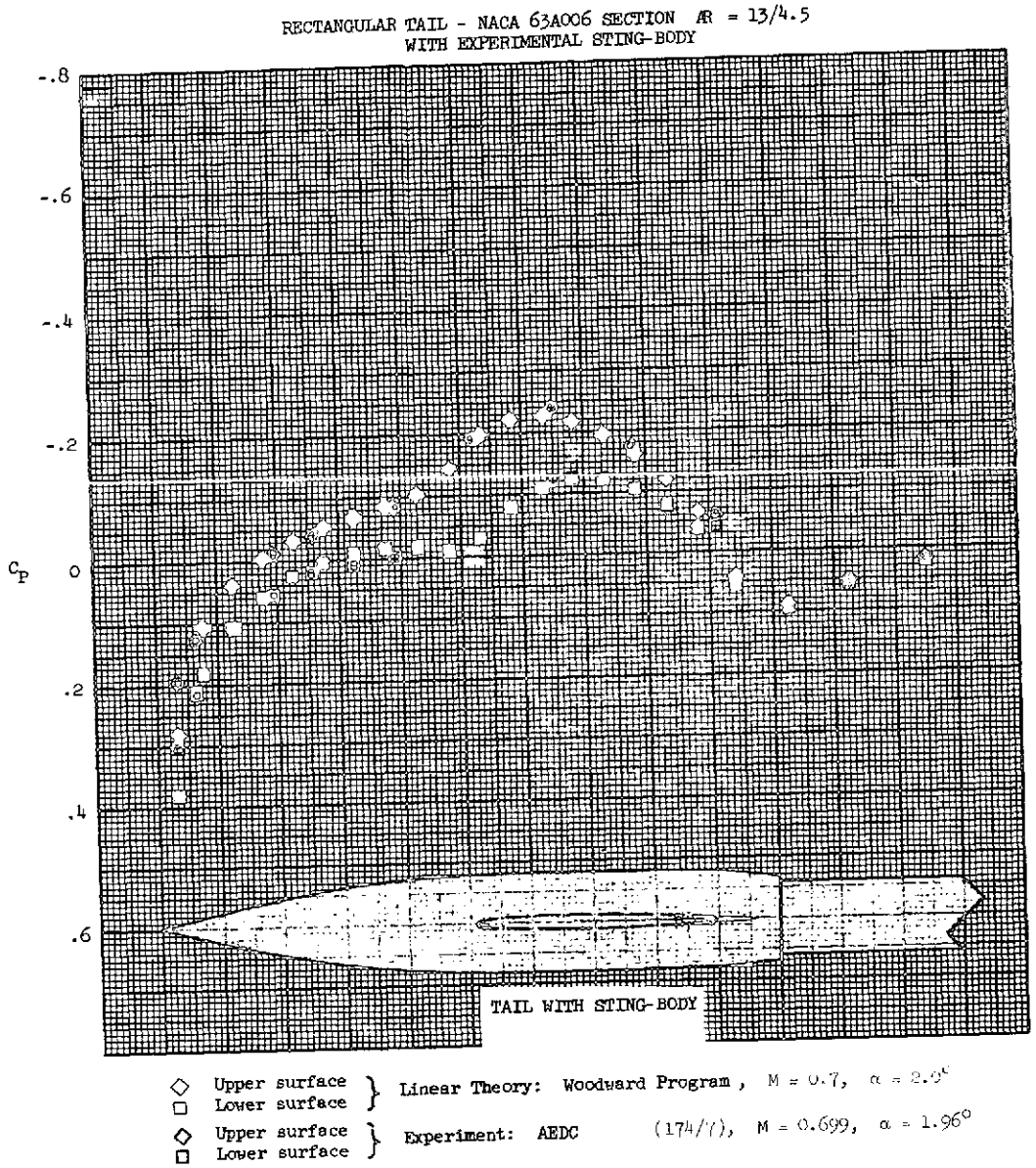


Figure 63.- Axial distribution of surface pressure coefficients on the sting-body of the tail.

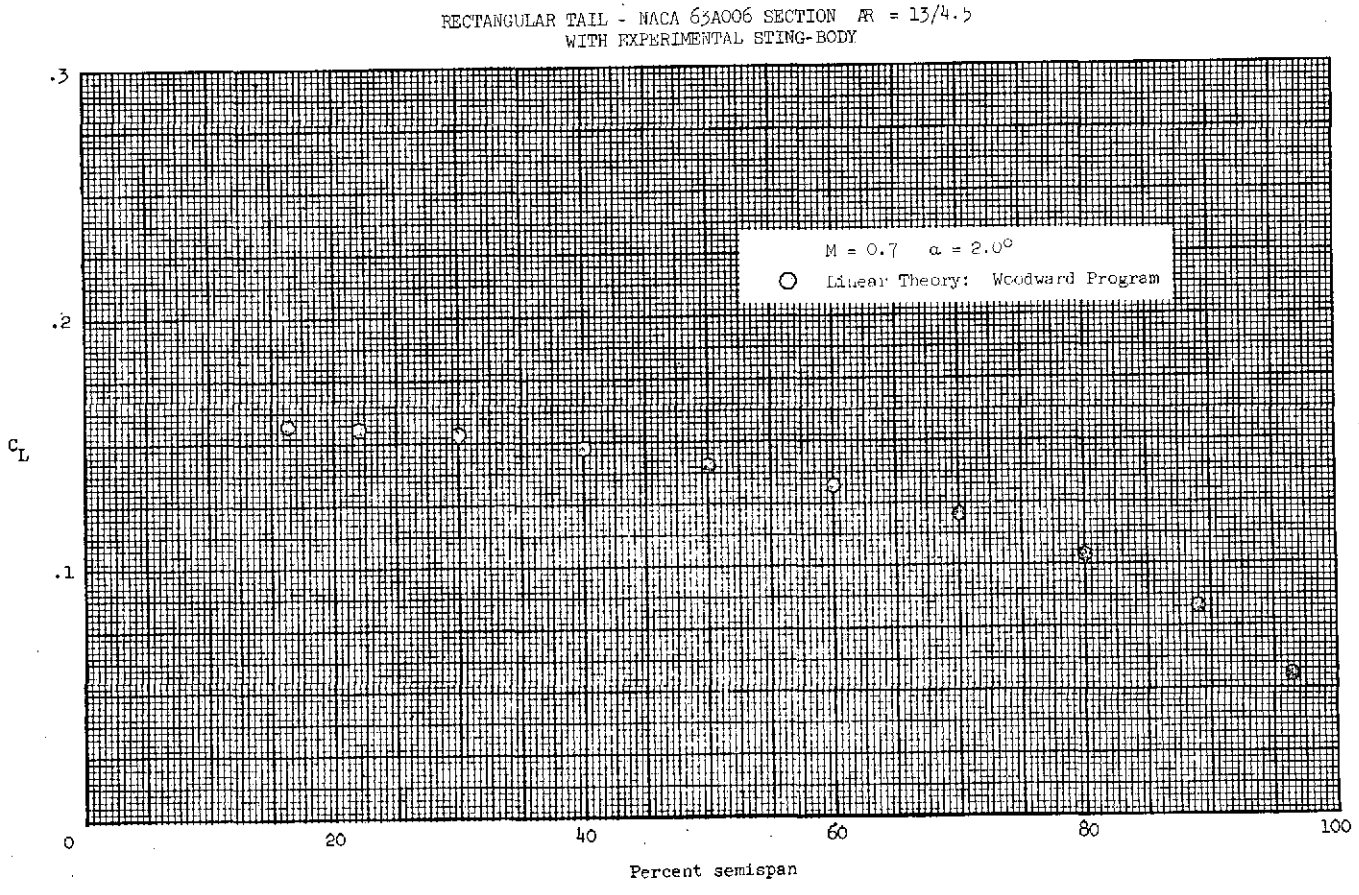


Figure 64.- Spanwise distribution of section lift coefficient.

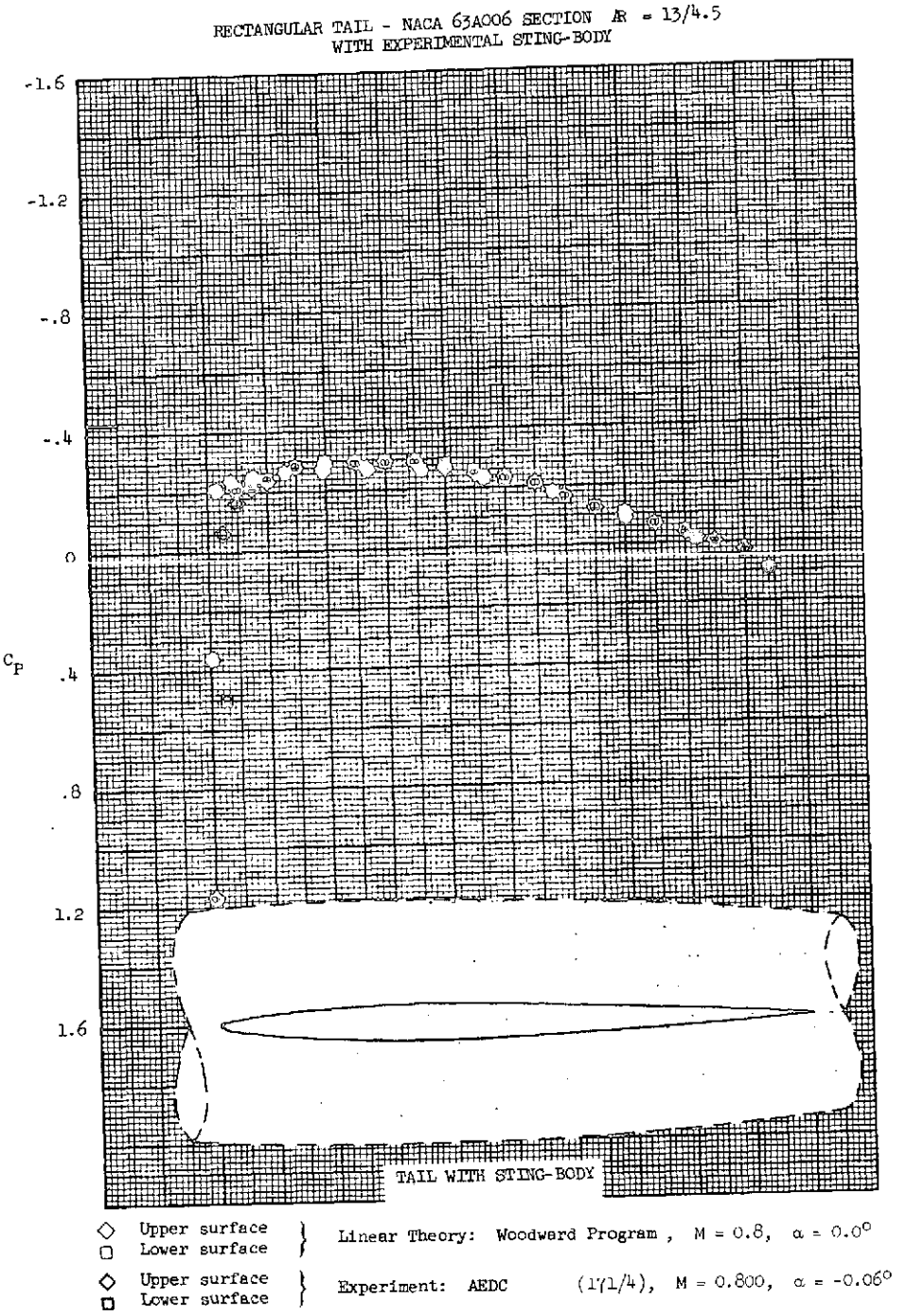


Figure 65.- Chordwise distribution of surface pressure coefficients at the 50 percent semispan location on the tail.

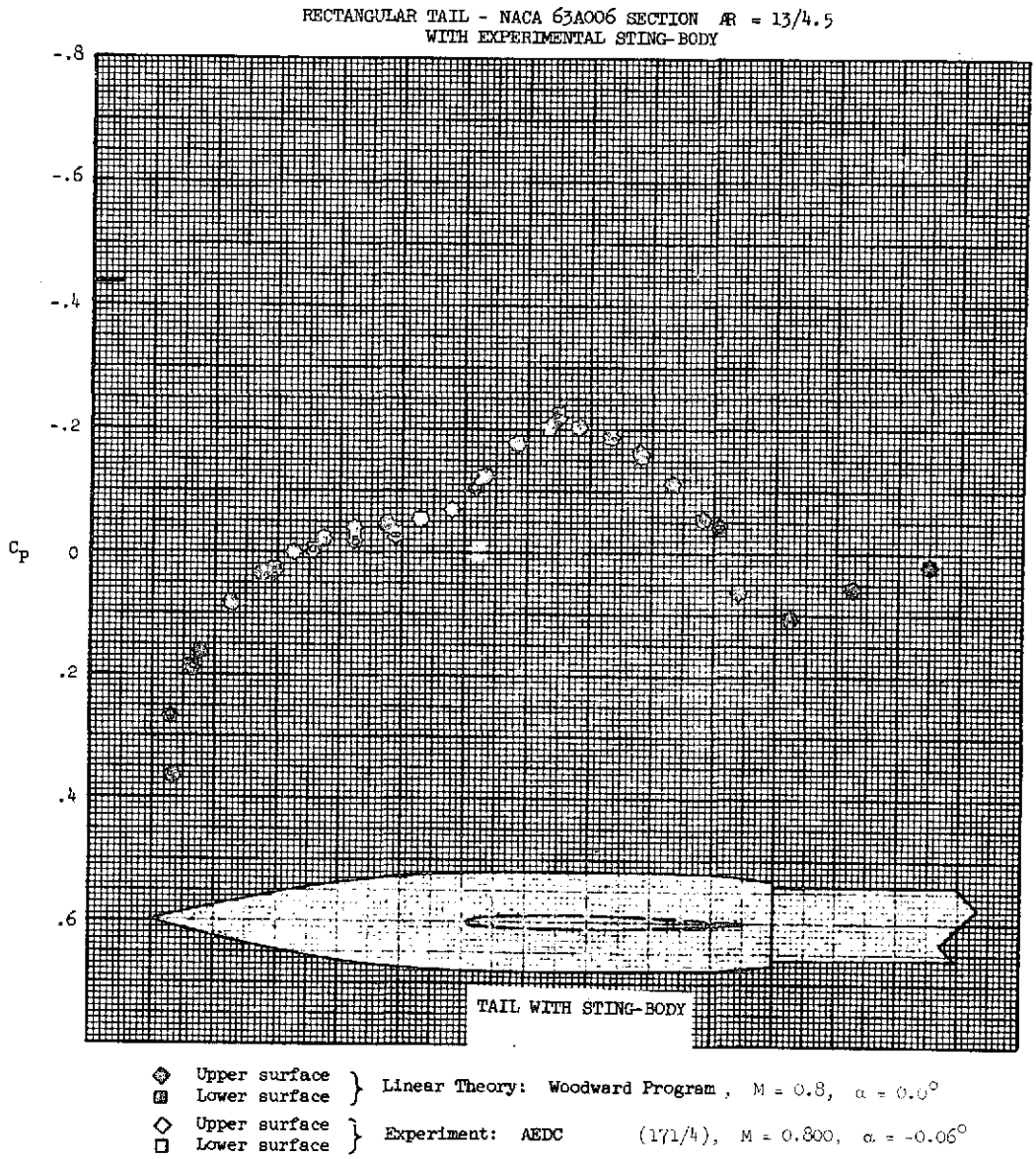


Figure 66.- Axial distribution of surface pressure coefficients on the sting-body of the tail.

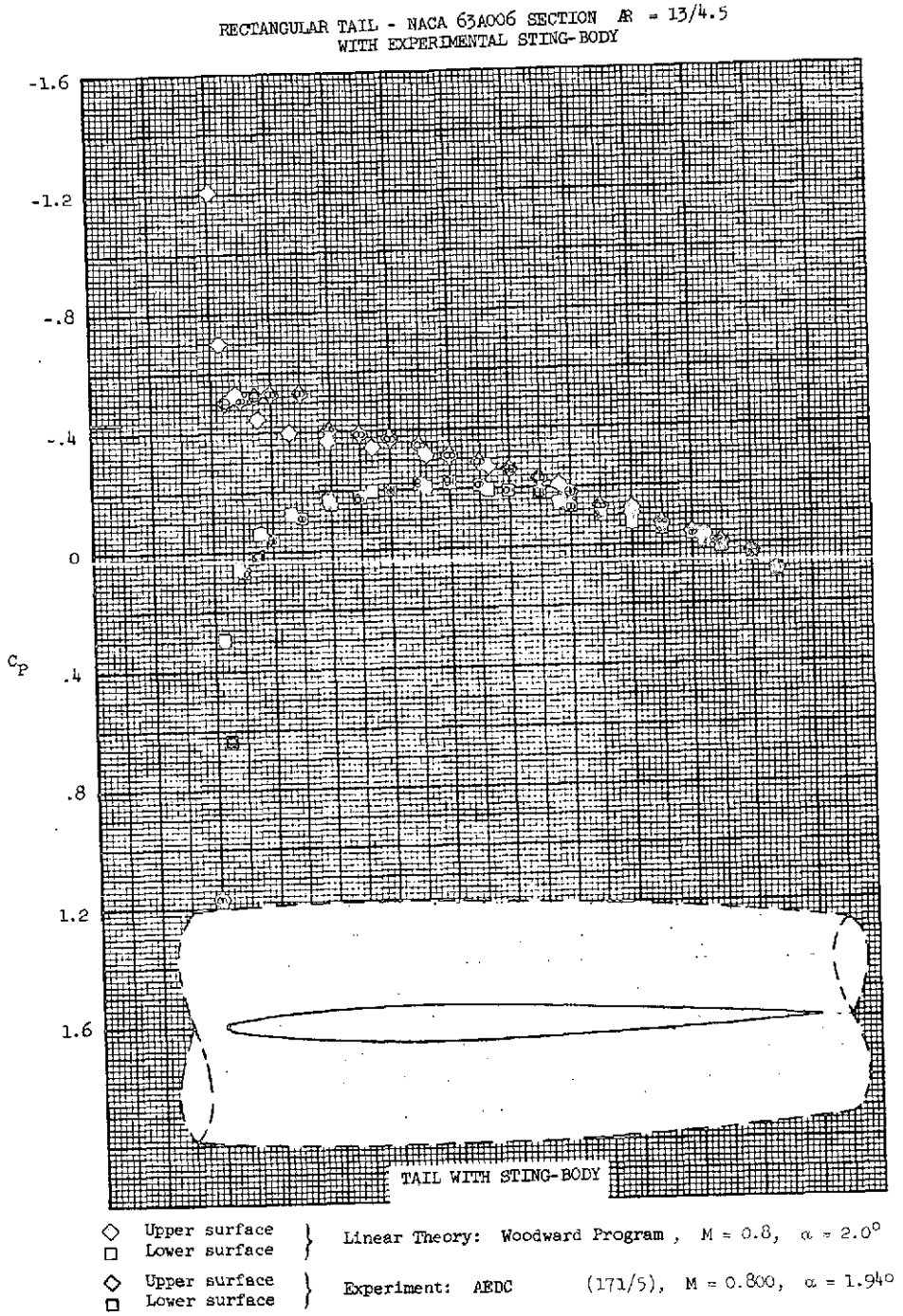


Figure 67.- Chordwise distribution of surface pressure coefficients at the 50 percent semispan location on the tail.

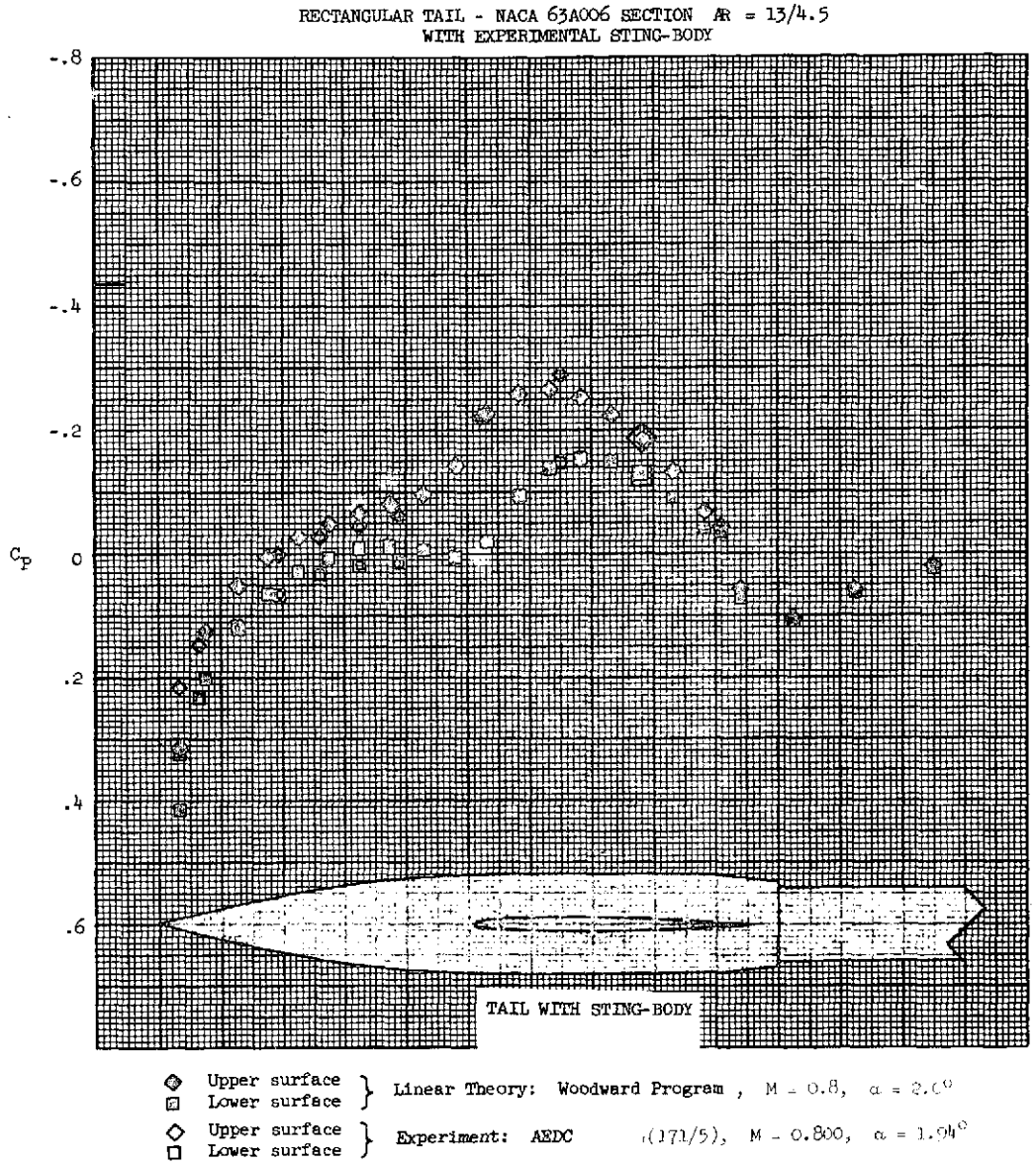


Figure 68.- Axial distribution of surface pressure coefficients on the sting-body of the tail.

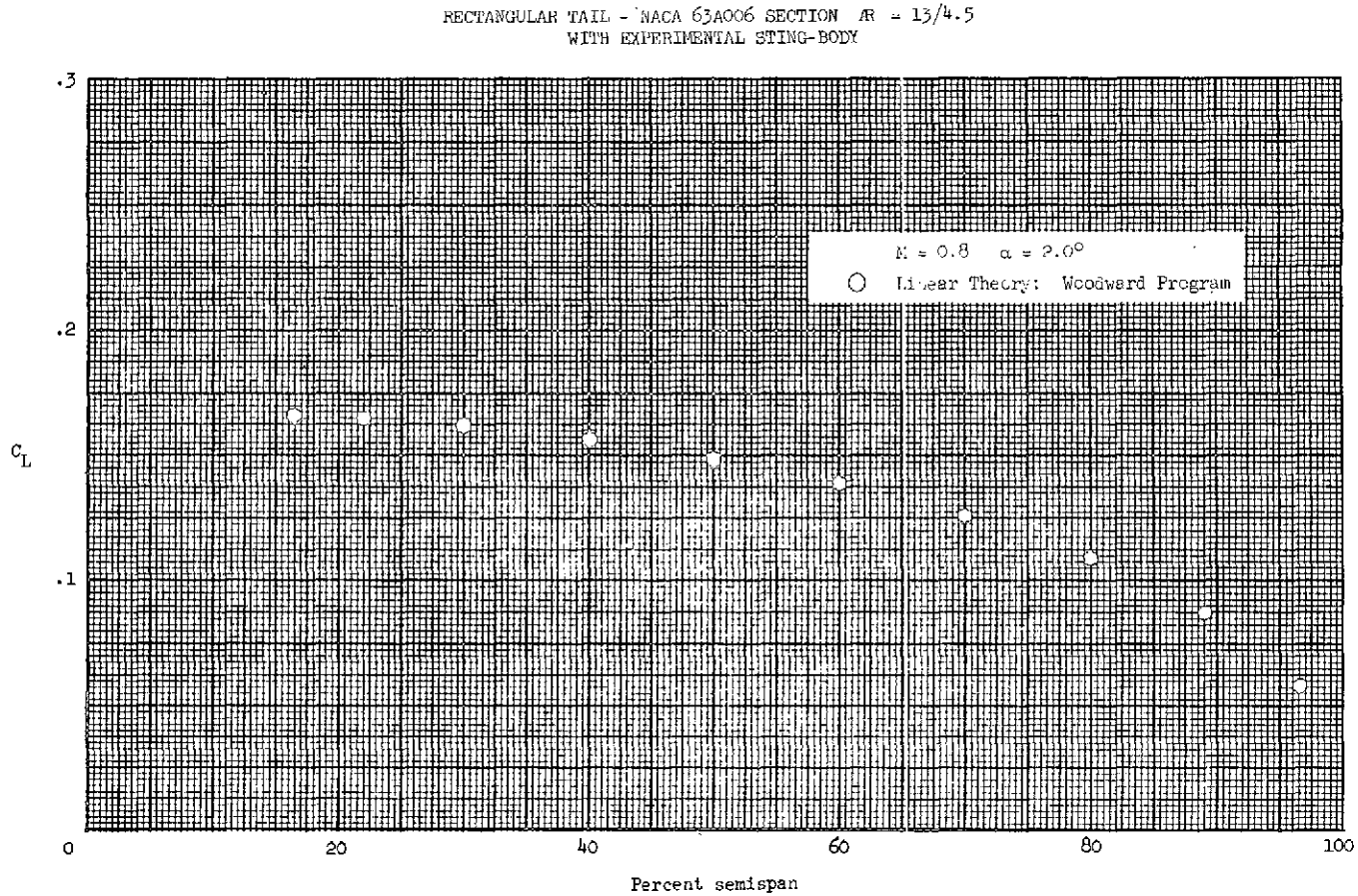


Figure 69.- Spanwise distribution of section lift coefficient.

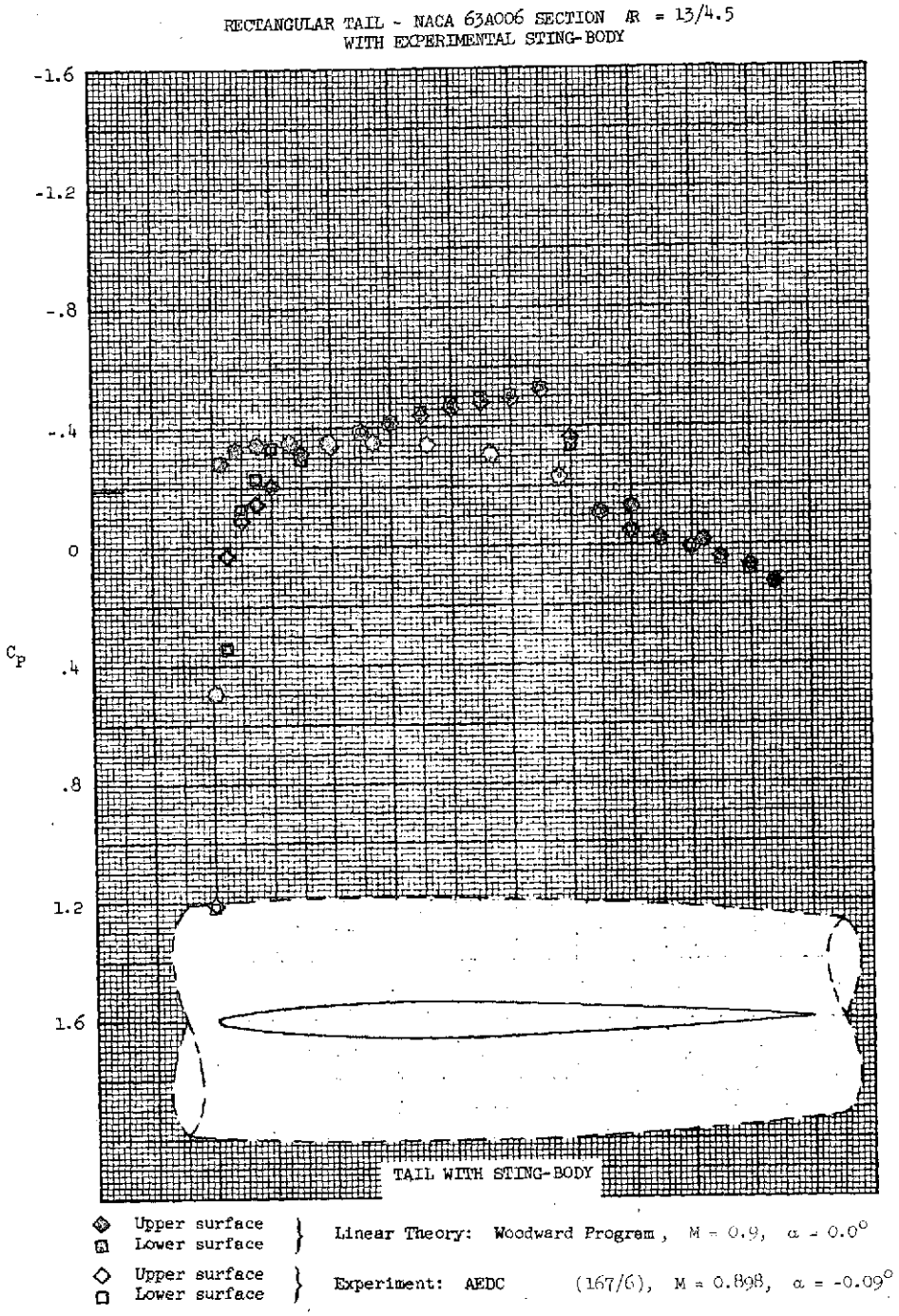


Figure 70.- Chordwise distribution of surface pressure coefficients at the 50 percent semispan location on the tail.

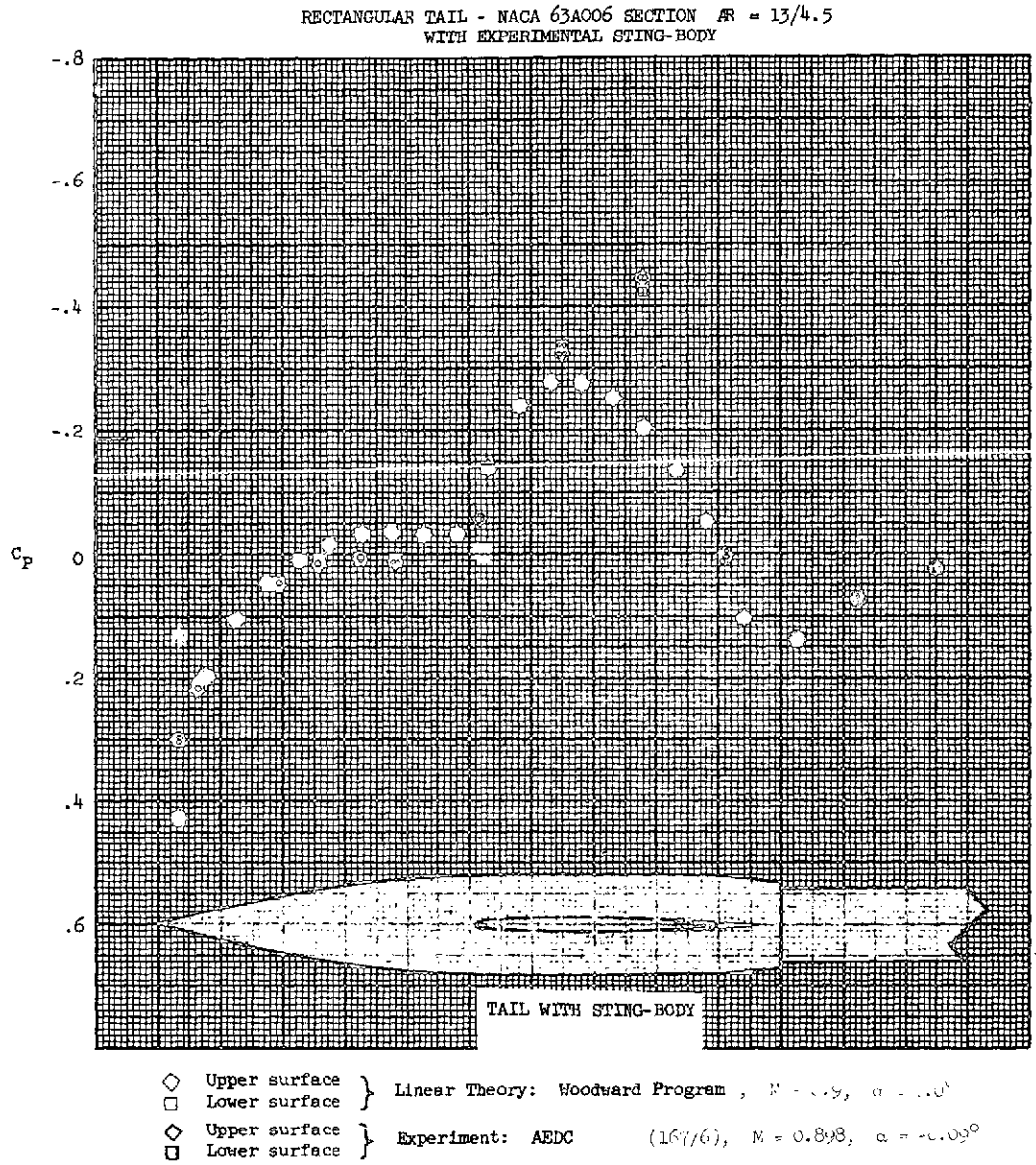


Figure 71.- Axial distribution of surface pressure coefficients on the sting-body of the tail.

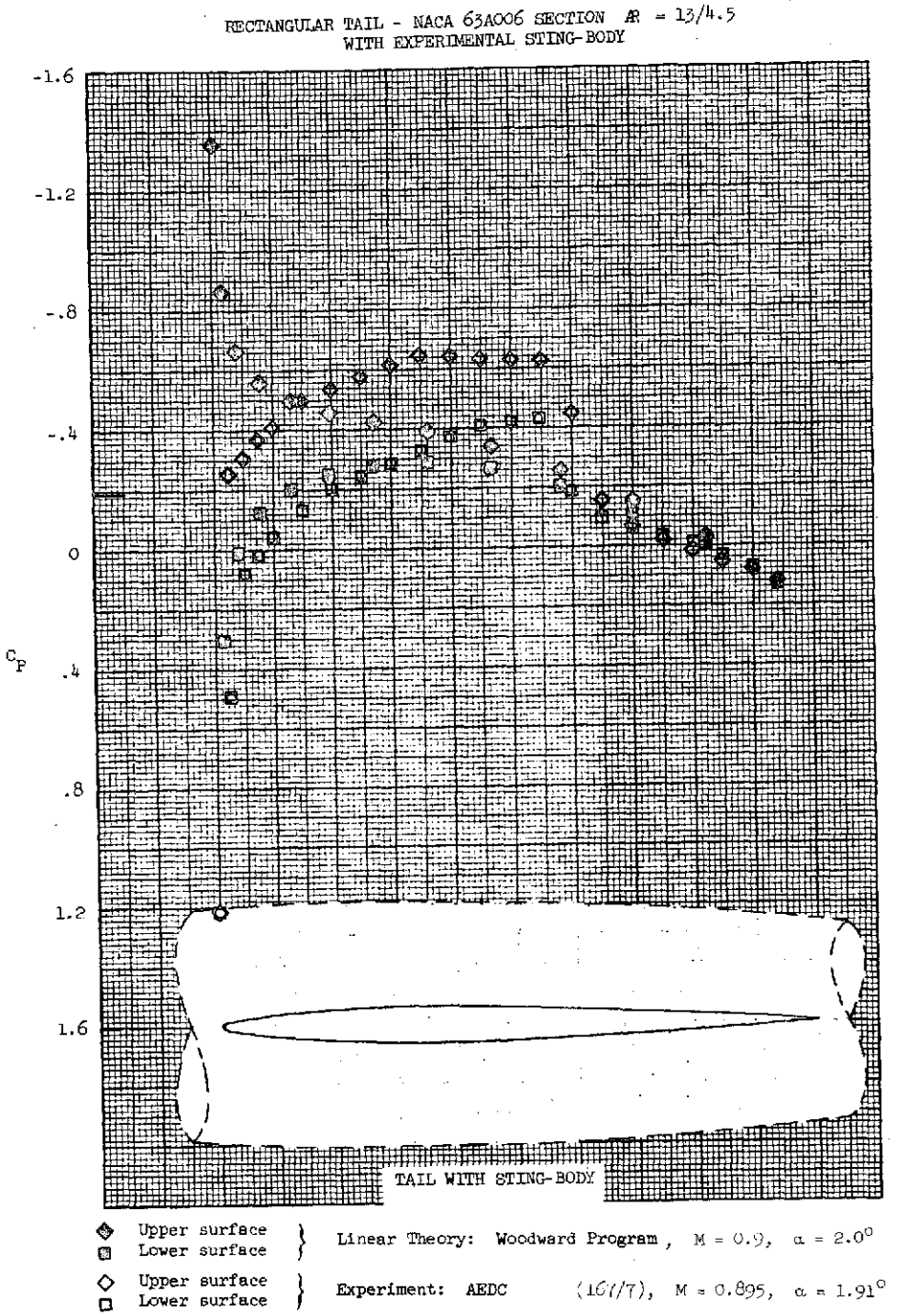


Figure 72.- Chordwise distribution of surface pressure coefficients at the 50 percent semispan location on the tail.

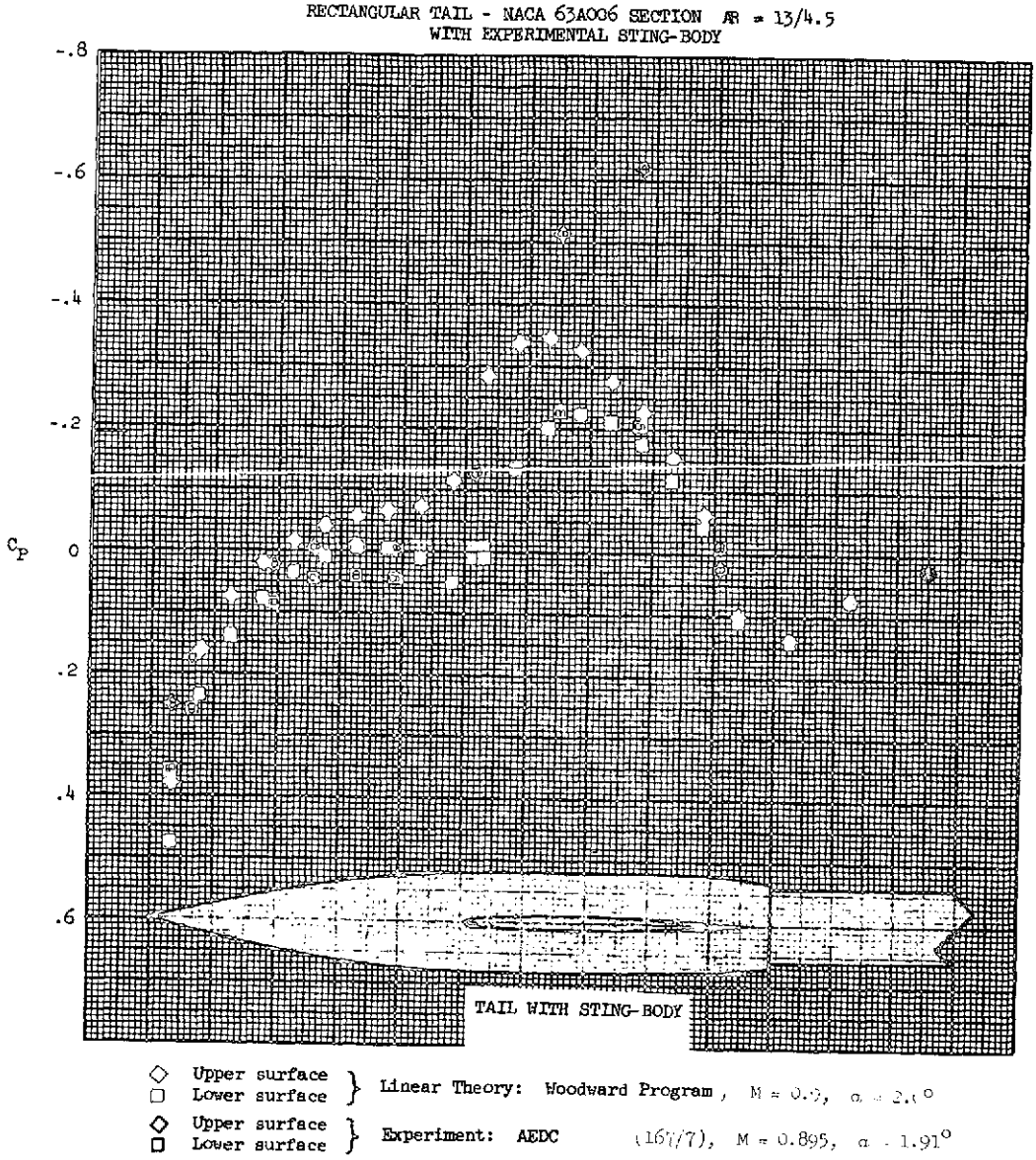


Figure 73.- Axial distribution of surface pressure coefficients on the sting-body of the tail.

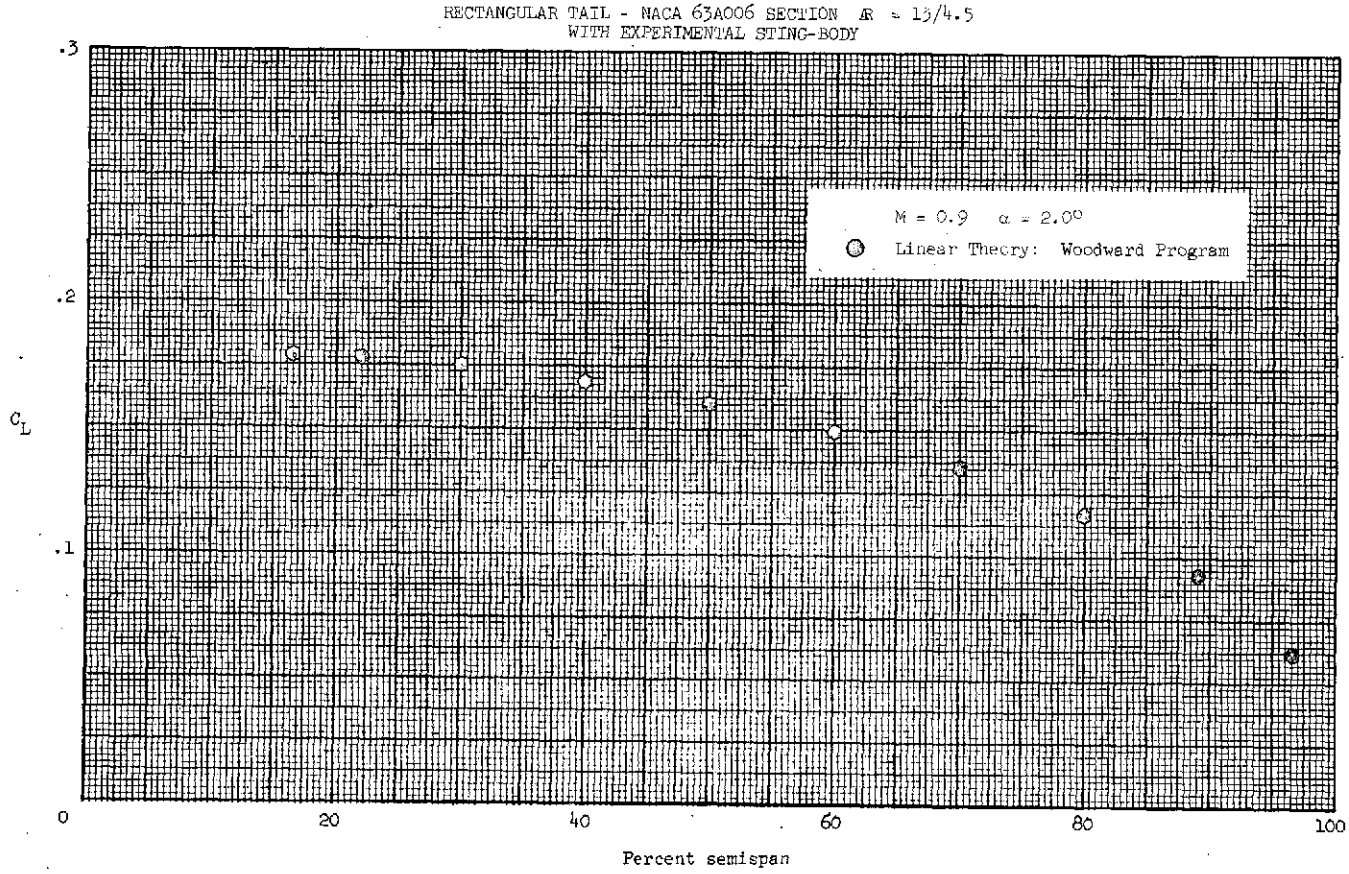


Figure 74.- Spanwise distribution of section lift coefficient.

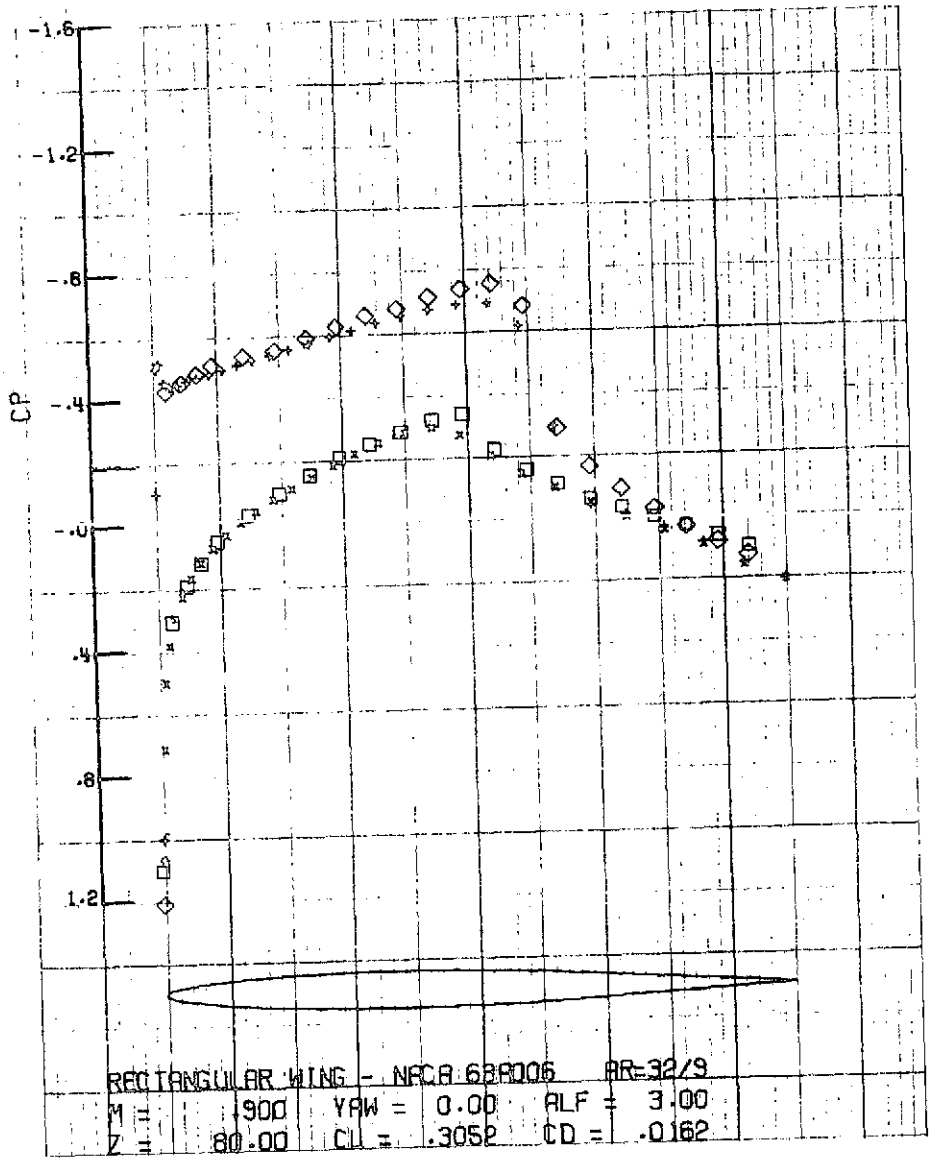


Figure 75.- Chordwise distribution of surface pressure coefficients at the 50 percent semispan location. The angle of attack used in the Jameson program was guessed so as to approximate the apparent experimental section lift.

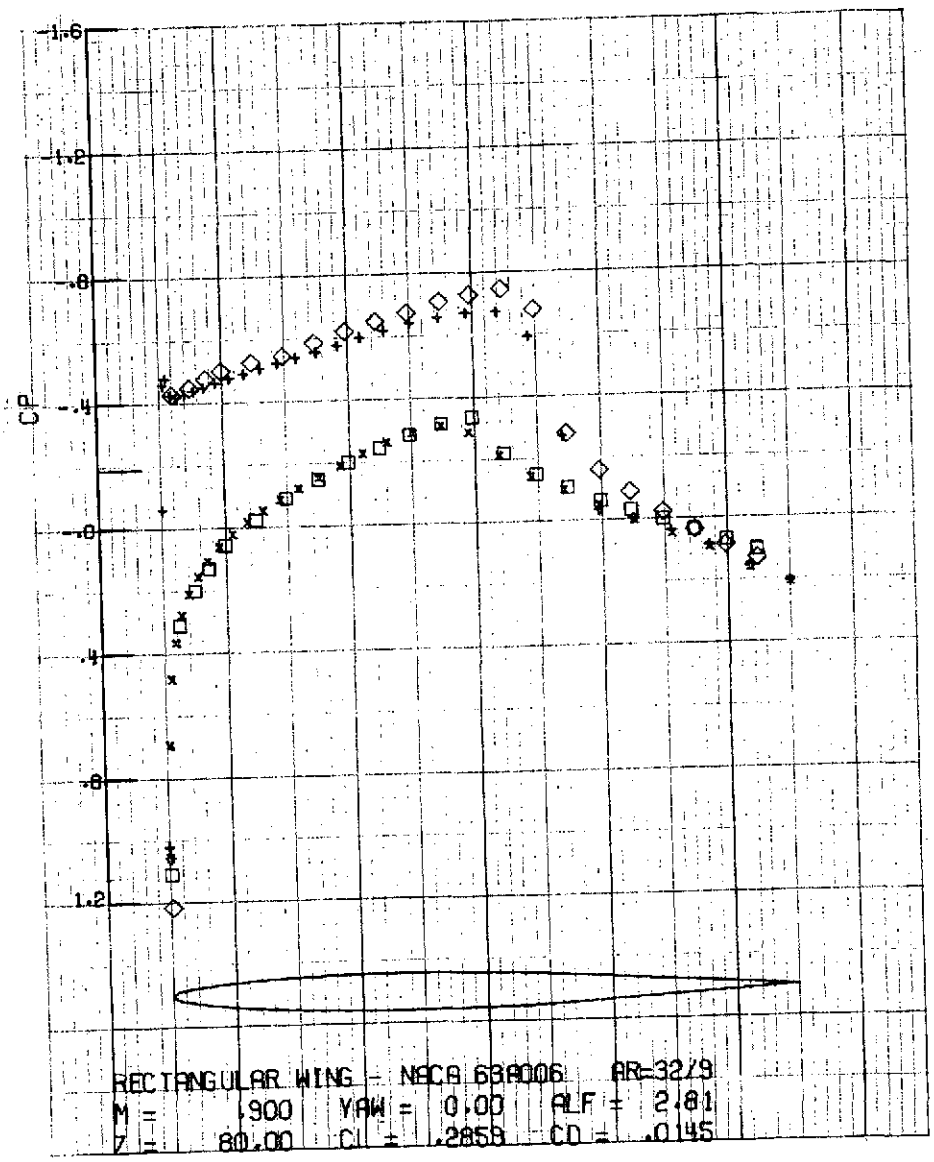


Figure 76.- Chordwise distribution of surface pressure coefficients at the 50 percent semispan location. The angle of attack used in the Jameson program was adjusted to account for sting deflection as determined by an approximate stress analysis.

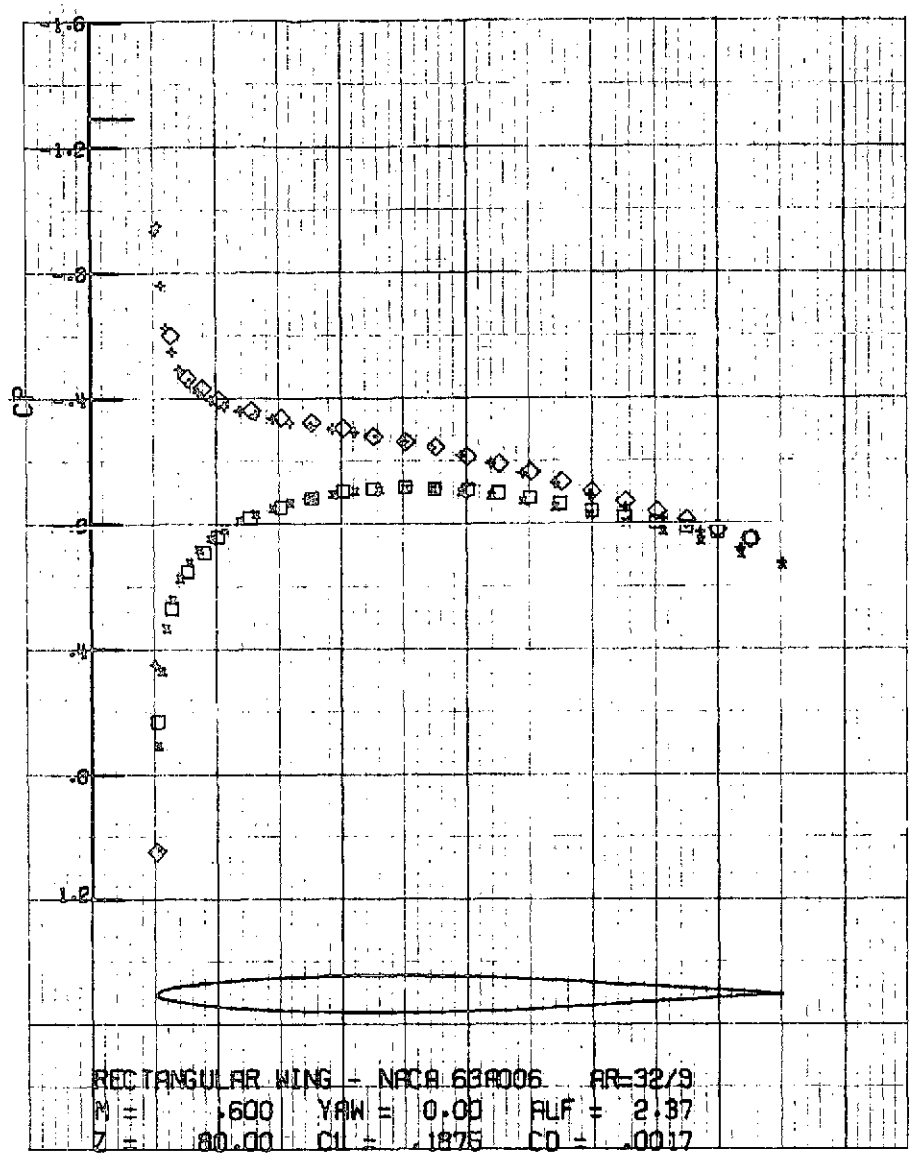


Figure 77.- Chordwise distribution of surface pressure coefficients at the 50 percent semispan location. The angle of attack used in the Jameson program was adjusted to account for sting deflection as determined by an approximate stress analysis.